Leg 197 Preliminary Report

Motion of the Hawaiian Hotspot: A Paleomagnetic Test

1 July–27 August 2001

Shipboard Scientific Party

PUBLISHER'S NOTES

This report was prepared from shipboard files by scientists who participated in the cruise. The report was assembled under time constraints and does not contain all works and findings that will appear in the *Initial Reports* of the ODP *Proceedings.* Reference to the whole or to part of this report should be made as follows:

Distribution: Electronic copies of this series may be obtained from the Ocean Drilling Program's World Wide Web site at http://www-odp.tamu.edu/publications.

This publication was prepared by the Ocean Drilling Program, Texas A&M University, as an account of work performed under the international Ocean Drilling Program, which is managed by Joint Oceanographic Institutions, Inc., under contract with the National Science Foundation. Funding for the program is provided by the following agencies:

DISCLAIMER

Any opinions, findings, and conclusions or recommendations expressed in this publication are those of the author(s) and do not necessarily reflect the views of the National Science Foundation, the participating agencies, Joint Oceanographic Institutions, Inc., Texas A&M University, or Texas A&M Research Foundation.

The following scientists and personnel were aboard the *JOIDES Resolution* for Leg 197 of the Ocean Drilling Program:

SHIPBOARD SCIENTIFIC PARTY

John Anthony Tarduno
Co-Chief Scientist
Department of Earth and Environmental Sciences
University of Rochester
227 Hutchison Hall
Rochester NY 14627
USA
Work: (716) 275-5713
Fax: (716) 244-5689
john@earth.rochester.edu

Robert A. Duncan
Co-Chief Scientist
Oceanic and Atmospheric Sciences
Oregon State University
104 Ocean Administration Building
Corvallis OR 97331-5503
USA
Work: (541) 737-5206
Fax: (541) 737-2064
rduncan@oce.orst.edu

David W. Scholl
Staff Scientist
Department of Geophysics
Stanford University
Stanford CA 94305
USA
Work: (650) 329-4762
Fax: (650) 329-5163
dscholl@pangea.stanford.edu

Rosalba Bonaccorsi
Sedimentologist
Geological, Environmental and Marine Sciences
Universitá degli Studi di Trieste
Via Weiss, 2
c/o Comprensorio di S. Giovanni
34127 Trieste
Italy
Work: (39) 040 6762026
Fax: (39) 040 6762048
bonaccor@univ.trieste.it

Arno Buysch
Logging Staff Scientist
Angewandte Geophysik
RWTH-Aachen
Lochnerstrasse 4-20
D-52056 Aachen
Germany
Work: (49) 241 80 94826
Fax: (49) 241 80 92132
a.buysch@geophysik.rwth-aachen.de

Claire Carvallo
Paleomagnetist
Department of Physics, Geophysics Division
University of Toronto
3359 Mississauga Road North
Mississauga ON L5L 1C6
Canada
Work: (905) 828-5336
Fax: (905) 828-5425
carvallo@physics.utoronto.ca

Rory D. Cottrell
Paleomagnetist
Department of Earth and Environmental Sciences
University of Rochester
227 Hutchison Hall
Rochester NY 14627
USA
Work: (716) 275-8810
Fax: (716) 244-5689
rory@earth.rochester.edu

Florence Einaudi
Logging Staff Scientist
Laboratoire de Mesures en Forage
ODP/Naturalia et Biologia (NEB)
ISTEEM, 056
34095 Montpellier Cedex 5
France
Work: (33) 4 67 14 93 09
Fax: (33) 4 67 14 93 08
florence.einaudi@dstu.univ-montp2.fr

Frederick A. Frey
Petrologist
Department of Earth, Atmospheric and Planetary
  Sciences
Massachusetts Institute of Technology
54-1226
77 Massachusetts Avenue
Cambridge MA 02139
USA
Work: (617) 253-2818
Fax: (617) 253-7102
fafrey@mit.edu

Jill A. Gudding
Undergraduate Student Trainee
Michigan State University
3340 Eastwood Drive
Rochester Hills MI 48309
USA
guddingj@msu.edu

Sarah Haggas
Physical Properties Specialist
Department of Geology
University of Leicester
University Road
Leicester LE1 7RH
United Kingdom
Work: (44) 116-252-3327
Fax: (44) 116-252-3918
slh19@leicester.ac.uk

Shichun Huang
Inorganic Geochemist
Department of Earth, Atmospheric and Planetary
  Sciences
Massachusetts Institute of Technology
54-1210
77 Massachusetts Avenue
Cambridge MA 02139
USA
Work: (617) 253-2869
Fax: (617) 253-7102
huangs@mit.edu

Randall A. Keller
Petrologist
College of Oceanic and Atmospheric Sciences
Oregon State University
104 Ocean Administration Building
Corvallis OR 97331-5503
USA
Work: (541) 737-2354
Fax: (541) 737-2064
rkeller@oce.orst.edu

Bryan C. Kerr
Geophysicist
Department of Geophysics
Stanford University
Mitchell Building Room H13A
Stanford CA 94305
USA
Work: (650) 723-2751
Fax: (650) 725-7244
bckerr@pangea.stanford.edu

Sten Lindblom
Sedimentologist
Department of Geology and Geochemistry and
  Unit for Paleogeophysics and Geodynamics
Stockholm Universitet
106 91 Stockholm
Sweden
Work: (46) 8-674-7837
Fax: (46) 8-674-7897
sten.lindblom@geo.su.se

Clive R. Neal
Petrologist
Department of Civil Engineering and Geological
  Sciences
University of Notre Dame
156 Fitzpatrick Hall
Notre Dame IN 46556
USA
Work: (219) 631-8328
Fax: (219) 631-9236
neal.1@nd.edu

Marcel Regelous
Petrologist
Abteilung Geochemie
Max-Planck-Institüt für Chemie
Johannes J-Becherweg 27
55128 Mainz
Germany
Work: (47) 6131 305304
Fax: (47) 6131 371051
regelous@mpch-mainz.mpg.de

Sidonie Rèvillon
Petrologist
Universitè J. Fourier
15, rue de la Piscine
38031 Grenoble Cedex
France

Present address:
Southampton Oceanography Centre
School of Ocean and Earth Sciences
Waterfront Campus, European Way
Southampton SO1 43ZH
United Kingdom
sido-revillon@yahoo.com

William G. Siesser
Paleontologist (nannofossils)
Department of Geology
Vanderbilt University
Box 46 Station B
Nashville TN 37235
USA
Work: (615) 322-2984
Fax: (615) 322-2138
william.g.siesser@vanderbilt.edu

Bernhard Steinberger
Physical Properties Specialist
Institut für Meteorologie und Geophysik
Johann Wolfgang Goethe-Universitaet
Feldbergstrasse 47
60323 Frankfurt am Main
Germany

Present address:
CIRES
University of Colorado
Campus Box 216
Boulder CO 80309-0216
USA
Work: (303) 492-1149
Fax: (303) 492-2606
bernhars@cires.colorado.edu

Johannes Stoll
JOIDES Logging Scientist/Physical Properties
  Specialist
Institut für Geophysik
Universität Göttingen
Herzberger Landstrasse 180
37075 Göttingen
Germany
Work: (49) 551-397466
Fax: (49) 551-3959
josto@uni-geophys.gwdg.de

Patricia M.E. Thompson
Petrologist
Department of Geology
University of Leicester
University Road
Leicester
Leicestershire LE1 7RH
United Kingdom
Work: (44) 116 252 3638
Fax: (44) 116 252 3918
pmet1@leicester.ac.uk

Thorvaldur Thordarson
Petrologist
Department of Geology and Geophysics/SOEST
University of Hawaii at Manoa
1680 East-West Road
POST Building 6th Floor
Honolulu HI 96822
USA
Work: (808) 956-7640
Fax: (808) 956-5512
moinui@soest.hawaii.edu

Masayuki Torii
Paleomagnetist
Department of Biosphere-Geosphere System Science
Okayama University of Science
1-1 Ridai-cho
Okayama 700-0005
Japan
Work: (81) 86-256-9601
Fax: (81) 86-256-9601
torii@big.ous.ac.jp

Fabrizio Tremolada
Paleontologist (nannofossils)
Dipartimento di Scienze della Terra Università degli
Studi di Milano
via Mangiagalli, 34
20133 Milano
Italy
Work: (39) 02-2369 8257
Fax: (39) 02-7063 8261
fabrizio.tremolada@unimi.it

TRANSOCEAN SEDCO FOREX OFFICIALS

Tom Hardy
Master of the Drilling Vessel
Overseas Drilling Ltd.
707 Texas Avenue South, Suite 213D
College Station TX 77840-1917
USA

Wayne Malone
Drilling Superintendent
Overseas Drilling Ltd.
707 Texas Avenue South, Suite 213D
College Station TX 77840-1917
USA

ODP SHIPBOARD PERSONNEL

Charles A. Endris
Marine Laboratory Specialist (Paleomagnetism)

Randy W. Gjesvold
Marine Electronics Specialist

Dennis Graham
Marine Laboratory Specialist (Chemistry)

Ronald M. Grout
Operations Manager

Ted Gustafson
Marine Laboratory Specialist
   (Downhole Tools/Thin Sections)

Margaret Hastedt
Marine Computer Specialist

Michiko Hitchcox
Marine Laboratory Specialist (Yeoperson)

Maniko Kamei
Marine Laboratory Specialist (Core)

Anastasia Ledwon
Marine Laboratory Specialist (Physical Properties)

Martin Leven
Marine Electronics Specialist

Mike Meiring
Marine Electronics Specialist

Bill Mills
Laboratory Officer

Erik Moortgat
Marine Computer Specialist

Robert Olivas
Marine Laboratory Specialist (X-Ray)

Chad Peddy
Marine Laboratory Specialist (Core)

Chieh Peng
Marine Laboratory Specialist (Chemistry)

Cyndi J. Prince
Marine Laboratory Specialist (Photographer)

Kerry Swain
Schlumberger Logging Engineer

Paula Weiss
Marine Laboratory Specialist
    (Curation/Underway Geophysics)

Granville Wright
Programmer

ABSTRACT

The bend in the Hawaiian-Emperor chain is the best example of a change in plate motion recorded in a fixed-hotspot frame of reference. Alternatively, the bend might primarily record differences in motion of the Hawaiian hotspot relative to the Pacific lithosphere. Four lines of inquiry support the latter view: (1) global plate motions predicted from relative plate motion data, (2) spreading rate data from the North Pacific Basin, (3) mantle flow modeling utilizing geoid and seismic tomography constraints, and (4) paleomagnetic data from the Emperor chain. Although the rate of motion has been difficult to constrain because previous drilling was limited, the best available paleomagnetic data suggest Pacific hotspots may have moved rapidly, at rates comparable to those of lithospheric plates in Late Cretaceous to early Tertiary times (81-43 Ma).

Basements sites were drilled in the Emperor Seamount trend during Leg 197 to test the hypothesis of southward motion of the Hawaiian hotspot. The principal drilling objective was to achieve moderate basement penetration at these sites to obtain cores from lava flows suitable for paleomagnetic paleolatitude and radiometric age determinations. Because of the record-setting basement penetration (1220 m) during Leg 197 at Detroit (Sites 1203 and 1204; ~71–76 Ma), Nintoku (Site 1205; ~56 Ma) and Koko (Site 1206; ~48 Ma) Seamounts, we were able to meet our objectives. Paleolatitudes for these sites suggested by our preliminary shipboard paleomagnetic analysis clearly differ from the latitude of Hawaii. The values are consistent with and confirm prior results from Suiko (Deep Sea Drilling Project Site 433) and Detroit (Ocean Drilling Program Site 884) Seamounts. Our shipboard analysis of paleolatitude vs. age for the Emperor Seamounts must be supported by shorebased paleomagnetic studies and radiometric age determinations. However, the available data suggest that the Emperor Seamounts record the rapid southward motion of the Hawaiian hotspot in the mantle, requiring a major change in how we view this classic age-progressive volcanic lineament as a record of mantle convection and plate motions.

Another important science objective of the leg was to determine the geochemical variation of the volcanic products of the Hawaiian hotspot through time. Observations of lava flow thickness, vesicularity, crystallinity, and morphology, together with analysis of volcaniclastic sediments, has provided a picture of eruptions in subaerial to shallow-water conditions at Detroit and Koko Seamount Sites 1203, 1204, and 1206 and waning subaerial activity at Nintoku Seamount (Site 1205). Shipboard geochemical measurements suggest we have captured the transition from Hawaiian tholeiitic shield stage to alkalic postshield stage at each of the volcanic complexes. Between Sites 1203 and 1204 and previously studied Sites 883 and 884, we have a range of compositions at Detroit Seamount that covers most of the variability seen in volcanoes of the island of Hawaii.

The variability of trace element ratios (e.g., Ti/Zr) provide hints that we have sampled different source compositions. It will remain for shorebased studies to evaluate and define these suspected source heterogeneities through the examination of additional trace elements and isotopic compositions.

INTRODUCTION

Many of our ideas of where mantle plumes originate, how they interact with the convecting mantle, and how plates have moved in the past rest on interpretations of the Hawaiian-Emperor hotspot track. One reason this volcanic lineament has attained this conceptual stature lies in its prominent bend at 43 Ma. The bend, which separates the westward-trending Hawaiian islands from

the northward-trending Emperor Seamounts (Fig. F1) has no equal among the Earth's hotspot tracks; it is the clearest physical manifestation of a change in plate motion in a fixed hotspot reference frame. Because the bend is so distinct, it can be used to estimate plume diameters and to place bounds on the convecting mantle wind that may deflect plumes (Duncan and Richards, 1991). However, shortly after hotspots were used as a frame of reference (Morgan, 1971), apparent discrepancies involving the Hawaiian-Emperor track arose (Molnar and Atwater, 1973). Attempts to model past plate motions failed to predict the bend; instead, a more westerly track was derived (Solomon et al., 1977). Tests of the fixed hotspot hypothesis based on global plate circuits suggested large relative motions between Hawaii and hotspots in the Atlantic and Indian Ocean basins (Molnar and Atwater, 1973; Molnar and Stock, 1987), but uncertainties in the relative plate motions employed in these tests limited their resolving power (Acton and Gordon, 1994).

Several works have readdressed these questions. Norton (1995) suggested that the Hawaiian-Emperor bend records the time when the moving hotspot became fixed in the mantle. Prior to 43 Ma, Norton argues that the hotspot moved southward, creating the Emperor Seamount chain. This work is difficult to assess because of the lack of formal error analyses, but the interpretation reiterates findings of updated plate circuit studies that consider rotation pole errors (Cande et al., 1995). In addition, no obvious change occurs in the spreading rate at 43 Ma for the well-studied marine magnetic anomaly record of the North Pacific (Atwater, 1989). Many feel the lack of such a response by overlying plates to a change of absolute plate motion as large as that indicated by the Hawaiian-Emperor bend is reason enough to question hotspot fixity. New modeling efforts, utilizing a viscosity structure based on geoid constraints, mantle flow fields consistent with tomographic data, and plate motion estimates, also predict motion of hotspot groups (Steinberger and O'Connell, 1997). For the Emperor trend, the predicted motion is 10–15 mm/yr (Steinberger, 1996) (Fig. F2).

Whereas these recent studies have revitalized discussions regarding hotspot fixity (see also Christensen, 1998; Wessel and Kroenke, 1998), they face some fundamental data limitations. However, the hypothesis of hotspot motion can be tested independently using paleomagnetism (e.g., Duncan et al., 1972; McElhinny, 1973; Hargraves and Duncan, 1973). The most direct approach is to sample volcanoes that construct a given hotspot track. In the example of the Hawaiian hotspot, the paleolatitudes of extinct volcanic edifices of the Emperor chain should match the present-day latitude of Hawaii if the hotspot has remained fixed with respect to the Earth's spin axis. But this type of test is difficult, in practice, to apply. Paleolatitude values derived from the paleomagnetic analysis of deep-sea sediment overlying seamounts must be interpreted carefully because compaction can induce a flattening of inclinations (Celaya and Clement, 1988; Arason and Levi, 1990; Tarduno, 1990). Such problems can be avoided through the study of drill cores from well-dated lava flows. But until recently, only a few sites had sufficient depth penetration to conduct direct paleomagnetic tests of hotspot fixity. This situation improved after Pacific drilling during Ocean Drilling Program (ODP) Legs 143–145. Data from Legs 143 and 144 indicate significant motions between hotspot groups in the Atlantic and Pacific Oceans during the mid-Cretaceous (128–95 Ma) (Tarduno and Gee, 1995). The motion is rapid, at speeds within the range of lithospheric plate velocities (30 mm/yr).

These findings indicate an older episode of hotspot motion and, coupled with the inferences based on relative plate motions, suggest that Hawaiian hotspot motion is a viable hypothesis that should be tested further; this test became the primary objective of ODP Leg 197. Data obtained from the analysis of cores obtained during ODP Leg 145 (Tarduno and Cottrell, 1997) and Deep Sea Drilling Project (DSDP) Leg 55 (Kono, 1980) on the Emperor chain (Fig. F1), summarized below, allowed a preliminary test (Cottrell and Tarduno, in press) that guided the drilling plan of Leg 197.

The sites chosen to address the question of hotspot fixity also were designed to obtain geochemical data needed for understanding the compositional variability of volcanic products from the Hawaiian hotspot, another important goal of Leg 197.

BACKGROUND AND PREVIOUS RESULTS

During Leg 145, 87 m of lava flows was penetrated on Detroit Seamount Site 884 (Fig. F1) (Rea et al., 1995). ^{40}Ar-^{39}Ar radiometric analyses yield an age (81.2 ± 1.3 Ma) (Keller et al., 1995) older than that predicted (~75 Ma) from hotspot-based best-fit linear plate motion models (Duncan and Clague, 1985). Characteristic magnetizations derived from basalt samples have mainly negative inclinations, indicating reversed polarity. This polarity assignment is consistent with the radiometric age data, suggesting eruption of the basalt during Chron 33R (Tarduno and Cottrell, 1997).

A potential problem in obtaining reliable paleomagnetic data from any basalt drill hole is the uncertain timescale between eruptions. If most flows reflect rapid eruptions, one could easily obtain a biased paleolatitude estimate by giving equal weight to each flow unit. To address this concern, the inclination-only averages derived from each flow unit (McFadden and Reid, 1982) must be checked for serial correlation (Cox, 1970; Kono, 1980; Tarduno and Sager, 1995). These analyses lead to inclination group models (Fig. F3). The directional angular dispersion, estimated from the inclination model data and transformed into pole space (Cox, 1970; Tarduno and Sager, 1995), is indistinguishable from the predicted virtual geomagnetic pole scatter from global data sets (McFadden et al., 1991) (Fig. F3). As discussed below, only one other paleomagnetic data set exists for the Emperor trend that satisfies these geomagnetic sampling requirements.

The preferred inclination group model, where groups are distinct at >95% confidence (N = 10) (Tarduno and Cottrell, 1997), produces a paleolatitude of 36.2˚ (+6.9˚/–7.2˚), clearly discordant from the present-day latitude of Hawaii (~19˚) (Fig. F3). This discrepancy is too large to be explained by tectonic tilt. Tilts of 1˚–3˚ have been previously reported for some of the northern Emperor Seamounts (Lonsdale et al., 1993). Because these tilts are small and the angle between the remanent magnetization vector and downdip azimuth of tilt is large (>60˚), the effect on the paleolatitude is negligible. Measurements made at unit contacts also fail to indicate significant dips.

The new paleomagnetic result directly questions the validity of the Late Cretaceous Pacific apparent polar wander path (APWP) (Fig. F3). But how could these prior results be so errant? Previous Late Cretaceous poles are dominantly or solely based on the inversion of magnetic surveys over seamounts (Gordon, 1983; Sager and Pringle, 1988). Reviews of the methods used to fit these poles suggest they are far more uncertain than commonly supposed (Parker, 1991). Viscous and induced magnetizations can also bias the resulting pole positions (Gee et al., 1989; Cottrell and Tarduno, 2000b). Interestingly, high-latitude poles similar to the new colatitude result (Fig. F3) have been reported from preliminary analyses of the skewness of marine magnetic anomaly data of comparable age (Vasas et al., 1994).

The other paleolatitude value from the Emperor trend that adequately averages secular variation was derived from Suiko Seamount (65 Ma) (Kono, 1980) (Fig. F1). The 8˚ discrepancy between the Suiko Seamount paleolatitude and the present-day latitude of Hawaii has been previously attributed to early Cenozoic true polar wander (Gordon and Cape, 1981; Sager and Bleil, 1987), which is defined as a rotation of the entire solid Earth in response to mass redistribution (e.g., changes in density heterogeneities in the mantle and growth and disappearance of glacial ice) (Goldreich and Toomre, 1969). True polar wander predictions based on global paleomagnetic data from the

continents (Besse and Courtillot, 1991), however, do not agree with the new Detroit Seamount data (Tarduno and Gee, 1995; Tarduno and Cottrell, 1997). Furthermore, renewed tests of Cretaceous true polar wander models show that the solid Earth rotations proposed are not seen in paleomagnetic data from regions where large changes in latitude should be observed (Cottrell and Tarduno, 2000b; Tarduno and Smirnov, 2001). Therefore, the proposed true polar wander rotations appear to be artifacts related to the fixed hotspot reference frame employed.

Because Late Cretaceous true polar wander predictions are inconsistent with Pacific observations, we must now consider hotspot motion as an explanation for the new paleomagnetic data. Although limited in number, paleomagnetic data from the Hawaiian chain younger than the age of the Hawaiian-Emperor bend do not suggest large southward latitudinal displacement relative to the fixed hotspot model (Gromme and Vine, 1972), nor do results from relative plate motion models (e.g., Cande et al., 1995). Thus, the possibility of large latitudinal motion of the Hawaiian hotspot is best examined by focusing our examination on the time interval during which the Emperor Seamounts were formed. We can isolate the latitudinal history of the Emperor Seamounts from that of the Hawaiian chain by subtracting the difference between the present-day latitudes of the 43-Ma bend and Hawaii from the present-day latitudes of each of the Emperor Seamounts. In effect, we slide the Emperor trend down the Hawaiian chain to the present-day latitude of Hawaii (Fig. F4). In so doing, we produce a plot predicting the paleolatitude of the Emperor Seamounts if they were formed by a hotspot moving at constant velocity beneath a stationary plate. Site 884 Detroit Seamount results together with the Suiko Seamount data (Kono, 1980) parallel this predicted trend and provide support for the hotspot motion hypothesis. Differences between the data and predicted values also allow for some northward plate motion. It is difficult to place error bounds on the rate of motion because only two estimates of paleolatitude are available. Nevertheless, the data suggest that the Hawaiian hotspot could have moved southward from 81 to 43 Ma (Norton, 1995) at a constant rate of 30–50 mm/yr while the Pacific plate moved slowly northward, in a paleomagnetic (spin axis) frame of reference (Fig. F4).

Interpretations of the Hawaiian-Emperor bend have had a tremendous impact on our understanding of the history and dynamics of plate motions. But the data sets described above suggest that these interpretations may be wrong or, at best, largely incomplete. Our primary motivation during Leg 197, as outlined in "Scientific Objectives" below, was to test the hypothesis of Hawaiian hotspot motion with further drilling in the Emperor Seamounts. This objective provided additional opportunities to learn more about the geometry and paleointensity of the Late Cretaceous to Tertiary geomagnetic field and to study the source and melting history of the Hawaiian hotspot.

SCIENTIFIC OBJECTIVES

Determining the Paleolatitude and Age of the Emperor Seamounts

The primary goal of Leg 197 was to obtain accurate and precise paleolatitude and age estimates for each of the sites drilled. These data, when compared with fixed and moving hotspot predictions, form the basis of our paleomagnetic test. To accomplish our goal, we targeted moderate penetration of lava flow sections with the aim of obtaining an average of secular variation (>15 independent paleomagnetic inclination units) at each site.

Our objectives differed slightly from site to site. At Detroit Seamount, we hoped to improve the precision of prior paleolatitude estimates and, possibly, obtain new time-average paleolatitude data

with ages different from those of Detroit Seamount ODP Site 884. At Nintoku Seamount and Koko Guyot we hoped to investigate the mechanisms for discrepancies between paleomagnetic data and predictions based on fixed hotspot models. Combined with data from Suiko Seamount (Kono, 1980), time-averaged paleomagnetic data of known age from these seamounts should allow us to test existing models and potentially develop new models for the generation of the Emperor Seamount trend and the Hawaiian-Emperor bend.

New paleomagnetic data from Detroit, Nintoku, and Koko Seamounts could also allow for the construction of an improved Pacific apparent polar wander path. In addition to its utility in the study of Pacific plate kinematics, a refined APWP could provide the basis for improved paleogeographic reconstructions important for paleoclimate studies. Such reconstructions are needed when proxy climate data are used to define past latitudinal gradients (e.g., Huber et al., 1995; Zachos et al., 1994). APWP data may serve as a more stable reference frame for Pacific plate reconstructions than one based on fixed hotspots (Cottrell and Tarduno, 1997b.)

Through our drilling approach (obtaining time-averaged paleomagnetic data at each site), we also hoped to address other aspects of the geomagnetic field through Late Cretaceous to early Teriary time (Fig. F5). For the present field and models of the Late Cretaceous to early Tertiary field, the axial dipole term is overwhelmingly dominant. Therefore, other terms will not greatly affect the accuracy of data used to test the hotspot motion hypothesis. However, the data obtained can be used to better constrain the Gauss coefficients of the past field. Data from the Pacific basin are essential because of its sheer size; no global description of the field can be considered complete without data from the region.

Although the general importance and need for Pacific data are generally appreciated, the methods used to summarize past data prior to modeling (spherical harmonic analysis) have been given less consideration. For the early Tertiary and Late Cretaceous, plate motion can not be neglected, as it can for analyses of data over the past 5 m.y. (Constable, 1992), but instead the data must be first rotated into a common reference. The few analyses that have tried to incorporate data from the Pacific (principally older seamount results) have relied on a fixed hotspot frame of reference; hence, previous estimates of Gauss coefficients may contain considerable errors if the hotspot motion hypothesis is correct.

Interestingly, these analyses show a dramatic change in the Gauss coefficients (a change in sign) during the critical Late Cretaceous to early Tertiary interval we targeted for study (Livermore et al., 1984). Therefore, we hoped that the data collected at the Leg 197 sites could simultaneously address the hypothesis of hotspot motion and the reality of this change in sign of the spatially varying Late Cretaceous–early Tertiary geomagnetic field.

When compared to the considerable success of studies that utilize directional data derived from paleomagnetic measurements, work devoted to understanding the past intensity of the geomagnetic field has advanced more slowly. However, the long-term variations of paleointensity are essential for a complete description of the field, as well as for understanding the long-term magnetic signature of ocean crust.

One reason progress has been slow is related to selection criteria needed to ensure reliable paleointensity determination. The preferred method of paleointensity measurement, Thellier-Thellier double heating experiments of basalt (Thellier and Thellier, 1959; modified by Coe, 1967), often encounters problems due to chemical alteration during heating. Significant recent progress has been made in studying basaltic glass (Pick and Tauxe, 1993) that shows ideal magnetic properties.

The available DSDP and ODP sites where basaltic glass was sampled have now been analyzed (Juarez et al., 1998), so further progress requires additional drilling.

The Leg 197 drilling plan included the potential recovery of reference sites for Late Cretaceous–early Tertiary paleointensity. We planned whole-rock, basaltic glass, and single plagioclase crystal (Cottrell and Tarduno, 1997a, 2000a; Tarduno et al., 2001) approaches to analyze the recovered cores and to derive Late Cretaceous to early Tertiary interval paleointensity data through shore-based study.

Source and Melting History of the Hawaiian Hotspot

Hotspots are of continuing interest to mantle geochemists because they provide "windows" into parts of the mantle that lie beneath the upper mantle source region for mid-ocean ridges. An observed range of distinct mantle compositions offers the means to investigate such important issues as the geochemical evolution of the mantle, temporal and spatial scales of mantle convection, and lithosphere-mantle interactions. No hotspot has been more intensely examined from a geochemical perspective than Hawaii, through compositional studies of lava sequences from the islands at the southeast end (e.g., Chen and Frey, 1985; Garcia et al., 1998) to dredged and drilled rocks from about 30 sites along this prominent and long-lived lineament (e.g., Lanphere et al., 1980; Clague and Dalrymple, 1987; Lonsdale et al., 1993; Keller et al., 2000).

As an example, the Sr isotope ratios of tholeiitic basalt from the Hawaiian hotspot track show a systematic trend through time (Fig. F6). These ratios are approximately constant along the Hawaiian Ridge (out to the 43-Ma bend) then decrease steadily northward along the Emperor Seamounts to Suiko Seamount. This decrease has been attributed to a decrease in distance between the hotspot and the nearest spreading ridge (Lanphere et al., 1980). Only the tholeiitic basalt from the shield phase of volcano construction show this trend because only these magmas appear to have escaped contamination by the oceanic lithosphere (Chen and Frey, 1985). Keller et al. (2000) have extended this analysis to Detroit and Meiji Seamounts, and they find that Sr isotope ratios continue to decrease northward, with a minimum value at Detroit Seamount well within the range of compositions for Pacific mid-ocean-ridge basalt (MORB). This composition (confirmed with other isotopic and elemental ratios) is unprecedented in the Hawaiian hotspot-produced volcanism to the south, but is consistent with the interpretation from plate reconstructions that the hotspot was located close to a spreading ridge at ~80 Ma. The seamount magmas, then, appear to be derived from a mixture of plume ("enriched") and predominantly aesthenosphere ("depleted") mantle sources. The plume end-member is more like the "Kilauea" than the "Koolau" component of the modern hotspot.

Plate reconstructions (e.g., Mammerickx and Sharman, 1988; Atwater, 1989) place a spreading ridge close to the Hawaiian hotspot at ~80 Ma. In other locations where a plume is close to a ridge (Galapagos Islands, Easter Island, and Iceland) the isotopic compositions of hotspot products extend toward MORB values. Several processes may lead to this effect. The nearby spreading ridge could have provided a higher temperature and lower viscosity and density regime, leading to significant entrainment of aesthenosphere within the rising plume. Thinner lithosphere near the ridge would promote a longer melting column in the plume, leading to greater degrees of partial melting and homogenization of geochemical heterogeneities (M. Regelous et al., unpubl. data). Also, younger, hotter lithosphere may be more readily assimilated by the ascending plume melts. Thus, the thickness of the lithosphere could determine how much aesthenosphere contributes to hotspot

volcanism or how possible isotopic heterogeneities within the plume itself are expressed through partial melting. The (deep mantle?) region where the Hawaiian plume acquires its geochemical characteristics has probably not been homogeneous and static. But the degree of geochemical variability at given sites within the Emperor Seamounts has not been established on the basis of the few analyses reported so far.

The Leg 197 study plan called for the generation of geochemical data from lava flows recovered from the Emperor Seamount sites to document the compositional and thermal characteristics of mantle sources and melting conditions of the early history of the Hawaiian hotspot. We planned to measure major and trace element abundances to place limits on the depth and extent of melting and track magma evolution (fractionation and contamination) to the surface. We also planned to use such data to categorize rocks as tholeiitic shield, alkalic postshield, or posterosional lavas for comparison with models of Hawaiian Islands construction. Shore-based isotopic work (Sr, Nd, Pb, and Hf isotope ratios and parent-daughter measurements of whole rocks and He for glasses and fresh olivine) and trace element analyses were planned to help identify mantle source components. Studies of volatiles in recovered glasses and melt inclusions in phenocryst phases were also planned, as well as microanalyses of opaque minerals (Fe-Ti oxides) that will reveal alteration and cooling conditions and aid in the rock magnetic and paleomagnetic investigations of the leg.

Knowledge of the physical volcanology of the lava flows at Emperor Seamount sites is important for understanding the mechanisms and timescales of eruptions. Studies of the physical characteristics of historic lava flows at Hawaii have led to the means of linking outcrop-scale observations to important eruption parameters, such as flow volume, velocity, viscosity, relative eruption rate, and distance from source. We planned to measure flow thickness, direction, structure, vesicularity, and crystallinity in the recovered cores. We planned to integrate this information with evidence for an eruptive environment (submarine vs. subaerial and volcano flank vs. summit) and secular variation measurements from the paleomagnetic studies to estimate timescales for the recovered sections.

DRILLING STRATEGY AND OPERATIONS

Secular Variation in Previous Deep-Sea Drilling Studies

A key question concerning paleomagnetic tests such as those conducted during Leg 197 is the penetration needed to adequately average secular variation. Analysis of cores from Site 884 on the eastern flank of Detroit Seamount indicates that at some sites as little as 85 m of basement penetration is sufficient to obtain an average of secular variation. Where basement penetration was >120 m at Cretaceous plateaus, seamounts, and guyots in the Pacific, enough independent time units were recovered to average secular variation (Tarduno and Sager, 1995; Tarduno and Gee, 1995). This depth does not differ greatly from the that over which secular variation is averaged (100–200 m) in analyses (Holt et al., 1996) of cores from lava flows obtained by drilling on Hawaii.

However, it is not possible to determine the time sequence represented by the volcanic section at a given site prior to drilling. It is necessary to evaluate the angular dispersion of independent lava flows (inclination units) and compare this with global paleomagnetic data to confirm whether secular variation has been adequately sampled at a given site. We planned to collect on-site paleomagnetic data and to make angular dispersion calculations to evaluate whether the resulting record provides an adequate average.

Paleolatitude Experiment

We planned basement penetration to moderate depth (150–250 m) at the Emperor Seamount sites (Fig. F1). Our preferred strategy was to employ minicones for reentry. The nominal depths for basement penetration were based on drilling of other Pacific seamounts and plateaus (Tarduno and Gee, 1995). Whereas these estimates were needed for the planning process, we envisioned an interactive process based on recovery. Ideally, we hoped to recover at least 15 flow units (distinct lava flows rather than lobes of compound flows) from each hole for detailed paleomagnetic and radiometric age (^{40}Ar-^{39}Ar incremental heating) analysis. Below, we include a brief description and rationale for each of the drilling sites. This approach, with age information provided by micropaleontology and relative time information provided by physical volcanology, guided our decisions at sea.

Originally, the northernmost site to be drilled during Leg 197 was on Meiji Guyot. Unfortunately, clearance for drilling was denied by the Russian government in May 2001. Consequently, drilling on Detroit Seamount (~81 Ma) became the highest priority for Leg 197. We planned single holes at two sites; two summit sites (proposed Sites HE-3A and HE-3B) were given high priority and were included in a seismic survey by the *JOIDES Resolution* en route. Proposed Site HE-3A became our first site drilled (Site 1203).

The relatively thick sequences of volcaniclastic rocks recovered at Site 1203 indicated proximity of a Campanian volcanic source; we felt that nearby proposed Site HE-3B might largely repeat the section already cored. Therefore, we elected to return to Site 883 (proposed Site HE-3) to drill deeper and obtain more flow units than previously acquired (during Leg 145) to increase the precision of the oldest paleomagnetic data to be used in our paleolatitude test. The final selected location near Site 883 became Site 1204, where two holes were drilled.

In addition to confirming the already recognized discrepancy between the paleolatitudes of Suiko and Detroit Seamounts and the present latitude of Hawaii, we saw an opportunity to investigate how this difference accumulated with time. We planned sites on Nintoku, Ojin, and Koko Seamounts (Fig. F1) to obtain this record. Because of time devoted to deepening Site 1203 below volcaniclastic intervals (to obtain additional time-independent lava flows) and operational delays related to a clogged drill bit at Site 1204 (forcing the drilling of a second hole), drilling at Ojin Seamount was canceled. We allotted the time saved in roughly equal proportions to deeper drilling at Nintoku Seamount and Koko Guyot (which became Sites 1205 and 1206, respectively).

If the Emperor trend represents southward motion of the Hawaiian hotspot, we expected to obtain a paleolatitude of 25°–27° for Nintoku Seamount. Our planned Site HE-4A was positioned at DSDP Hole 432A, near the northwest edge of the seamount on flat-lying, stratified sediment that could be used to stabilize the bottom hole assembly (BHA). Previous drilling indicated that the sediment was 42 m thick, above basement, and that the uppermost lava flows were separated by a soil horizon. Soils indicate significant time intervals between lava flows and ideal conditions for deeper drilling.

Our planned site on Koko Guyot (proposed Site HE-6A) was positioned at DSDP Site 308. Previous drilling penetrated ~70 m of clay and volcaniclastic sandstone. Biostratigraphic data indicated an Eocene age for the base of the section, suggesting the hole was terminated (due to sea conditions) near basement.

SITE 1203

Principal Results

Site 1203, at 50˚57.00′N, 167˚44.40′E, is located toward the central region of the summit area of Detroit Seamount (Fig. F7). This position was initially selected along an available, high-exaggeration (12–15:1) single-channel (analog) seismic reflection profile collected in 1988. An underway geophysical survey was conducted to gather digital seismic reflection data to more adequately characterize the stratigraphic and structural setting of the site; high-resolution profiles were collected using a single 80-in^3 water gun firing at a rate of 6 s. Basement was clearly imaged, and Site 1203 was positioned along the crossing points of three survey lines.

Hole 1203A was spudded at a water depth of 2593 m. In the vicinity of the selected site, an acoustically prominent basement reflection is overlain by a 400- to 500-m-thick carapace of sedimentary deposits. The greater part of this sequence consists of late Oligocene and younger beds of the Meiji drift (Rea et al., 1995). Coring began at a depth of 300 meters below seafloor (mbsf) in diatom and nannofossil ooze beds of late, middle, and early Miocene age. At ~390 mbsf, diatomaceous material gave way to chalk with abundant but poorly preserved nannofossils of late Oligocene age. Lower Eocene (upper part of Zone NP12; ~51 Ma) (Berggren et al., 1995) chalky and sandy-silty sediment immediately overlies basaltic lava flows of the basement rock sequence. Beds of volcaniclastic sediment and chalk within the upper part of the cored basement complex contain Campanian nannofossils assigned to Zones CC22–CC23, the estimated age of which is 71.3–76.0 Ma. Toward the base of the basement section (~400 m into basement or ~865 mbsf), nannofossils characteristic of Zone CC22 were identified, indicating an age of 75–76 Ma (Berggren et al., 1995).

We reached basement at 462 mbsf. The underlying ~453 m of cored basement consists of 18 lava units and 14 volcaniclastic interbeds (Fig. F8). The average recovery in basement was 56.5%. The upper part of the basement sequence defines deposition or emplacement in a distal environment relative to eruptive centers and at relatively shallow water depths. It is characterized by nonvesicular pillow lavas and thick, sparsely vesicular pahoehoe lava flow units interbedded with volcaniclastic sedimentary sequences of primary and resedimented basaltic tuff (ash fall deposits) and vitric siltstone and sandstone.

The lower part of the basement succession is dominated by highly vesicular compound pahoehoe lavas (up to 65 m thick) and includes subordinate lapillistone (i.e., scoria fall deposits), pillow lava, hyaloclastite tuff, and breccia, along with thin vitric siltstone to sandstone sequences. The highly vesicular pahoehoe flows and the lapilli scoria deposits are characteristic of eruption and emplacement in a subaerial setting close to a source vent. The presence of pillow lavas, hyaloclastite tuff, and marine vitric sandstone and siltstone within the sequence indicates emplacement (or deposition) in water (Fig. F9). These contrasting indicators imply that the depositional environment extended from shallow marine to land, an interpretation consistent with an early subaqueous emplacement and then subsequent emergence of the lava section as it thickened.

Similarities are noted between the Site 1203 basalt units and those recovered during Leg 145 at Sites 883 and 884, positioned, respectively, on the summit and at the base of the eastern flank of Detroit Seamount (Rea et al., 1995). For example, a plagioclase-phyric basalt containing centimeter-size glomerocrystic plagioclase phenocrysts (Fig. F10) is similar to seven of the ten igneous units described from Site 884. Differences include the presence of olivine-rich zones (that also contain Cr spinel) in Hole 1203A (Fig. F11).

Geochemically, tholeiitic to transitional basalt is present at the top of the sequence and alkali basalt occurs intercalated lower down (Fig. F12). Some alkali basalt lavas are geochemically distinct in that they have a substantially lower Ti/Zr ratio (Fig. F13). Whereas Na and K are subject to mobility during alteration, at Site 1203 the designation of basalt units as alkalic is supported by elevated abundances of Ti, Zr, and Y relative to the tholeiitic basalt. The Site 1203 alkalic basalt, which erupted as subaerial pahoehoe lavas, may be analogous to the dominantly alkalic postshield-stage lavas that erupt as Hawaiian volcanoes migrate away from the hotspot. However, the shift upsection to tholeiitic pillow lavas is not easily understood with reference to the evolution of single Hawaiian volcanoes. This sequence could have developed from interfingering of lava flows from two distinct volcanic centers that were in different stages of growth. This possibility is supported by the observation that at least one flow unit within the lower alkalic section is compositionally related to lavas in the upper tholeiitic section.

The igneous rocks recovered at Site 1203 have undergone secondary alteration and weathering. Evidence for pervasive low-temperature alteration is exhibited by vesicle- and vein-filling secondary minerals. The degree of alteration increases downsection (Fig. F14). Mineral paragenesis in the upper part of the hole is dominated by calcite, Fe oxyhydroxide, and brown and green (saponite) clay. Associated secondary minerals are sulfide (pyrite), blue-green clay (celadonite), and zeolite. Most vesicles are filled with calcite or saponite. Near the bottom of the hole (~415 m into basement) vesicles are mostly filled with zeolite and Fe oxyhydroxide.

Bulk density measurements for that part of the sedimentary section cored (300–462 mbsf) show an increase with depth from ~1.5 to 2.3 g/cm^3. This gradient correlates with an overall decrease in porosity downhole, from ~65% to ~40%, which probably largely reflects increasing compaction, although the proportion of calcareous material with respect to diatomaceous debris also increases below ~390 mbsf.

In the basement section, variations in index properties, gamma ray counts, and thermal conductivity correspond to the alternation of volcaniclastic sediment and basaltic lava flows. In the volcaniclastic sediment, bulk density and thermal conductivity are generally low, whereas porosity is high (>40%). Conversely, in the basalt units, bulk density and thermal conductivity are high and porosity correspondingly low (<20%). For the basalt, natural gamma ray measurements uncorrected for background radiation generally range between ~15 and 30 counts per second. To orient core segments to their in situ position, digital photos of 200 m of whole-round cores were taken to compare with Formation MicroScanner (FMS) logging images.

Logging operations in Hole 1203A were extensive, including the collection of downhole natural gamma ray, density, porosity, electrical resistivity, and temperature data with the triple combination (triple combo) tool and FMS and velocity measurements in a second tool string. Downhole magnetometer data were also collected with the Goettingen borehole magnetometer (GBM) in a third run (Figs. F15, F16). Excellent data quality and repeatability were observed along the entire section during the three runs. Basaltic sections are characterized by high electrical resistivity (up to 10 Ωm), low porosity (<0.5%), high density (up to 2.5 g/cm^3), and low natural gamma ray (<20 gAPI). In contrast, sediment and volcaniclastic units exhibit low resistivity, high porosity, and high natural gamma ray counts. FMS electrical images are of high quality and can be used to distinguish pillow basalt and more massive units (Fig. F17). The borehole magnetometer, which employed three fluxgate sensors and an innovative fiber-optic sensor to record tool rotation, yielded data that can be used to identify sequences of basalt and volcaniclastic sediment (Fig. F18). The strength of the

recorded vertical to the horizontal component of the anomalous field suggests that within the basalt section the combined remanent and induced magnetic field has an inclination >45°.

A total of 258 discrete samples were taken from cores of volcanic basement rock. These samples were measured for natural remanent magnetization and then were alternating-field demagnetized to 80 mT in 5- and 10-mT steps. Inclination, declination, and intensity were measured and orthogonal vector plots employed to determine the stability of remanence and the number of magnetic components present (Figs. F19, F20). Principal component analysis was used to determine the characteristic remanent magnetization direction. All samples exhibit normal polarity.

The average inclination of volcaniclastic units is 54.7° (+3.1°/–6.4°; 95% confidence level), which is a minimum value because compaction processes in sediment can rotate the remanent magnetic vector toward a reading shallower than originally set (Fig. F21). The minimum paleolatitude is thus 35.2° (+3.2°/–5.9°). Paleomagnetic inclination data for the lava flows were grouped according to flow unit and averaged. The means of the individual flow units were averaged to determine an overall mean inclination for the thickness of the basement section penetrated. Based on 16 units, the average inclination is 48.0° (+6.8°/–10.1°), a value that corresponds to a paleolatitude of 29.0° (+6.3°/–7.7°) (Fig. F22). This reading will change with improved age control (several flows may together represent a short period of time) and shore-based thermal demagnetization studies to address evidence that a high-coercivity component of magnetization present in some units was not adequately demagnetized with the alternating-field treatments applied.

The significant result of shipboard measurement is that the range of preliminary mean paleolatitude determinations extracted from volcaniclastic sediment and lava flow units (29°–35°) and the distributions of the data are distinct from the value predicted by the fixed hotspot model (i.e., ~19°N).

SITE 1204

Principal Results

The two holes drilled at Site 1204 (Hole 1204A: 51°11.68′N, 167°46.36′E, and Hole 1204B: 51°11.64′N, 167°46.42′E, respectively) are located toward the northern end of the summit platform of Detroit Seamount in international waters ~18 km southeast of the Russian Exclusive Economic Zone. Prior to spudding in Hole 1204A, an underway geophysical survey was run to more fully characterize the stratigraphic and structural setting of the site. Crossing high-resolution seismic reflection profiles were collected using a single 80-in³ water gun firing at a rate of 6 s. Basement was cleanly imaged at the site as an upward-terminated sequence of discontinuous reflection events beneath a prominently layered set of reflectors representing sedimentary beds ~850 m thick. The bulk of these sedimentary beds are part of the areally extensive Meiji drift sequence of Oligocene and younger age (Rea et al., 1995).

The location for Site 1204 was selected on the basis of two seismic lines digitally recorded during the underway survey and information from previously drilled Leg 145, Site 883, at virtually the same location (Fig. F23). Because lengths of drilling pipe were left behind at Site 883, Hole 1204A was moved ~460 m southeast along one of the new seismic lines where a flat basement reflector could be distinguished. After a clogged bit forced us to abandon the first hole, Hole 1204B was spudded ~100 m southeast of Hole 1204A.

Coring in Hole 1204A began beneath the Meiji drift sequence at a depth of ~762 mbsf, where a relatively condensed sequence of chalk with volcanic ash containing middle Eocene to upper Paleocene nannofossils was recovered. Parts of this section could be correlated to the geomagnetic polarity timescale through shipboard paleomagnetic measurements. The lower Eocene carbonate units contain an interesting zone of sedimentary beds deformed and disrupted by sliding. Similar units are also preserved at Site 883 and at Site 884, which is at the base of the eastern flank of Detroit Seamount (Fig. F24). Ash in the sequence produces elevated magnetic susceptibility values that helped distinguish sedimentary subunits. The chalk beds overlie low-carbonate clay, diamictite, and ash-rich strata containing ~71- to 76-Ma Campanian nannofossils (CC22/CC23). Coring began in Hole 1204B at a depth of 810 mbsf in sediment immediately overlying basement containing the same nannofossil assemblage as that found in Hole 1204A. This age suggests that the Site 1204 basement may be roughly coeval with that at Sites 1203 and 883.

The Site 1204 basement consists of basalt that occurs as pahoehoe lava flows constructed of multiple lobes (Fig. F25). The association of pahoehoe lava, carbonate sand, and low-density lapilli and vesicular basalt breccia (Fig. F26) suggests that these flows originated from subaerial vents and that the lava was emplaced in a nearshore environment. The sequence was altered at low temperature within the seafloor weathering and alkali mobility zone. Prominent reduced zones with saponite clay and secondary pyrite are intermixed with more common oxidized zones characterized by Fe oxyhydroxide. Particularly noteworthy are unaltered glassy margins of flow lobes (Figs. F27, F28). The lava flows recovered at Site 1204 have alkali basalt compositions, but with significantly lower abundances of incompatible elements than postshield-stage alkalic basalt lava flows erupted at Hawaiian volcanoes such as Mauna Kea. The abundance and ratios of certain trace elements (e.g., Ti and Zr) in the Site 1204 lavas fall along the trend for Suiko Seamount and most other Detroit Seamount compositions (Fig. F29).

Detailed shipboard paleomagnetic analyses of basalt at Site 1204 (Figs. F30, F31) yielded an average inclination of 58.9° (+5.8°/–6.4°; 95% confidence level) and a preliminary paleolatitude estimate of 39.7° (+4.4°/–3.7°). The estimated angular dispersion of the data, however, indicates that the full range of geomagnetic secular variation important for obtaining a high-resolution paleolatitude value has not been sampled. Nevertheless, the Site 1204 values are in agreement with our preliminary data collected at Site 1203 and data from Site 884 (a data set known to average secular variation) (Tarduno and Cottrell, 1997). Together, these data suggest that Detroit Seamount formed some 1500 km north of the present latitude of Hawaii.

SITE 1205

Principal Results

Site 1205, the third site to be occupied during Leg 197, was targeted at DSDP Site 432 (Leg 55) at the northwestern edge of Nintoku Seamount, a guyot or flat-topped volcanic complex in the central sector of the Emperor chain. Nintoku Seamount, at ~41°N, is positioned approximately two-thirds the distance southward along the line of north-northeast–south-southeast–trending Emperor volcanoes extending from Meiji Seamount (~53°N) in the north to Kammu Seamount (~32°N) at the chain's southern terminus near the Hawaiian-Emperor bend. Like many of the Emperor Seamounts, Nintoku was named by Robert Dietz in 1954 after the 16th emperor of Japan.

To provide acoustic images of the stratigraphic and structural setting of the proposed site, a short underway geophysical survey was conducted. Hole 1205A was spudded ~100 m southwest of Site 432 over what appeared to be a broad sediment-filled (~70 m) swale in the surface of the main volcanic shield of Nintoku Seamount (Fig. F32). Coring sampled the entire sedimentary section before encountering basement at 42 mbsf, a depth similar to that reported at Site 432. Further penetration showed that the "sediment fill" was largely a stack of lava flows (~95%) with interbedded soil horizons. Coring continued to a final depth of 326 mbsf.

Five sediment cores (only 2%–16% recovery) established that Nintoku Seamount's sediment carapace consists of sandstone and siltstone containing well-rounded to subrounded basalt clasts (Fig. F33), volcanic ash, and fossil fragments of molluscs, benthic foraminifers, bryozoans, and coralline red algae. These observations document a relatively shallow-water, high-energy depositional environment.

Drilling in Hole 1205A penetrated 283 m into the volcanic basement of Nintoku Seamount and recovered parts of at least 25 different lava flow units (Fig. F34). Little systematic variation with depth was recorded in average *P*-wave velocity, bulk density, grain density, and porosity, except for interbedded low-density, high-porosity soil horizons. It is presumed that these low-velocity interbeds are the underlying cause for the acoustically recorded layering in the upper 200–230 m of basement rock, below which the occurrence of soil horizons diminishes.

The age of the youngest volcanic rocks in Hole 1205A is constrained by nannofossils (Zone NP10) in the sediment immediately overlying basement to be older than 53.6–54.7 Ma, an age range that is just younger than a radiometric age of 56.2 ± 0.6 Ma (Dalrymple et al., 1980) obtained for alkali basalt from nearby Hole 432A. The thickness and vesicularity of the flows from Site 1205, the presence of oxidized flow tops and soil horizons, together with the lack of pillow structure indicate that the flows erupted subaerially. They range from aphyric to highly plagioclase and olivine-phyric basalt. At 230–255 mbsf, two flows of tholeiitic basalt are intercalated within alkalic basalt flows. Above these flows the degree of alkalinity tends to increase upsection. Intraflow soil horizons are also most common in this interval, suggesting that eruption rates may have been lower during this period. Internal flow gradients within very thick lava flows have produced aligned groundmass crystals (Fig. F35) that help delineate flow structure. Clasts of hawaiite recovered in the basal conglomerate of the sedimentary section were not found as flow units within the underlying basement sequence.

Lavas from Nintoku Seamount have similar major element compositions to lavas erupted during the postshield stage of Hawaiian volcanoes such as Mauna Kea (Fig. F36). Slight differences in trace element composition between lavas from Nintoku Seamount and active Hawaiian volcanoes probably result from differences in source composition or variations in the degree of mantle melting (Fig. F37).

All the lava flows recovered at Site 1205 are only slightly altered except thin, highly weathered flow tops. The low-temperature (30˚–60˚C) alteration assemblage is homogeneous downhole and is composed of Fe oxyhydroxide, saponite and/or nontronite, celadonite, and zeolite. Veining is sparse, indicating small-scale fluid circulation. In contrast to the first two sites (1203 and 1204) drilled during Leg 197 at Detroit Seamount, K_2O was not mobilized during alteration event(s) at Nintoku Seamount Site 1205.

Rock magnetic data (low-field magnetic susceptibilities, Koenigsberger ratios, and median destructive field values) obtained from oriented minicores suggest that the lava flows from Site 1205 carry a remanent magnetization suitable for paleolatitude analysis (Figs. F38, F39). Although the

demagnetization characteristics of some samples indicate the need for thermal demagnetization studies, most samples yielded data suitable to make a preliminary determination of magnetic inclinations (Fig. F40).

Twenty-two independent paleomagnetic inclination groups were identified, yielding a mean inclination of –45.7° (+10.5°/–6.3°; 95% confidence interval) (Fig. F41). The preliminary mean inclination suggests a latitude of formation of an early Eocene Nintoku Seamount at 27.1° (+5.5°/–7.7°). This value, together with paleolatitudes from paleomagnetic analyses of basement rocks at DSDP Site 433 (Kono, 1980), Site 884 (Tarduno and Cottrell, 1997), and Sites 1203 and 1204 (Leg 197), form a consistent data set indicating southward motion of the Hawaiian hotspot from Late Cretaceous to early Tertiary time.

SITE 1206

Principal Results

The last and most southern drilling site occupied during Leg 197, Site 1206, was located on the southeastern side of the lower summit terrace of Koko Seamount. Koko Seamount is a flat-topped seamount or guyot with a crowning ornamentation of small reefal bodies. It rises from the abyssal floor (~5000 m) of the western subtropical Pacific at 35.3°N, thus just north of the "bend" (~32°N) in the ~5000-km-long Hawaiian-Emperor Seamount chain. The seamount was named by Thomas Davies and colleagues in 1972 for the 58th emperor of Japan (Davies et al., 1972).

A short seismic survey was conducted to locate a suitable structural and stratigraphic setting for Site 1206, which was initially targeted for the vicinity of DSDP Site 308 drilled in 1973 during Leg 32 (Larson, Moberly, et al., 1975). Weather conditions prevented Leg 32 from reaching basement during drilling at this site, which penetrated to a depth of 68.5 m in Koko Seamount's sediment cover. In consideration of the short time remaining in Leg 197 to conduct basement coring at Koko Seamount, a location was sought where a thin sedimentary section covered its main shield-building volcanic mass. Site 1206, at a water depth of ~1545 m, was located ~6.2 km south of Site 308 in an area where the surficial section of acoustically layered material, presumably all or mostly sedimentary beds, was less than one-half that recorded at Site 308 (Fig. F42). At Site 1206 (34°55.55′N; 172°8.75′E), basement was reached at a subsurface depth of 57 m. Coring continued to a depth of 335 mbsf, or 278 m into basement.

The top 57 m of sediment was washed with the core barrel in place. Recovered debris in the wash core included fragments of fossiliferous calcarenite and calcareous mudstone and siltstone indicative of shallow-water depositional settings. The lower part of the wash core recovered a 15- to 20-cm-long section of laminated, shell debris–bearing mudstone containing a nannofossil assemblage typical of Zones NP14 and NP15, of the early to middle Eocene (43.5–49.7 Ma). This age is similar to a radiometric analysis reported for a dredged rock (48.1 Ma) (Clague and Dalrymple, 1973) from Koko Seamount. Although volcaniclastic beds commonly rich in shell fragments were recovered from Hole 1206A in the underlying sequence of volcanic basement rock, none of these deposits contained identifiable nannofossils.

Lava flows in Hole 1206A dominated in number over volcaniclastic beds and thin lenses of calcarenite (Fig. F43). Many lavas are pahoehoe flows interbedded with subordinate a'a units that show evidence of subaerial extrusion. A large degree of scatter with depth was recorded in bulk density, grain density, and porosity of these basement rocks. Although *P*-wave velocity varies widely

(2215–4820 m/s) with depth, velocity correlates strongly with bulk density, and thus inversely with the degree of vesicularity. The bulk of the basalt flows are aphyric to olivine-phyric lava (Fig. F44) and tholeiitic or transitional to alkalic in composition. With respect to major and trace element geochemistry, the basaltic lavas from Koko Seamount resemble those drilled during DSDP Leg 55 at Suiko Seamount (Figs. F45, F46).

All the basalt flows recovered at Site 1206 are slightly altered and show a homogeneous assemblage of Fe oxyhydroxide, clay (brown clay, saponite, aliettite, and celadonite), carbonate, and zeolite. Unaltered olivine was characteristic of many of tholeiitic lava flows. The occurrence of aliettite (alternating talc and saponite-layered smectite), which expands in contact with water, caused the mechanical disintegration of some massive basalt intervals. Possibly, this phenomenon led to the onset of unstable hole conditions that, with respect to probable tool loss, made logging too risky to conduct.

Low-field magnetic susceptibilities, Koenigsberger ratios, and high median destructive field values (Figs. F47, F48, F49) suggested that the lava flow units from Hole 1206A carry a stable remanent magnetization and are suitable for the determination of preliminary paleomagnetic inclinations. Three early Tertiary polarity chrons were recognized within the lava flow units. Geomagnetic polarity reversals were not found at other Leg 197 sites. At Koko Seamount, 14 independent paleomagnetic inclination groups were identified, yielding a mean inclination of 38.5° (+8.4°/–10.9°; 95% confidence interval) (Fig. F50). The preliminary mean inclination of the lava flow units suggests a paleolatitude of 21.7° (+6.4°/–7.0°) for Koko Seamount.

The paleolatitude result gained at Koko Seamount strengthens confidence in the correctness of the implications of the paleomagnetically determined latitude of formation for Nintoku, Suiko, and Detroit Seamounts. These volcanic edifices, each located progressively north of Koko Seamount, also formed paleomagnetically progressively farther north of the present location of the Hawaii hotspot (~19°N). Thus, singularly and as a linear group, the latitudes of formation of these four Emperor Seamounts establish that to reach its present position, the Hawaii hotspot moved rapidly southward during the Late Cretaceous and early Tertiary (i.e., from ~81 to 43 Ma).

SUMMARY

Paleomagnetism and the Hotspot Test

The main goal of Leg 197 was to obtain sufficient basement penetration at several Emperor Seamount sites to test the idea that the Hawaiian hotspot migrated southward during Late Cretaceous to early Tertiary time. This hypothesis further challenges long-standing notions about the tectonic implications of the bend in the Hawaiian-Emperor Seamount chain. The bend is usually considered to represent a large change in Pacific plate motion at 43 Ma; this interpretation can be found in nearly all textbook descriptions of hotspots and plate motions.

Because of the record-setting basement penetration achieved during the leg, we were able to meet all of our goals. A key part of our study plan involved assessing whether secular variation had been averaged by lava flows recovered at a given site through a large number of shipboard paleomagnetic and rock magnetic measurements. These data have provided a firm basis both for an initial assessment of the results of the Leg 197 paleolatitude experiment and for guiding the shore-based work that must be completed to finalize the hotspot test.

Prior to the leg, only two time-averaged paleomagnetic data sets were available to address fixity of the Hawaiian hotspot during formation of the Emperor Seamounts. Paleolatitudes derived from analyses of basement cores recovered from Site 433 on Suiko Seamount (Kono, 1980) and Site 844 on Detroit Seamount (Tarduno and Cottrell, 1997) clearly differ from the latitude of Hawaii (~19°N) (Fig. F54). Although each paleolatitude represents the summary of a large data set composed of many paleomagnetic measurements, rates of motion ultimately depend on time-independent values; therefore, additional data were needed both to confirm the motion suggested and to better constrain potential hotspot drift rates. Our shipboard data allow us to draw preliminary conclusions on both of these aspects.

The paleolatitudes suggested from our preliminary paleomagnetic analysis of the basement cores recovered at Sites 1203, 1204, 1205, and 1206 also clearly differ from the latitude of Hawaii. The values are consistent with prior data from Suiko and Detroit Seamounts and the hypothesis that the Hawaiian hotspot moved southward from 81 to 43 Ma at rates of 30–50 mm/yr. These values, which are within the range of velocities typical of lithospheric plates, force us to reconsider the cause of the Hawaiian-Emperor bend, rates of mantle convection, and Pacific plate reconstructions based on the fixed hotspot assumption. The latter issue is of particular interest for ODP studies, as Leg 198 and Leg 199 scientists will require accurate paleolatitude control in their studies of Paleogene paleoceanography in the Pacific basin.

Whereas the implications of the Leg 197 shipboard paleomagnetic data are exciting and multifaceted, the results are nevertheless preliminary and must be supported by shore-based paleomagnetic and rock magnetic measurements. In particular, analyses employing detailed stepwise thermal demagnetization are needed to better resolve our estimates, which are currently based solely on alternating-field demagnetization data. Thermal demagnetization is necessary because secondary magnetic minerals with intermediate to high coercivities could carry important magnetizations that might contaminate the characteristic directions we have isolated in our shipboard analyses.

Evidence for such magnetic mineral carriers has indeed been found in cores from some sites (especially Site 1204), as recorded in observations under reflected-light microscopy and in the results of rock magnetic measurements. Additional shore-based rock magnetic analyses including magnetic hysteresis, Curie temperature, and low-temperature measurements, are needed to further characterize the magnetic carriers in the basement rocks recovered at each site.

The shore-based thermal demagnetization and rock magnetic data hold the promise of achieving much more than confirming our preliminary paleolatitude values. Because thermal demagnetization is a more efficient means of magnetic cleaning than the application of alternating magnetic fields (given the presence of high-coercivity magnetic minerals), the data may allow us to better constrain the uncertainty limits of each paleolatitude data set. Several units with limited recovery were reserved for shore-based thermal demagnetization study; inclusion of data from these units will increase the precision of the mean paleolatitudes. In addition, for Sites 1205 and 1206 thermal demagnetization analysis of recovered soils and deeply weathered lava flow tops (Fig. F51) will provide paleolatitude constraints based on a natural recording medium that averages significantly more time than a given lava flow. Finally, the application of thermal demagnetization analyses together with a host of rock magnetic measurements will allow us to isolate and identify magnetic overprints. If properly understood, such overprints can be used to reorient cores and obtain paleodeclination information (Cottrell and Tarduno, in press). Complementary studies of zeolite assemblages in the recovered cores (Fig. F52) may allow us to fingerprint the processes responsible for magnetic overprints and use them with greater confidence for tectonic studies.

The principal motivation for obtaining paleodeclination data is to address predictions of relative plate motion studies (e.g., Cande et al., 1995) that call for a rotational component of Hawaiian hotspot motion during Late Cretaceous to early Tertiary time. In addition to the use of magnetic overprints, we will use FMS, general purpose inclinometer tool (GPIT), and Deutsche Montan Technologie (DMT) color scanner data to reorient basement cores. Veins and fractures have been imaged in the recovered cores with the DMT system (Fig. F53). Similar features can be seen in the high-quality FMS images (which are automatically oriented with respect to north with the GPIT data) obtained from logging at Detroit Seamount Site 1203 (Fig. F54). We plan to use these data to orient declinations derived from core pieces having veins and fractures and to use the information to constrain a Late Cretaceous paleomagnetic pole for the Pacific plate.

Additional constraints on paleodeclination may become available through shore-based analyses of downhole data collected with the GBM. This was the first deployment of a magnetometer at an ODP site with a sensor to record tool rotation. Preliminary analyses of the data indicate the rotation history of the tool was successfully recorded (Fig. F55).

In addition to obtaining cores and data needed for the test of the hotspot hypothesis, during Leg 197 we recovered an outstanding collection of basement rocks that will be used to investigate inclination anomalies of geomagnetic origin. These anomalies, although much smaller than those associated with the debate over hotspot drift rates, are nevertheless important for our understanding of the geodynamo. In fact, because few data are available of Late Cretaceous to early Tertiary age from the Pacific region, the paleomagnetic data resulting from thermal demagnetization studies of the Leg 197 sites will carry considerable weight in efforts to study the geometry of the past geomagnetic field. Similarly, the recovery of basaltic glass and whole rocks with favorable rock magnetic characteristics bodes well for paleointensity investigations that will be part of postcruise science studies.

Source and Melting History of the Hawaiian Hotspot

One of the significant initial achievements of Leg 197 has been the remarkable depth of penetration at drilling sites on three seamounts. In fact, during Leg 197 we set a new record for total basement penetration (1220 m; 52% recovery). This augurs well for a variety of planned postcruise investigations, including the long-term petrochemical variability of source and melting, volcano-stratigraphic and environmental setting of eruptions, the timing and duration of volcanism, and the cooling and alteration conditions of lava flows produced by the Hawaiian hotspot.

Observations of lava flow thickness, vesicularity, crystallinity, and morphology, together with analysis of volcaniclastic sediment, have provided a picture of eruptions in subaerial to shallow-water conditions at Detroit and Koko Seamounts and waning subaerial activity at Nintoku Seamount (Fig. F56). Further study of core material from all sites and integration with the downhole logging data, particularly FMS images from Site 1203 (Fig. F17), promises to reveal additional details about eruption rate, volume of flows, and distance from source.

From a limited number of shipboard geochemical measurements, we believe we have captured the transition from Hawaiian tholeiitic shield stage to alkalic postshield stage at each of the volcanic complexes. Between Sites 1203 and 1204 and previously studied Sites 883 and 884, we have a range of compositions at Detroit Seamount that covers most of the variability seen in the volcanoes of the island of Hawaii (Fig. F57). Site 1205 (Nintoku Seamount) basalt is dominantly alkalic but includes tholeiitic compositions, whereas Site 1206 (Koko Seamount) basalt is dominantly tholeiitic but

include alkalic basalt compositions. We did not sample any of the posterosional stage of evolved compositions that occur at the end of Hawaiian island volcanic activity, except as cobbles in a conglomerate above basement at Site 1205.

We have hints that we have sampled different source compositions through the variability of trace element ratios, such as Ti/Zr (Fig. F58). It will remain for shore-based studies of additional trace elements and isotopic compositions (Sr, Nd, Pb, Hf, and He) to evaluate and define these suspected source heterogeneities. We are assured, however, that appropriate material has been recovered in the cores for such a comprehensive geochemical program. Unaltered olivine (Fig. F59), which will be separated for He-isotopic studies, was observed at all sites. We will probe melt inclusions in olivine and feldspar (Fig. F60) to discover parental melt compositions. Fresh glass is common and will be the source of information about melt volatile content and magma evolution. The latter subject will also be addressed through studies of zoned feldspars (Fig. F10). Opaque minerals provide a rich source of information about cooling rates of lava flows and subsequent alteration history (Fig. F61). Low-temperature alteration will be studied through the composition of secondary minerals in multiple generations of vesicle and vein fillings (Fig. F62).

Time is an important aspect of the volcanic history recorded at each site. Excellent material was recovered for both mineral (feldspar) and whole-rock age determinations to estimate the timing and duration of volcanism through ^{40}Ar-^{39}Ar incremental heating radiometric dating. In particular, the evidence for prolonged volcanic activity (soil horizons at Site 1205 and alternating shallow-water volcaniclastic sediment with subaerial lava flows at Site 1206) will be investigated, as will the apparent underestimate of current ages from Nintoku and Koko Seamounts relative to the long-term age progression within the Emperor Seamounts (Clague and Dalrymple, 1987).

OPERATIONS SYNOPSIS

Site 1203

Transit to Site 1203 and Underway Survey

In the early afternoon of 5 July 2001, the *JOIDES Resolution* departed Yokohama, Japan, and sailed northeasterly to Detroit Seamount. This volcanic edifice, in the northwest corner of the Pacific Basin at the northern tip of the north-northwest–trending Emperor Seamount chain, was the first of four Emperor Seamounts (Detroit, Nintoku, Ojin, and Koko) scheduled to be drilled during Leg 197.

The *JOIDES Resolution* arrived in the vicinity of Detroit Seamount in the early morning of 11 July and began a ~14-hr seismic reflection survey to record multicrossings of two proposed sites, HE-3A and HE-3B. These sites had been selected along single-channel analog records gathered in 1988 by the *Thomas Washington* (Lonsdale et al., 1993). Profiles of good quality were digitally recorded and presented at low exaggeration on EPC line-scan recorders. At 1645 hr on 11 July, the survey was concluded and the seismic equipment retrieved. The thrusters and hydrophones were extended and the vessel situated over the coordinates of proposed Site HE-3A (which became Site 1203) at 1715 hr. The beacon was deployed at 1807 hr.

Hole 1203A

After the vessel settled on location, the corrected precision depth recorder (PDR) depth referenced to the dual elevator stool (DES) was obtained and indicated 2604.4 m. The bottom-hole assembly

(BHA) was made up of a 9.875-in rotary core barrel (RCB), a medium-hard formation C-4 bit, a mechanical bit release, a modified head sub, an outer core barrel, a modified top sub, a modified head sub, seven 8.25-in drill collars, a tapered drill collar, six 5.5-in drill pipe sections, and one crossover sub. Hole 1203A was spudded with the RCB at 0145 hr on 11 July. The drill string was drilled ahead with a wash barrel in place to a depth of 70.6 mbsf, when an electrical fault forced coring operations to be prematurely terminated.

Loss of Power

According to the engine room data management system records, at 0259 hr on 12 July, a fault alarm occurred in the power control console for thruster 1. The console housing these control circuits and breaker (Thyrig Bay 1) is located in the forward thyrig room just below the galley in the forward part of the vessel. The electrical fault forced one of the three main generators providing ship's power to drop off-line. As a result of the rapid drop in the supplied power, the power management system compensated by load-shedding noncritical demand. The main power was stabilized when an additional generator was powered up only 4 min after the event.

At 0305 hr, smoke was detected emanating from the forward thyrig room, and at the same time all thrusters were automatically dropped off-line. The vessel began to drift off location. The drill crew was instructed to immediately stop drilling and hang the drill string off at the DES with the 500-ton elevators. The vessel had drifted off location by as much as 200 m (9% of water depth) before positioning control could be restored. To ensure that no damage was inflicted on the BHA or drill string by the excursion off location, the drill string was recovered and the pin and box connections of the BHA components subjected to a magnetic particle inspection. No cracks or bent tubulars were found.

At 1630 hr on 12 July, Hole 1203A was respudded and drilled ahead with a center bit to 300 mbsf at an average rate of penetration (ROP) of 124 m/hr. After the center bit was recovered, the core barrel was dropped and coring initiated. Sediment coring proceeded rapidly to 462.0 mbsf, where basaltic basement was contacted. A total of 162.0 m of nannofossil calcareous ooze and chalk were cored at an average ROP of 58.9 m/hr. Seventy-eight meters of sediment was recovered for an average recovery of 48.2%.

Rotary coring continued 232.7 m into basement (694.7 mbsf) when operations were suspended to change the bit. The average recovery for basement was 55.8%, representing 129.7 m of basalt and volcaniclastic sediment. The average ROP in basement was 3.8 m/hr. The ROP in basement ranged from a lethargic 1.7 m/hr (Core 197-1203A-34R [608.3–612.3 mbsf]) to a frenetic 115.2 m/hr (Core 197-1203A-24R [521.5–531.1 mbsf]). No problems were encountered with hole stability or erratic torque during the first bit run. The bit accumulated 66.9 hr of rotation before being recovered.

Reentry

The top drive was set back and the drill string pulled back in the hole to 142 mbsf. A free-fall funnel (FFF) was rigged up in the moonpool and launched at 1015 hr on 17 July. The subsea vibration-isolated television (VIT) camera was then deployed and positioned over the hole to observe the condition of the FFF during the extraction of the drill string. The BHA was pulled clear of the seafloor at 1205 hr. As the bit cleared the throat of the FFF, a 1- to 2-m-long squid was observed embracing the outer core barrel.

A new C-7 hard-formation rotary bit was affixed to a fresh mechanical bit release and made up to the BHA. The FFF was reentered at 0008 hr on 18 July. The drill string was advanced to a depth of 655 mbsf. The top drive was picked up and the drill bit positioned at the bottom of Hole 1203A at 694.7

mbsf. Approximately 3.5 m of soft fill was found at the bottom of the hole. Rotary coring resumed in Hole 1203A at 0400 hr on 18 July and advanced through alternating layers of veined and vesicular basalt flows interbedded with volcaniclastic sediment. Coring continued until, at a total depth of 914.6 mbsf, the time allocated for Site 1203 expired. The ROP while coring with the second bit varied from 1.0 m/hr (Core 197-1203A-48R [727.1–732.0 mbsf]) to 16.5 m/hr (Core 197-1203A-64R [866.6–876.2 mbsf]). Core recovery ranged from 1% to 103% (average recovery = 57.4%).

A total of 219.9 m of basement was cored with the second bit at an average ROP of 2.6 m/hr. The second bit acquired 88.3 rotating hours and was still viable when released at the bottom of the hole. The thickness of basement cored was 452.6 mbsf with 255.87 m recovered (recovery = 56.5%) at an average ROP of 3.1 m/hr. The overall results in Hole 1203A were 300 m drilled, 614.6 m cored, and 333.91 m recovered (recovery = 54.3%). The only hole trouble experienced while drilling or coring was when the drill string stuck after picking off bottom to retrieve Core 197-1203A-49R (732.0–741.6 mbsf). After the driller worked the drill string for 30 min with applications of up to 100,000 lb of overpull, the pipe was freed.

The weather on site was, although foggy, mild and under the influence of a large Pacific high. The air temperatures ranged from 6° to 9°C. Seas and swell never exceeded 5 ft and heave ranged from 1 to 5 ft with 2 ft being typical. These agreeable conditions contributed to the good recovery and extended bit life.

Because of a high oil temperature problem due to a misadjustment of the pump controls, the active heave compensator (AHC) was not online until 16 July. The AHC was used continuously while coring from 665.9 to 905.0 mbsf. It was intentionally turned off while cutting the final core (905.0–914.6 mbsf) to see if recovery would be affected. The recovery dropped from 47.5% to 39.5% on the last two cores. The AHC acquired 92 hr of operation on this site.

Logging

In preparation for logging, a 30-bbl sepiolite mud flush was circulated in the hole and a wiper trip conducted between 145 and 914.6 mbsf. Following the routine displacement of the borehole with 280 bbl of sepiolite, the bit was released at the bottom of the hole. The Schlumberger equipment was assembled, and the bottom end of the BHA was placed at 202 mbsf.

During the first logging run, the triple combo was lowered to the bottom of the hole at 915 mbsf without difficulty and logging proceeded downhole (dual laterolog and gamma ray). The second pass was conducted uphole at 274 m/hr from 915 mbsf to the base of the pipe. Excellent data quality and repeatability were recorded along the entire section scanned during these two passes.

During the second logging run, the FMS/sonic tool string also succeeded in reaching the bottom of the hole without difficulty and logging proceeded uphole at 274 m/hr. The first pass recorded FMS and sonic data only in the basement section, from 915 to 420 mbsf. The tool string was lowered to the bottom of the hole, and a second pass was conducted in the basement as well as the sedimentary section. Data quality in the basement was excellent. However, in the sedimentary section overlying basement and within some of the volcaniclastic interbeds within the basalt, the borehole was washed, out and, consequently, the FMS data are not usable.

The third logging run was made with the GBM. The first pass was interrupted by an apparent oversaturation of the x-component of the three-axis measured magnetic field. The problem was quickly repaired and the tool lowered; good quality data were recorded downhole and uphole. The fourth logging run was devoted to the magnetic susceptibility tool. This run was canceled when an

electronic power supply fault could not be repaired in a timely fashion. The logging operations were secured at 0200 hr on 25 July.

After the logging equipment was rigged down, the drill string was recovered and the BHA was dismantled in preparation for the short trip to Site 1204. The beacon was successfully recalled and retrieved. After the drilling equipment was secured, the vessel departed at 0730 hr on 25 July to run an underway survey over a northern proposed site, HE-3, which is at ODP Site 883.

Site 1204

Transit to Site 1204 and Underway Survey

The provisional location of Site 1204 was at or close to Site 883, where ~38 m of basalt had been penetrated and partly cored during Leg 145. The site survey was under way 1 hr after departing Site 1203.

After the vessel slowed to 6 kt, seismic equipment and a magnetometer were deployed and the survey started using one 80-in^3 water gun and a single-channel Teledyne hydrophone streamer. Good-quality reflection profiles were displayed on two software-controlled EPC recorders operating at different scanning speeds. The position selected was ~0.5 km from the six holes cored and drilled during Leg 145 at Site 883. At 1500 hr on 25 July 2001, the seismic equipment was retrieved as the vessel came about to return to Site 1204. Thrusters were lowered and the vessel maneuvered to the Global Positioning System (GPS) coordinates of the new location by 1534 hr. The hydrophones were then lowered concurrent with the making up of a new BHA. A beacon was deployed at 1614 hr. The 37-nmi survey was accomplished in 6.2 hr at an average speed of 6.0 kt.

Hole 1204A

After the vessel settled on location, the corrected PDR depth referenced to the DES was obtained and indicated 2604.4 m. The BHA was made up of a 9.875-in RCB, a medium-hard formation C-4 bit, a mechanical bit release, a modified head sub, an outer core barrel, a modified top sub, a modified head sub, seven 8.25-in drill collars, a tapered drill collar, six 5.5-in drill pipe sections, and one crossover sub.

Hole 1204A was spudded with the RCB at 2015 hr on 25 July. The drill string was drilled ahead with a center bit in place to a depth of 761.9 mbsf, where coring was initiated in nannofossil ooze and chalk. Coring advanced through 57.6 m of sediment at an average ROP of 28.8 m/hr with 66.3% recovery. Basement coring began with Core 197-1204A-7R (819.5–829.0 mbsf). As coring progressed, a low-pressure system developed and the weather deteriorated. By the early morning hours of 28 July, vessel heave was occasionally measured at 16 ft. Winds were 25–30 kt from the northwest, and seas were estimated between 10 and 12 ft and from the northwest. The main swell emanated from the north-northeast. The barometer was steady at 1000 Mb.

After Core 197-1204A-10R (843.3–857.9 mbsf) (ROP = 2.0 m/hr) was recovered with 79% recovery (fresh basalt), seawater was observed flowing back at the rig floor connection, indicating that the float valve was jammed open (probably with basalt fragments). Three runs were made with the deplugger before the flow was stopped. Coring resumed with Core 197-1204A-11R (857.9–862.7 mbsf), representing a 4.8-m advance. No recovery was achieved, but the appearance of the core catcher with one missing finger suggested that the core had possibly slipped out during the recovery of the core barrel. A fresh core barrel was dropped, and Core 197-1204A-12R (862.7–867.5 mbsf) (ROP = 3.8 m/hr) was cored an additional 4.8 m. The core barrel was recovered empty. A deplugger

was deployed with paint on the latch dogs to verify the engagement of the core barrel within the BHA. The deplugger was recovered and appeared to have engaged in the latch sleeve. It was surmised that a formation change signaled by the increased ROP could have involved the coring of volcaniclastic sediment, and because of the large heave, the sediment was not recovered. A fresh core barrel was dropped and Core 197-1204A-13R (867.5–877.1 mbsf) (ROP = 2.6 m/hr) advanced 9.6 m. The core barrel was recovered empty.

In a last attempt to save the hole, a fifth deplugger run was made and engagement with the latch sleeve was suggested by the abrasion on the latch dogs of the rotary assembly. This time, Core 197-1204A-14R (877.1–880.3 mbsf) (ROP = 5.5 m/hr) was intentionally advanced only 3.2 m. When there was no recovery, the drill string was tripped to the surface to determine the mechanical reason for the failure to recover core. Because of rough sea conditions, the deployment of a FFF was not attempted. Total core recovered from Hole 1204A was 55.86 m and recovery was 47.2%.

When the BHA was recovered, the bit was removed and the throat of the bit was found to be full of basaltic debris, some of which were current-rounded pebbles. The bottom of the mechanical bit release below the float valve was also jammed with basalt. The total amount of recovered basalt filled one 1.5-m section. The bit was found to be in very good condition (1, 1, NO, E, 1/16, HP, RR) after accumulating 30.3 total rotating hours. Of the total rotating hours, 10 hr were required to drill 762 m and an additional 2 hr needed to core the ~58 m of sediment. The remaining 18.3 hr was expended penetrating 60 m into basement.

The latch sleeve was inspected and found to be in gage with no apparent wear. A new C-4 bit was affixed to a fresh mechanical bit release and the drill string deployed to spud Hole 1204B. This incident was classified as weather induced. The AHC was in operation during this incident.

Hole 1204B

The vessel was offset 100 m southeast of Hole 1204A, and Hole 1204B was spudded at 2015 hr on 28 July. The seafloor was tagged at 2381.0 m relative to the DES on the rig floor.

The RCB system was drilled ahead with an average ROP of 73.7 m/hr to a depth of 810.7 mbsf. This depth was estimated to be within 5–10 m of basement. The first core (197-1204B-1R [810.7–820.3 mbsf]) contacted basement at a depth of 816.0 mbsf. Coring then advanced without incident to a depth of 906.3 mbsf. After recovering Core 197-1204B-11R, seawater was flowing back at the rig floor level from the open end of the drill string, indicating that basalt had jammed in the float valve. This was the same phenomenon that forced the early cancellation of Hole 1204A. It required six deployments of the deplugger and one core barrel round trip to clear the obstruction from the float valve. The time expended in this process was 8.8 hr.

Coring resumed, and Hole 1204B was deepened to 954.5 mbsf when time expired on site. A total of 138.5 m of basaltic basement was cored with an average recovery of 38.0%. The cored sedimentary section was 5.3 m with 62.5% recovery. The average ROP in basement was 3.6 m/hr. The basement ROP ranged from 0.9 m/hr (Core 197-1204B-9R [887.1–888.8 mbsf]) to 5.5 m/hr in the bottom 19.3 m of the hole. An operation problem required using the aft coring line to retrieve Core 197-1204B-17R. Total core recovered from Hole 1204B was 55.93 m (recovery = 38.9%).

The drilling equipment was secured in preparation for the 2-day transit to Site 1205. This included the complete disassembly of the BHA. Although the bit had acquired 50.4 hr, it appeared to be in excellent shape with only two plugged nozzles to show that it had been in service. The bit was

slightly under gage with all the inserts in the cones and had no chipped teeth. The beacon was successfully recovered. The vessel began the transit to the next site at 2100 hr on 1 August.

Site 1205

Transit to Proposed Site HE-4A (DSDP Site 432) and Underway Survey over Nintoku Seamount

The position of Site 1205 was located nearly 600 nmi south-southeast of Site 1204, at the northwestern corner of the summit platform of Nintoku Seamount. This site was last visited during DSDP Leg 55 (Site 432) in early August 1977.

The 596-nmi transit to the first survey waypoint was accomplished at an average speed of 11.6 kt. During the 52-hr voyage, the skies were overcast with occasional showers and fog hampering visibility. The sea and swell did not exceed 7 ft. The air temperature increased from 10° to 17°C as the vessel entered the Kuroshiro Current during the early evening of 7 August 2001.

Prior to spudding Hole 1205A, a geophysical survey was conducted to acoustically image the stratigraphic and structural setting of the site. Crossing high-resolution seismic reflection profiles were obtained using a single 80-in³ water gun with a firing rate of 6 s. At 0030 hr on 4 August, the vessel slowed to 6 kt to deploy the seismic equipment, and by 0600 hr the survey was completed. The 29.5-nmi survey was conducted at an average speed of 5.6 kt. To provide adequate sediment thickness to insure lateral stability of the BHA while spudding, Site 1205 was positioned where the sedimentary blanket was estimated to be at least 60 m thick.

The thrusters were lowered as the vessel established location using the GPS coordinates selected from the site survey, ~100 m southwest of proposed Site HE-4A (DSDP Site 432) in the Leg 197 prospectus. After the vessel was on station at 0632 hr, the hydrophones were lowered concurrent with the making up of a new BHA. A beacon was deployed at 0735 hr.

Hole 1205A

The corrected PDR depth referenced to the DES was obtained and indicated 1319.4 m. The BHA was made up of a 9.875-in RCB, a hard formation C-7 bit, a mechanical bit release, a modified head sub, an outer core barrel, a modified top sub, a modified head sub, seven 8.25-in drill collars, a tapered drill collar, six 5.5-in drill pipe sections, and one crossover sub.

Hole 1205A was spudded with the RCB at 1230 hr on 4 August and tagged the depth of the seafloor at 1321.0 m. Coring advanced slowly through 42.7 m of sandstone and breccia rich in basalt fragments at an average ROP of 12.5 m/hr with 9.1% recovery. Basement coring began with Core 197-1205A-6R (42.7–52.2 mbsf) and proceeded to a depth of 132.9 mbsf, when operations were suspended to change the bit, which had accumulated 52.1 hr of rotation.

Progress in the mostly fresh, fine-crystalline basaltic basement was the slowest thus far during the leg and was only uncommonly interrupted by sudden spurts of rapid penetration through thin soil horizons between lava flows. Until a depth of 59 mbsf was attained, the slow penetration rate in basement was also attributed to the BHA not being sufficiently buried to allow the driller to apply more than 15,000 lb of weight on bit.

A total of 90.2 m of basaltic basement was cored with an average recovery of 61.3%. The cored sedimentary section was 42.7 m with 9.1% recovery. The ROP in basement varied from 4.8 m/hr (Core 197-1205A-6R [42.7–52.2 mbsf]) to 0.5 m/hr (Core 197-1205A-8R [56.9–58.9 mbsf]). The

average ROP in basement was 1.9 m/hr. The average total recovery for the 132.9 m of cored sedimentary and basement sequences was 49.0%.

Reentry

The bit cleared the FFF at 1330 hr on 7 August and was captured by the VIT camera. The bit cleared the rotary table at 1630 hr and was quickly removed and replaced with another new C-7 hard-formation rotary bit. The used bit was inspected and found to be in excellent condition with only 0.0625-in loss of outside gage. The cones were intact with no chipped or missing teeth. All nozzles were clear. Because of the excessive hours of rotation, most of which was accumulated in basement, the bit was retired from service in spite of the outward excellent appearance.

The used mechanical bit release was also replaced with a fresh unit. After spacing out the new assembly, the drill string was deployed and positioned over the FFF by 2115 hr. As the driller was making a near-perfect reentry, the bit lightly tapped the throat of the cone, which immediately toppled over on its side, rendering it useless for reentry purposes. Apparently, the sandy surface formation was too firm to allow the 2.5-m length of 13.375-in casing to sufficiently penetrate the hard seafloor during deployment. The FFF was perched on, rather than nestled within, the hard sandy bottom of the summit platform of the Nintoku Seamount. The bit tapping the FFF was enough to upset the unstable installation.

Considerable bottom mud was stirred up as a result of the FFF tipping over, which obscured the now unadorned Hole 1205A. However, the driller and dynamic positioning personnel persevered, and the reentry of the open hole was achieved by 2209 hr.

Coring resumed in Hole 1205A and advanced to 215.8 mbsf when flowback at the drill floor connection indicated that the float valve was jammed open. It required seven runs with the depluggers and core barrel to clear the obstruction. This effort consumed 5 hr and involved two runs with the long deplugger, two runs with fresh core barrels, another run with the long deplugger, and two runs with the chisel deplugger.

Basement coring again resumed and penetrated to 274.6 mbsf when once again flowback at the rig floor required one run with the deplugger and one run with a fresh core barrel to clear the obstruction from the float valve. Time-scheduled coring in Hole 1205A was terminated at a final depth of 326.0 mbsf. The cored interval was 326.0 m with a recovery of 165.6 m of sediment and basalt (recovery = 50.8%). The total basement penetration was 283.3 m with 161.8 m recovered (recovery = 57.1%). The coring effort required two bits with a total rotating time of 110.8 hr. The average ROP in basement was 2.6 m/hr. The cored sediment was 42.7 m with 3.87 m recovered (recovery = 9.1%). At this juncture during Leg 197, 935.2 m of basement had been cored with 487.9 m recovered (recovery = 52.2%).

Logging Attempt

Following the retrieval of the last core, the hole was conditioned with a wiper trip up to 69 mbsf and down to 279 mbsf. The hole was washed and reamed from 279 to 326 mbsf with no apparent fill detected at the bottom. Following the displacement of the hole with 100 bbl of sepiolite mud, the bit was placed at the logging depth of 90 mbsf. The first planned logging run was with the triple combo. Unfortunately, it was not possible for the loggers to deploy the tool deeper than 136 mbsf because the hole was blocked by a bridge and swelling formation. The logging effort was aborted and the drilling equipment retrieved.

The drilling equipment was secured and the BHA dismantled in preparation for the 400-nmi journey to proposed Site HE-6A, Koko Seamount. The beacon was recovered and the thrusters and

hydrophones retracted. The moonpool was secured for the transit as the vessel got under way to the last site of Leg 197 at 0600 hr on 12 August.

Site 1206

Transit to Proposed Site HE-6A (DSDP Site 308) and Underway Survey over Koko Seamount

The position of Site 1206 was located nearly 400 nmi south-southeast of Site 1205, Nintoku Seamount, and situated on the southeastern sector of the lower summit platform of Koko Seamount. The site area was last visited during the DSDP Leg 32, in mid-September 1973, when drilling took place at Site 308.

The 377-nmi transit to the first survey waypoint was accomplished at an average speed of 11.6 kt. During the 32.5-hr voyage, the skies were mostly cloudy with good visibility. Seas were flat with a gentle 4-ft swell from the east-northeast. Sea temperature continued to rise from 15° to 24°C during the 1.5-day voyage.

Prior to spudding Hole 1206A and consonant with the routine established during Leg 197, a geophysical survey was conducted to augment the paucity of seismic reflection data available for the site area, to locate a suitable site, and to acoustically characterize its structural and stratigraphic setting. Crossing high-resolution seismic reflection profiles were obtained using a single 80-in^3 water gun with a firing rate of 4 s. At 1430 hr on 13 August 2001, the vessel slowed to 6 kt to deploy the seismic equipment, and by 2115 hr the survey was completed. The 33.0-nmi survey was completed at an average speed of 5.5 kt.

Our arrival over Koko Seamount was greeted by Russian fishing trawlers whose crews were tending nets and long lines. We also encountered a small container vessel utilizing the great-circle route. The thrusters were lowered as the vessel, using the GPS, established the location for Site 1206 selected during the survey. Site 1206 was positioned ~6.2 km south of Site 308 (proposed Site HE-6A identified in the Leg 197 prospectus). After the vessel was on station at 2116 hr, the hydrophones were lowered concurrent with making up a new BHA. A beacon was deployed at 2300 hr.

Hole 1206A

The corrected PDR depth referenced to the DES was obtained and indicated a water depth of 1544.1 m. The BHA was made up of a 9.875-in RCB, a hard-formation C-7 bit, a mechanical bit release, a modified head sub, an outer core barrel, a modified top sub, a modified head sub, seven 8.25-in drill collars, a tapered drill collar, six 5.5-in drill pipe sections, and one crossover sub.

Hole 1206A was spudded at 0215 hr on 14 August with the RCB and a wash barrel in place. The bit tagged the seafloor depth at 1557.0 m relative to the DES. The bit was drilled ahead to 57 mbsf when the penetration slowed, suggesting basement contact. The wash barrel contained a composite of sedimentary material, most of which was a dark, calcareous, sandy siltstone and silty sandstone. Volcanic basement coring began with Core 197-1206A-2R (57.0–58.5 mbsf) and proceeded to a depth of 79.8 mbsf, when operations were suspended to conduct a small wiper trip to 35.0 mbsf to reduce high erratic torque.

Coring resumed and continued slowly as frequent deplugger operations were required to free debris jamming the throat of the bit and the float valve. The recovery dropped off markedly below 104.4 mbsf (47 m into basement). After the hole was deepened an additional 23.8m (128.2 mbsf)

with only 0.45 m obtained (recovery = 1.9%), it was clear that a round trip of the drill string was required to investigate the reason for poor core recovery.

A FFF was deployed at 0010 hr on 16 August. The bit cleared the top of the FFF at 0110 hr and was monitored via the VIT. The FFF was erect following the withdrawal of the bit. After the drill string was recovered, the bit and the area directly under the float valve in the mechanical bit release were found to be full of basalt fragments as well. Many of the fragments were obviously cored segments that apparently fell out of the core barrel during earlier operations. The reclaimed cored material added an additional 2.0 m to the 0.02-m recovery of the last core barrel (Core 197-1206A-14R). The bit was otherwise in excellent shape, but because it had accumulated 24 rotating hours in drilling 57 m of sediment and cored an additional 71.2 m of basement, it was retired from service. The average recovery for the cored interval of 71.2 m was 39.9%, corresponding to 28.39 m of cored material. The average ROP in basement coring was 3.3 m/hr.

Reentry (Third of Leg 197)

A new C-7 bit and a fresh mechanical bit release were made up to the BHA, and by 1015 hr on 16 August the bit was suspended above the open hole of Hole 1206A. Sometime in the interval between the extraction of the old bit and reentry positioning, the FFF had tipped over when the 2.5-m length of 13.375-in casing failed to sufficiently penetrate the hard surface of the seafloor. The dynamic positioning operator adroitly maneuvered the vessel and at 1021 hr, the bare hole was successfully reentered.

Basement coring resumed in Hole 1206A and by the evening of 19 August proceeded without incident from 128.2 to 323.2 mbsf. The hole was flushed with mud, and a wiper trip was made to 65 mbsf to prepare the hole for logging. The drill string stuck at two positions in the borehole, 101 and 171 mbsf. The driller had to apply 100,000 lb of overpull to free the pipe at a depth of 171 mbsf. The hole was washed and reamed from 65 to 323 mbsf after which 2 m of fill was found at the bottom of the hole. After considering the unstable nature at the top of the hole and factoring in the 11-ft heave of the vessel, the prospects for a successful logging endeavor appeared dim. The decision was made to extend coring for the few remaining hours until time expired on site. Coring resumed and deepened the hole to 335.2 mbsf when we decided to terminate operations and recover the drill string.

An additional 207.0 m of basaltic basement was cored with the second bit with an average recovery of 54.6%. The ROP varied from 1.2 m/hr (Core 197-1206A-23R [191.0–192.7 mbsf]) to 5.8 m/hr (Core 197-1206A-20R [162.2–171.8 mbsf]). The average ROP in basement with the second bit was 3.2 m/hr. The total cored interval in Hole 1206A was 278.2 m with 50.8% average recovery. The average ROP for the two bits was 3.2 m/hr.

The drill string was recovered and the BHA was inspected before being disassembled. The hydrophones and thrusters were retracted, the beacon was recovered, and all drilling equipment was secured by 2230 hr on 20 August, when the vessel left location for Yokohama.

REFERENCES

Acton, G.D., and Gordon, R.G., 1994. Paleomagnetic tests of Pacific plate reconstructions and implications for motions between hotspots. *Science,* 263:1246–1254.

Arason, P., and Levi, S., 1990. Compaction and inclination shallowing in deep-sea sediments from the Pacific Ocean. *J. Geophys. Res.,* 95:4501–4510.

Atwater, T., 1989. Plate tectonic history of the northeast Pacific and western North America. *In* Winterer, E.L., Hussong, D.M., and Decker, R.W. (Eds.), *The Eastern Pacific Ocean and Hawaii,* Geol. Soc. Am., Geol. of North America Ser., N:21–72.

Berggren, W.A., Kent, D.V., Swisher, C.C., III, and Aubry, M.-P., 1995. A revised Cenozoic geochronology and chronostratigraphy. *In* Berggren, W.A., Kent, D.V., Aubry, M.-P., and Hardenbol, J. (Eds.), *Geochronology, Time Scales and Global Stratigraphic Correlation.* Spec. Publ.—Soc. Econ. Paleontol. Mineral. (Soc. Sediment. Geol.), 54:129–212.

Besse, J., and Courtillot, V., 1991. Revised and synthetic apparent polar wander paths of African, Eurasian, North American and Indian plates, and true polar wander since 200 Ma. *J. Geophys. Res.,* 96:4029–4051.

Cande, S.C., Raymond, C.A., Stock, J., and Haxby, W.F., 1995. Geophysics of the Pitman Fracture Zone and Pacific-Antarctic plate motions during the Cenozoic. *Science,* 270:947–953.

Celaya, M.A., and Clement, B.M., 1988. Inclination shallowing in deep sea sediments from the North Atlantic. *Geophys. Res. Lett.,* 15:52–55.

Chen, C.-Y., and Frey, F.A., 1985. Trace element and isotopic geochemistry of lavas from Haleakala Volcano, East Maui, Hawaii: implications for the origin of Hawaiian basalts. *J. Geophys. Res.,* 90:8743–8768.

Christensen, U., 1998. Fixed hotspots gone with the wind. *Nature,* 391:739–740.

Clague, D.A., and Dalrymple, G.B., 1973. Age of Koko Seamount, Emperor Seamount chain. *Earth. Planet. Sci. Lett.,* 17:411–415.

————, 1987. The Hawaiian-Emperor volcanic chain, Part I. Geologic evolution. *In* Decker, R.W., Wright, T.L., and Stauffer, P.H. (Eds.), *Volcanism in Hawaii.* Geol. Surv. Prof. Pap. U.S., 1350:5–54.

Coe, R.S., 1967. Paleo-intensities of the Earth's magnetic field determined from Tertiary and Quaternary rocks. *J. Geophys. Res.,* 72:3247–3262.

Constable, C., 1992. Link between geomagnetic reversal paths and secular variation of the field over the past 5 Myr. *Nature,* 358:230–233.

Cottrell, R., and Tarduno, J.A., 1997a. Magnetic hysteresis properties of single crystals: prelude to paleointensity studies, Suppl. *Eos,* Am. Geophys. Union, 78:F185.

————, 1997b. Tectonic and paleoclimatic implications of a high latitude Late Cretaceous pole position for the Pacific plate. Suppl. *Eos,* Am. Geophys. Union, 78:S117.

————, 2000a. In search of high fidelity geomagnetic paleointensities: a comparison of single plagioclase crystal and whole rock Thellier-Thellier analyses. *J. Geophys. Res.,* 105:23579–23594.

————, 2000b. Late Cretaceous true polar wander: not so fast. *Science,* 288:2283a.

————, in press. A Late Cretaceous pole for the Pacific plate: implications for apparent and true polar wander and the drift of hotspots. *Tectonophysics.*

Cox, A.V., 1970. Latitude dependence of the angular dispersion of the geomagnetic field. *Geophys. J. R. Astron. Soc.,* 20:253–269.

Dalrymple, G.B., Lanphere, M.A., and Clague, D.A., 1980. Conventional and $^{40}Ar/^{39}Ar$ K-Ar ages of volcanic rocks from Ojin (Site 430), Nintoku (Site 432) and Suiko (Site 433) Seamounts and the chronology of volcanic propagation

along the Hawaiian-Emperor chain. *In* Jackson, E.D., Koizumi, I., et al., *Init. Repts. DSDP,* 55: Washington (U.S. Govt. Printing Office), 659–676.

Davies, T.A., Wilde, P., and Clague, D.A., 1972. Koko Seamount: a major guyot at the southern end of the Emperor Seamounts. *Mar. Geol.,* 13:311–321.

Duncan, R.A., and Clague, D.A., 1985. Pacific plate motion recorded by linear volcanic chains. *In* Nairn, A.E.M., Stehli, F.G., and Uyeda, S. (Eds.), *The Ocean Basins and Margins* (Vol. 7A): *The Pacific Ocean:* New York (Plenum), 89–121.

Duncan, R.A., Petersen, N., and Hargraves, R.B., 1972. Mantle plumes, movement of the European plate, and polar wandering. *Nature,* 239:82–86.

Duncan, R.A., and Richards, M.A., 1991. Hotspots, mantle plumes, flood basalts, and true polar wander. *Rev. Geophys.,* 29:31–50.

Fisher, F.A., 1953. Dispersion on a sphere. *Proc. R. Soc. London A,* 217:295–305.

Frey, F.A., Garcia, M.O., Wise, W.S., Kennedy, A., Gurriet, P., Albarede, F., 1991. The evolution of Mauna Kea Volcano, Hawaii; petrogenesis of tholeiitic and alkalic basalts. *J. Geophys. Res.,* 96:14347–14375.

Frey, F.A., Wise, W.S., Garcia, M.O., West, H., Kwon, S.T., Kennedy, A., 1990. Evolution of Mauna Kea Volcano, Hawaii; petrologic and geochemical constraints on postshield volcanism. *J. Geophys. Res.,* 95:1271–1300.

Garcia, M.O., Ito, E., Eiler, J.M., and Pietruszka, A.J., 1998. Crustal contamination of Kilauea volcano magmas revealed by oxygen isotope analyses of glass and olivine from Puu Oo eruption lavas. *J. Petrol.,* 39:803–817.

Gee, J., Staudigel, H., and Tauxe, L., 1989. Contribution of induced magnetization to magnetization of seamounts. *Nature,* 342:170–173.

Goldreich, P., and Toomre, A., 1969. Some remarks on polar wandering. *J. Geophys. Res.,* 74:2555–2567.

Gordon, R.G., 1983. Late Cretaceous apparent polar wander of the Pacific plate: evidence for a rapid shift of the Pacific hotspots with respect to the spin axis. *Geophys. Res. Lett.,* 10:709–712.

Gordon, R.G., and Cape, C., 1981. Cenozoic latitudinal shift of the Hawaiian hotspot and its implications for true polar wander. *Earth Planet. Sci. Lett.,* 55:37–47.

Gromme, S., and Vine, F.J., 1972. Paleomagnetism of Midway atoll lavas and northward movement of the Pacific plate. *Earth Planet. Sci. Lett.,* 17:159–168.

Hargraves, R.B., and Duncan, R.A., 1973. Does the mantle roll? *Nature,* 245:361–363.

Holt, J.W., Kirschvink, J.L., and Garnier, F., 1996. Geomagnetic field inclinations for the past 400 kyr from the 1-km core of the Hawaii Scientific Drilling Project. *J. Geophys. Res.,* 101:11655–11663.

Huber, B.T., Hodell, D.A., and Hamilton, C.P., 1995. Mid- to Late Cretaceous climate of the southern high latitudes: stable isotopic evidence for minimal equator-to-pole thermal gradients. *Geol. Soc. Am. Bull.,* 107:1164–1191.

Juarez, M.T., Tauxe, L., Gee, J.S., and Pick, T., 1998. The intensity of the Earth's magnetic field over the past 160 million years. *Nature,* 394:878–881.

Keller, R.A., Duncan, R.A., and Fisk, M.R., 1995. Geochemistry and [40]Ar/[39]Ar geochronology of basalts from ODP Leg 145 (North Pacific Transect). *In* Rea, D.K., Basov, I.A., Scholl, D.W., and Allan, J.F. (Eds.), *Proc. ODP, Sci. Results,* 145: College Station, TX (Ocean Drilling Program), 333–344.

Keller, R.A., Fisk, M.R., and White, W.M., 2000. Isotopic evidence for Late Cretaceous plume-ridge interaction at the Hawaiian hotspot. *Nature,* 405:673–676.

Kono, M., 1980. Paleomagnetism of DSDP Leg 55 basalts and implications for the tectonics of the Pacific plate. *In* Jackson, E.D., Koizumi, I., et al., *Init. Repts. DSDP,* 55: Washington (U.S. Govt. Printing Office), 737–752.

Lanphere, M.A., Dalrymple, G.B., and Clague, D.A., 1980. Rb-Sr systematics of basalts from the Hawaiian-Emperor volcanic chain. *In* Jackson, E.D., Koizumi, I., et al., *Init. Repts. DSDP,* 55: Washington (U.S. Govt. Printing Office), 695–705.

Larson, R.L., Moberly, R., et al., 1975. *Init. Repts. DSDP,* 32: Washington (U.S. Govt. Printing Office).

Le Pas, M.J., Le Maitre, R.W., Streckeisen, A., and Zanettin, B., 1986. A chemical classification of volcanic rocks based on the total alkali-silica diagram. *J. Petrol.* 27:745–750.

Livermore, R.A, Vine, F.J., and Smith, A.G., 1984. Plate motions and the geomagnetic field. II. Jurassic to Tertiary. *Geophys. J. R. Astron. Soc.,* 79:939–961.

Lonsdale, P., Dieu, J., and Natland, J., 1993. Posterosional volcanism in the Cretaceous part of the Hawaiian hotspot trail. *J. Geophys. Res.,* 98:4081–4098.

Lowrie, W., and Fuller, M., 1971. On the alternating field demagnetization characteristics of multidomain thermoremanent magnetization in magnetite. *J. Geophys. Res.,* 76:6339–6349.

Macdonald, G.A., and Katsura, T., 1964. Chemical composition of Hawaiian lavas. *J. Petrol.,* 5:82–133.

Mammerickx, J., and Sharman, G.F., 1988. Tectonic evolution of the North Pacific during the Cretaceous Quiet Period. *J. Geophys. Res.,* 93:3009–3024.

McElhinny, M.W., 1973. Mantle plumes, palaeomagnetism, and polar wandering. *Nature,* 241:523–524.

McFadden, P.L., Merrill, R.T., McElhinny, M.W., and Lee, S., 1991. Reversals of the Earth's magnetic field and temporal variations of the dynamo families. *J. Geophys. Res.,* 96:3923–3933.

McFadden, P.L., and Reid, A.B., 1982. Analysis of paleomagnetic inclination data. *Geophys. J. R. Astron. Soc.,* 69:307–319.

Molnar, P., and Atwater, T., 1973. Relative motion of hotspots in the mantle. *Nature,* 246:288–291.

Molnar, P., and Stock, J., 1987. Relative motions of hotspots in the Pacific, Atlantic, and Indian Oceans since Late Cretaceous time. *Nature,* 327:587–591.

Morgan, W.J., 1971. Convection plumes in the lower mantle. *Nature,* 230:42–43.

Norton, I.O., 1995. Plate motions in the North Pacific: the 43 Ma Nonevent. *Tectonics*, 14:1080–1094.

Parker, R.L., 1991. A theory of ideal bodies for seamount magnetization. *J. Geophys. Res.,* 96:16101–16112.

Pick, T., and Tauxe, L., 1993. Geomagnetic paleointensities during the Cretaceous normal superchron measured using submarine basaltic glass. *Nature,* 366:238–242.

Rea, D.K., Basov, I.A., Krissek, L.A., and the Leg 145 Scientific Party, 1995. Scientific results of drilling the North Pacific transect. *In* Rea, D.K., Basov, I.A., Scholl, D.W., and Allan, J.F. (Eds.), *Proc. ODP, Sci. Results,* 145: College Station, TX (Ocean Drilling Program), 577–596.

Rhodes, J.M., 1996. Geochemical stratigraphy of lava flows sampled by the Hawaii Scientific Drilling Project. *J. Geophys. Res.,* 101:11729–11746.

Sager, W., and Bleil, U., 1987. Latitudinal shift of Pacific hotspots during the Late Cretaceous and early Tertiary. *Nature,* 326:488–490.

Sager, W.W., and Pringle, M.S., 1988. Mid-Cretaceous to early Tertiary apparent polar wander path of the Pacific plate. *J. Geophys. Res.,* 93:11753–11771.

Solomon, S.C., Sleep, N.H., and Jurdy, D.M., 1977. Mechanical models for absolute plate motions in the early Tertiary. *J. Geophys. Res.,* 82:203–213.

Steinberger, B., 1996. Motion of hotspots and changes of the Earth's rotation axis caused by a convecting mantle. [Ph.D. Thesis]. Harvard Univ., Cambridge, MA.

————, 2000. Plumes in a convecting mantle: models and observations for individual hotspots. *J. Geophys. Res.,* 105:11127–11152.

Steinberger, B., and O'Connell, R.J., 1997. Changes of the Earth's rotation axis owing to advection of mantle density heterogeneities. *Nature,* 387:169–173.

————, 1998. Advection of plumes in mantle flow: implications for hotspot motion, mantle viscosity and plume distribution. *Geophys. J. Int.,* 132:412–434.

Tarduno, J.A., 1990. Absolute inclination values from deep sea sediments: a reexamination of the Cretaceous Pacific record. *Geophys. Res. Lett.,* 17:101–104.

Tarduno, J.A., and Cottrell, R., 1997. Paleomagnetic evidence for motion of the Hawaiian hotspot during formation of the Emperor Seamounts. *Earth Planet. Sci. Lett.,* 153:171–180.

Tarduno, J.A., Cottrell, R.D., and Smirnov, A.V., 2001. High geomagnetic field intensity during the mid-Cretaceous from Thellier analyses of single plagioclase crystals. *Science,* 291:1179–1183.

Tarduno, J.A., and Gee, J., 1995. Large scale motion between Pacific and Atlantic hotspots. *Nature,* 378:477–480.

Tarduno, J.A., and Sager, W.W., 1995. Polar standstill of the mid-Cretaceous Pacific plate and its geodynamic implications. *Science,* 269:956–959.

Tarduno, J.A., and Smirnov, A.V., 2001. Stability of the Earth with respect to the spin axis for the last 130 million years. *Earth Planet. Sci. Lett.,* 184:549–553.

Thellier, E., and Thellier, O., 1959. Sur l'intensité du champ magnétique terreste dans le passé historique et geologique. *Ann. Geophys.,* 15:285–375.

Vasas, S.M., Gordon, R.G., and Petronotis, K.E., 1994. New paleomagnetic poles for the Pacific plate from analysis of the shapes of anomalies 33N and 33R. *Eos*, Trans. Am. Geophys. Union, 75:203.

Wessel, P., and Kroenke, L.W., 1998. Factors influencing the locations of hotspots determined by the hot-spotting technique. *Geophys. Res. Lett.*, 25:555–558.

Yang, H.-J., Frey, F.A., Rhodes, J.M., Garcia, M.O., 1996. Evolution of Mauna Kea Volcano: inferences from lava compositions recovered in the Hawaii Scientific Drilling Project. *J. Geophys. Res.,* 101:11747–11767.

Zachos, J.C., Stott, L.D., and Lohmann, K.C., 1994. Evolution of early Cenozoic marine temperatures. *Paleoceanography,* 9:353–387.

TABLE CAPTIONS

Table T1. Coring summary, Leg 197.

Table T2. Operations summary, Leg 197.

FIGURE CAPTIONS

Figure F1. Location of Leg 197 sites and previous DSDP and ODP sites on the Emperor Seamounts (solid circles).

Figure F2. A. Preferred viscosity structure used to calculate hotspot motion from Steinberger and O'Connell (1998). A low-viscosity upper mantle is used to reproduce the Hawaiian-Emperor bend. A high-viscosity lower mantle is employed; otherwise, the relative motions between hotspots are greater than observations. Harvard tomographic model S12WM13 was used to infer mantle density heterogeneities. The gradual increase in viscosity was chosen to minimize disagreement with models based on postglacial rebound, which mainly constrain viscosity in the upper half of the mantle. **B.** The predicted motion of the Hawaiian plume between 90 and 43 Ma after Steinberger (2000). The model predicts a southward component of motion of ~10 mm/yr. This result is from the mantle flow at depth, which also tends to have a southward component of the same magnitude, partly due to a return flow opposite of Pacific plate motion in the model. The model predicts only a small relative motion between the Hawaiian and Louisville hotspots, in accordance with the age progressions observed along the two hotspot tracks. Other models with a lower viscosity in the lower mantle predict substantially higher flow speeds and substantially larger southward motion of the Hawaiian hotspot.

Figure F3. A. Average inclination values for three inclination group models from Detroit Seamount; error bars = 95% confidence intervals. The predicted inclination at 81 Ma based on prior Pacific apparent polar wander path (APWP) poles (Gordon, 1983) is also shown. **B.** Paleolatitude values with 95% confidence intervals for the inclination groups. The present-day latitude of the Hawaiian hotspot (solid line) is also shown. **C.** Estimated angular dispersion (S) of the inclination groups (solid line) vs. the predicted values for 45–80 Ma (dark field) and 80–110 Ma (light field) from McFadden et al. (1991). VGP = virtual geomagnetic pole. **D.** Orthographic projection of the colatitude (primary) for Detroit Seamount (star). The colatitude is distinct at the 99% confidence level (shaded) from previous 81–82 Ma poles (ellipses). Poles are derived from the following: 81 Ma (Gordon, 1983), 82 Ma (Sager and Pringle, 1988), and 33n (79.1–73.6 Ma) (Vasas et al., 1994). The sense of offset between the natural remanent magnetization data and the demagnetized (primary) data is the same as that between the new paleolatitude result and results based on prior Pacific pole positions. This is the expected effect if these previous pole positions are contaminated by secondary magnetizations. This figure is after Tarduno and Cottrell (1997).

Figure F4. Plot of latitudinal distance from the 43-Ma bend in the Hawaiian-Emperor hotspot track vs. age (light circles). Age data are not available for Meiji, Tenchi, and Jimmu Seamounts; their positions, based on a constant latitudinal progression, are shown for reference. Dark circles indicate positions after the difference between the present-day latitude of the 43-Ma bend and Hawaii is subtracted from each of the present-day latitudes of the Emperor Seamounts. In effect, we slide the Emperor trend down the Hawaiian chain so that the bend coincides with the position of Hawaii (inset). This reconstruction allows the following test. If the Emperor Seamounts record mainly motion of the Hawaiian hotspot, paleolatitudes should fall close to this corrected latitudinal trend; if the hotspot has been stationary, the paleolatitudes should fall close to the present-day latitude of Hawaii. Triangles = paleolatitudes of Suiko and Detroit Seamounts, with 95% confidence intervals. The null hypothesis that the paleolatitude result from the Suiko Seamount is drawn from the same population as the Detroit Seamount data can be rejected at the 95% confidence level using nonparametric tests (Kolmogorov-Smirnov). In the absence of a rotation of the entire Earth with respect to the spin axis, known as true polar wander (Tarduno and Cottrell, 1997; Cottrell and Tarduno, 2000b; Tarduno and Smirnov, 2001), the hotspot may have moved continuously southward at a rate of 30–50 mm/yr while the plate also drifted slowly northward (shaded area). This figure is after Tarduno and Cottrell (1997).

Figure F5. A. Estimates of zonal quadrupole Gauss coefficients (g20) relative to the axial dipole (g10), from Livermore et al. (1984). Pacific data are rotated using a fixed hotspot reference frame (see model "B" in Livermore et al., 1984). Our proposed sampling covers the range where Livermore et al. (1984) propose a change in sign of the quadrupole term. **B.** Paleointensity determined from studies of submarine basaltic glass complied by Juarez et al. (1998). The proposed sampling covers the transition from the Cretaceous Normal Polarity Superchron (K-N) to the Late Cretaceous–Cenozoic mixed polarity interval. VADM = virtual axial dipole moment.

Figure F6. Compositional changes in magmas produced by the Hawaiian hotspot through time. The shaded field shows the range of published $^{87}Sr/^{86}Sr$ ratios of tholeiitic basalt vs. age and distance along the Hawaiian-Emperor chain. Note that data from Detroit Seamount are significantly less radiogenic than those at younger volcanoes. The circles with crosses connected by the thick dotted line show the trend in age difference between seamounts and the underlying ocean crust (from Keller et al., 2000).

Figure F7. Site 1203 survey 1, line 6, 5-km-long migrated time section. Data are bandpass filtered between 40 and 100 Hz. Hole 1203A is situated at about shotpoint 7780. Trace-to-trace distance = ~18.8 m; vertical exaggeration at the seafloor = ~3:1; bottom of hole = ~4.34 s two-way traveltime.

Figure F8. Summary of Site 1203 basement rocks and biostratigraphic ages with provisional downhole logging data for comparison. TD = total depth.

Figure F9. Close-up photograph showing partially altered glassy lobe margins with calcareous interlobe sediment (interval 197-1203A-41R-2, 0–18 cm).

Figure F10. Photomicrographs in cross-polarized light of zonation in plagioclase (Sample 197-1203A-35R-4, 47–49 cm [Piece 1F]). **A.** Field of view = 10 mm; photomicrograph 1203A-59. **B**. Field of view = 2.5 mm; photomicrograph 1203A-60.

Figure F11. Photomicrograph of the olivine-rich zone in Unit 16 (Sample 197-1203A-37R-3, 10–13 cm [Piece 1A]) (cross-polarized light; field of view = 5.5 mm; photomicrograph 1203A-22).

Figure F12. A. Total alkali content ($Na_2O + K_2O$) vs. SiO_2 classification plot (from Le Bas et al., 1986) for volcanic rocks showing lava compositions from Detroit Seamount. The dashed line is the alkalic-tholeiitic dividing line for Hawaiian basalt. Lavas from Site 884 are tholeiitic basalt, whereas lavas from Site 883 are alkalic basalt, although Keller et al. (1995) inferred that prior to alteration these lavas were transitional between alkalic and tholeiitic basalt. Data for these two Leg 145 sites in this and all subsequent figures are from Keller et al. (2000) and M. Regelous et al. (unpubl. data). Lavas from Site 1203 range from tholeiitic, overlapping with Site 884 lavas, to alkalic, overlapping with Site 883 lavas. Most of the alkalic Site 1203 lavas have loss on ignition (LOI) >2 wt%. The volcaniclastite sample has high total alkalis, which is interpreted as a result of alkali gain during alteration. The two Site 1203 basalt samples in the tholeiitic field at <45% SiO_2 are picritic as a result of olivine accumulation. **B.** Total alkali content ($Na_2O + K_2O$) vs. SiO_2 comparing Detroit Seamount lava compositions with those from Mauna Kea Volcano (shield and postshield stage lavas—lower and upper shaded areas, respectively) on the island of Hawaii. Site 884 and some Site 1203 lavas overlap with the shield-stage tholeiitic basalt, whereas Site 883 and some Site 1203 lavas overlap with Hawaiian postshield alkalic basalt. The irregular line encloses postshield-stage lava erupted at Mauna Kea Volcano, Hawaii.

Figure F13. Ti/Zr abundance ratio vs. depth for Hole 1203A lavas. The alkalic basalt of Units 23 and 26 near the bottom of the hole have relatively low Ti/Zr ratios. This result contrasts with the classic Hawaiian trend of increasing alkalinity with decreasing eruption age during the transition from shield to postshield-stage volcanism.

Figure F14. Variations of loss on ignition (LOI), CaO, K_2O, Na_2O, Ba, and Sr with depth. Basaltic units are represented in blue and are labeled. Volcaniclastic units are represented in yellow.

Figure F15. Logging data summary for Hole 1203A. Circles plotted under bulk density, porosity, and *P*-wave log columns are values from discrete measurements on recovered core samples.

Figure F16. Comparison of FMS images and wireline measurements (electrical resistivity, natural gamma ray, porosity, and density) with the core-derived lithology and logging lithology in basement.

Figure F17. Example of detailed FMS image displaying the transition between basement Units 7 (layered volcaniclastic sediment) and 8 (pillow lava).

Figure F18. Downhole and uphole run of the Goettingen borehole magnetometer. Intensities of the horizontal and vertical field are compared to the sequences of volcaniclastic sediment and lava flows.

Figure F19. Example orthogonal vector plot showing well-defined, stable magnetic behavior recorded by Site 1203 volcaniclastic sediment samples. **A.** Sample 197-1203A-24R-1, 30–32 cm. **B.** Sample 197-1203A-38R-2, 77–79 cm. **C.** Sample 197-1203A-38R-4, 94–96 cm. **D.** Sample 197-1203A-63R-5, 127–129 cm. Open squares = vertical projection of magnetization, solid circles = horizontal projection of magnetization.

Figure F20. Example orthogonal vector plot showing well-defined, stable magnetic behavior recorded by Site 1203 basalt samples. **A.** Sample 197-1203A-25R-1, 29–31 cm. **B.** Sample 197-1203A-26R-1, 75–77 cm. **C.** Sample 197-1203A-31R-1, 65–67 cm. **D.** Sample 197-1203A-36R-3, 60–62 cm. **E.** Sample 197-1203A-37R-3, 113–115 cm. **F.** Sample 197-1203A-47R-4, 18–20 cm. **G.** Sample 197-1203A-55R-5, 17–19 cm. **H.** Sample 197-1203A-59R-4, 124–126 cm. Open squares = vertical projection of magnetization, solid circles = horizontal projection of magnetization.

Figure F21. Histogram of inclination values derived from principal component analyses on alternating-field demagnetization data from Hole 1203A volcaniclastic sediment samples. ΔI = difference between the inclination of Hawaii and that of Detroit Seamount, Δλ = difference in the latitude of Hawaii and the formative paleolatitude of Detroit Seamount.

Figure F22. Histogram of inclination values derived from principal component analyses on Hole 1203A basement basalt. ΔI = difference between the inclination of Hawaii and that of Detroit Seamount, Δλ = difference in the latitude of Hawaii and the formative paleolatitude of Detroit Seamount.

Figure F23. Site 1204 survey 2 line 3, 4-km-long migrated time section. Data are bandpass filtered between 40 and 100 Hz. Hole 883F occurs at about shotpoint 3517, Hole 1204A at shotpoint 3549, and Hole 1204B at shotpoint 3555. Trace-to-trace distance = ~16.5 m; vertical exaggeration at the seafloor = ~3:1; bottom of Hole 1204B = ~4.35 s two-way traveltime.

Figure F24. Photograph showing rotated, broken sediment block overlying a thick interval consisting of a thin, faulted, very finely laminated bed and convoluted laminations, likely indicating slumping. The 2-cm brown beds of silty volcanic material alternate with finely laminated, bioturbated, and burrowed nannofossil chalk (interval 197-1204A-3R-2, 50–69 cm).

Figure F25. Recovery, age, and major lithologic features of basement units from Holes 1204A and 1204B. TD = total depth, G = fresh glass.

Figure F26. Photograph of Unit 1b breccia containing angular fragments of altered glass and vesicular basalt in a carbonate cement (Section 197-1204A-7R-1 [Pieces 5 and 8]).

Figure F27. Photomicrograph showing unaltered olivine and plagioclase laths in a glassy lobe margin (Sample 197-1204B-3R-2, 97–100 cm) (plane-polarized light; field of view = 0.625 mm; photomicrograph 1204B-138).

Figure F28. Photomicrograph showing unaltered olivine and plagioclase laths in glassy lobe margin (Sample 197-1204B-3R-2, 97–100 cm) (cross-polarized light; field of view = 0.625 mm; photomicrograph 1204B-156).

Figure F29. Abundance of Ti vs. Zr showing a near-linear trend for most of the lavas from Detroit Seamount. Basalt from Suiko Seamount defines a similar trend (data from M. Regelous et al., unpubl. data). Site 884 lavas and the two picrites from Site 1203 have the lowest abundances and the alkalic basalt from Site 1203 has the highest abundances of Ti and Zr.

Figure F30. Example orthogonal vector plots showing well-defined, stable magnetic behavior recorded by Hole 1204B basalt samples. **A.** Sample 197-1204B-2R-2, 14–16 cm. **B.** Sample 197-1204B-14R-1, 14–16 cm. **C.** Sample 197-1204B-13R-4, 82–84 cm. **D.** Sample 197-1204B-17R-2, 104–106 cm. **E.** Sample 197-1204B-10R-1, 6–9 cm. **F.** Sample 197-1204B-15R-1, 11–13 cm. Open squares = vertical projection of magnetization, solid circles = horizontal projection of magnetization.

Figure F31. Example orthogonal vector plots showing well-defined, stable magnetic behavior recorded by Hole 1204B diabase samples. **A.** Sample 197-1204B-7R-3, 139–141 cm. **B.** Sample 197-1204B-9R-2, 8–10 cm. **C.** Sample 197-1204B-8R-2, 21–23 cm. **D.** Sample 197-1204B-10R-4, 40–42 cm. **E.** Sample 197-1204B-11R-2, 38–40 cm. **F.** Sample 197-1204B-13R-3, 33–35 cm. Open squares = vertical projection of magnetization, solid circles = horizontal projection of magnetization.

Figure F32. Site 1205 survey 3 line 4, 3-km-long, frequency wavenumber- or fk-migrated time section. Data are bandpass filtered between 60 and 150 Hz. Hole 1205A is at approximately shotpoint 4216. Trace-to-trace distance = ~9.9 m; vertical exaggeration at the seafloor = ~7:1; bottom of Hole 1205 = ~4.35 s two-way traveltime.

Figure F33. Photograph of conglomerate overlying basement showing clasts of hawaiite up to 8 cm in diameter embedded in a poorly sorted, fossiliferous sandy matrix (interval 197-1205A-5R-2, 9–25 cm).

Figure F34. Recovery, thickness, chemical composition, and major lithologic features of Hole 1205A basement units. TD = total depth.

Figure F35. Photomicrograph showing strain bands in trachytic texture in Unit 3b (Sample 197-1205A-10R-2, 73–75 cm) (cross-polarized light; field of view = 5 mm; photomicrograph 1205A-202).

Figure F36. Total alkali content ($Na_2O + K_2O$) vs. SiO_2 classification plot for lava flows from Nintoku Seamount. The solid diagonal line is the alkalic-tholeiitic dividing line for Hawaiian basalt. Only two Site 1205 lava units (18b and 19b) are composed of tholeiitic basalt. All other flow units at Site 1205 and nearby DSDP Site 432 (M. Regelous et al., unpubl. data) are alkalic basalt. At both sites, conglomerates overlying igneous basement contain hawaiite clasts that are distinguished by their high total alkali (>6 wt%) and relatively high SiO_2 content. Data for Suiko Seamount (Site 433), which is dominantly tholeiitic basalt (M. Regelous et al., unpubl. data), are shown for comparison.

Figure F37. Abundance of Y and Zr/Y vs. Zr content. In the Zr-Y panel the trends for East Pacific Rise (EPR) MORB (data from J.M. Sinton, pers. comm., 1998), three Hawaiian shields, and Suiko Seamount define a fan-shaped array of lines, but the trend for lavas from Nintoku Seamount crosscuts the trends for Suiko Seamount and the Hawaiian volcanoes. The Zr/Y-Zr panel shows that lavas from Nintoku Seamount display a wider range in Zr/Y than EPR MORB and Mauna Kea shield lavas. HSDP = Hawaiian Scientific Drilling Project.

Figure F38. Examples of Lowrie-Fuller tests (Lowrie and Fuller, 1971) conducted on Site 1205 basalt samples. ARM = anhysteretic remanent magnetization, SIRM = saturation isothermal remanent magnetization, AF = alternating field, SD = single domain, MD = multidomain. **A.** Sample 197-1205A-14R-2, 16–18 cm. **B.** Sample 197-1205A-19R-4, 143–145 cm. **C.** Sample 197-1205A-24R-2, 141–143 cm. **D.** Sample 197-1205A-27R-4, 44–46 cm. **E.** Sample 197-1205A-29R-3, 114–116 cm. **F.** Sample 197-1205A-35R-2, 36–38 cm.

Figure F39. Examples of isothermal remanent magnetization (IRM) acquisition and demagnetization (backfield IRM) used to calculate coercivity of remanence from Hole 1205A basalt samples. SD = single domain, MD = multidomain. **A.** Sample 197-1205A-14R-2, 16–18 cm. **B.** Sample 197-1205A-19R-4, 143–145 cm. **C.** Sample 197-1205A-24R-2, 141–143 cm. **D.** Sample 197-1205A-27R-4, 44–46 cm. **E.** Sample 197-1205A-29R-3, 114–116 cm. **F.** Sample 197-1205A-35R-2, 36–38 cm.

Figure F40. Example orthogonal vector plot showing well-defined, stable magnetic behavior recorded by Site 1205 basalt samples. **A.** Sample 197-1205A-13R-2, 39–41 cm. **B.** Sample 197-1205A-25R-2, 17–19 cm. **C.** Sample 197-1205A-26R-1, 117–119 cm. **D.** Sample 197-1205A-28R-3, 4–6 cm. **E.** Sample 197-1205A-29R-4, 126–128 cm. **F.** Sample 197-1205A-44R-1, 68–70 cm. Open squares = vertical projection of magnetization, solid circles = horizontal projection of magnetization.

Figure F41. Histogram of inclination values derived from principal component analyses on Site 1205 lava flows compared to a synthetic Fisher distribution (Fisher, 1953) having the same precision parameter (k) as the experimental data.

Figure F42. Site 1206 survey 4 line 6, 2.5-km-long, finite-difference migrated time section. Data are bandpass filtered between 45 and 120 Hz. Hole 1206A is at approximately shotpoint 4947. Trace-to-trace distance = ~13 m; vertical exaggeration at the seafloor = ~4.25:1; bottom of Hole 1206A = ~2.25 s two-way traveltime.

Figure F43. Diagram summarizing the recovery, thickness, chemical composition, and major lithologic features of Hole 1206A basement units. TD = total depth.

Figure F44. Photomicrograph of Unit 6 euhedral olivine with unaltered interior and rims altered to iddingsite and green clay (Sample 197-1206A-18R-1, 49–51 cm [Piece 4]). **A.** Plane-polarized light; field of view = 0.625 mm; photomicrograph 1206A-358. **B.** Cross-polarized light; field of view = 0.625 mm; photomicrograph 1206A-359.

Figure F45. Total alkali content ($Na_2O + K_2O$) vs. SiO_2 classification plot for basaltic lava flows from Koko Seamount. Data from Nintoku and Suiko Seamounts are shown for comparison. The solid diagonal line is the alkalic-tholeiitic dividing line for Hawaiian basalt. Only three Site 1206 samples plot in the alkalic basalt field.

Figure F46. Abundances of Na_2O, K_2O, TiO_2, CaO, Al_2O_3, and Zr vs. MgO content for lavas from Koko, Nintoku, and Suiko Seamounts. All trends show an inverse correlation except for CaO in Nintoku Seamount lavas with <5 wt% MgO. Note that some lavas from Suiko Seamount contain up to 30 wt% MgO.

Figure F47. Examples of Lowrie-Fuller tests (Lowrie and Fuller, 1971) conducted on Site 1206 lava flow samples. ARM = anhysteretic remanent magnetization, SIRM = saturation isothermal remanent magnetization, AF = alternating field. **A.** Sample 197-1206A-3R-2, 99–101 cm. **B.** Sample 197-1206A-4R-5, 55–57 cm. **C.** Sample 197-1206A-9R-2, 29–31 cm. **D.** Sample 197-1206A-16R-5, 75–77 cm. **E.** Sample 197-1206A-22R-1, 117–119 cm. **F.** Sample 197-1206A-28R-1, 97–99 cm.

Figure F48. Examples of isothermal remanent magnetization (IRM) acquisition and demagnetization (backfield IRM) used to calculate coercivity of remanence from Hole 1206A lava flow samples. **A.** Sample 197-1206A-3R-2, 99–101 cm. **B.** Sample 197-1206A-4R-5, 55–57 cm. **C.** Sample 197-1206A-9R-2, 29–31 cm. **D.** Sample 197-1206A-16R-5, 75–77 cm. **E.** Sample 197-1206A-22R-1, 117–119 cm. **F.** Sample 197-1206A-28R-1, 97–99 cm. DC = direct current.

Figure F49. Example orthogonal vector plot showing well-defined, stable magnetic behavior recorded by Site 1206 basalt samples. **A.** Sample 197-1206A-3R-4, 59–61 cm. **B.** Sample 197-1206A-7R-4, 64–66 cm. **C.** Sample 197-1206A-16R-1, 33–35 cm. **D.** Sample 197-1206A-18R-2, 17–19 cm. **E.** Sample 197-1206A-20R-2, 85–87 cm. **F.** Sample 197-1206A-23R-1, 109–111 cm. Open squares = vertical projection of magnetization, solid circles = horizontal projection of magnetization.

Figure F50. Histogram of inclination values derived from principal component analyses of Site 1206 lava flows compared to a synthetic Fisher distribution (Fisher, 1953) having the same precision parameter (k) as the experimental data.

Figure F51. Red-brown soil containing planar laminations (interval 197-1205A-26R-3, 92–111 cm).

Figure F52. Well-formed zeolites recovered at Nintoku Seamount Site 1205 (Section 197-1205A-36R-2, 104 cm).

Figure F53. Well-defined dipping veins showing sinusoidal pattern in the DMT image of Site 1203 basalt.

Figure F54. Example of fractures and veins seen in FMS images.

Figure F55. History of rotation about the vertical axis for the magnetometer tool during the downhole and uphole run at Site 1203. BOP = bottom of pipe.

Figure F56. Schematic drawing (not to scale) showing the inferred volcanic environments for the volcanic sections drilled at Detroit (Sites 1203 and 1204), Nintoku (Site 1205), and Koko (Site 1206) Seamounts during Leg 197. The Detroit lava flows at Site 1204 and the lower part of the Site 1203 section were subaerially erupted (although shown as a submerged sequence following posteruption subsidence). The lava flows and associated tephra fall deposits in the upper part of the Site 1203 section were emplaced into a low-energy shallow-marine environment. The Site 1205 lavas were entirely subaerial, as indicated by numerous soil horizons between flows. The Site 1206 section at Koko Seamount consists of lava flows that have flowed from land into water in a nearshore environment. Subscript "A" indicates subaerial lava emplacement.

Figure F57. Total alkalis ($Na_2O + K_2O$) vs. SiO_2 content showing shipboard Leg 197 data for lavas recovered from basement penetrations of Detroit, Nintoku, and Koko Seamounts. All samples are basalt except for the two hawaiite clasts from Nintoku Seamount that occur in a conglomerate overlying the basement. The alkalic-tholeiitic dividing line for Hawaiian basalt is from Macdonald and Katsura (1964). Fields for alkalic and tholeiitic basalt recovered from the shield of Mauna Kea volcano by the Hawaiian Scientific Drilling Project (data from Rhodes, 1996; Vollinger and Rhodes, unpubl. data) are shown for comparison. All data are given on a volatile-free basis with 90% of the iron as Fe^{2+}.

Figure F58. A. Ti/Zr and alkalinity vs. depth in basement for basalt from Detroit Seamount (Site 1203), Nintoku Seamount (Site 1205), and Koko Guyot (Site 1206). Alkalinity is a measure of the deviation from the tholeiitic-alkalic dividing line in Figure F59; positive values indicate alkalic basalt (solid symbols) and negative values indicate tholeiitic basalt (open symbols). At Detroit Seamount, dominantly alkalic basalt, some with an anomalously low Ti/Zr = ~60, are overlain by tholeiitic basalt with Ti/Zr = ~100, only slightly less than the primitive mantle estimate. This stratigraphic sequence of basalt types is not expected during the late shield and postshield growth stages of Hawaiian volcanoes (Clague and Dalrymple, 1987). **B.** At Nintoku Seamount the lavas are dominantly alkalic basalt with two flows of intercalated tholeiitic basalt at ~200 m in the basement. This sequence of basalt types is similar to that of the postshield stage at Mauna Kea Volcano (Frey et. al., 1990, 1991). In contrast, at Koko Guyot, the lavas are dominantly tholeiitic basalt with a few intercalated lavas of alkalic basalt. This sequence is similar to the late shield stage growth of Mauna Kea Volcano that were recovered by the Hawaiian Scientific Drilling Project (Rhodes, 1996; Yang et al., 1996).

Figure F59. Photomicrograph of Unit 1 olivine phenocryst with chrome spinel inclusion (Sample 197-1206A-4R-3, 72-74 cm [Piece 4A]) (cross-polarized light; field of view = 5 mm; photomicrograph 1206A-304).

Figure F60. Photomicrograph of melt inclusions in plagioclase phenocrysts from a glassy lobe margin in Unit 3 (Sample 197-1203A-19R-2, 24–26 cm [Piece 3]) (plane-polarized light; field of view = 1.25 mm; photomicrograph 1203A-55).

Figure F61. Reflected-light photomicrograph of titanomagnetite (gray-brown) showing variable degrees of replacement by maghemite (light gray-blue) in the Site 1204 basement sequence (Sample 197-1204A-9R-2, 50–51 cm) (field of view = 0.25 mm; photomicrograph 1204A-125).

Figure F62. Complex vein filling (interval 197-1203A-36R-2, 116–135 cm).

Table 1. Coring summary, Leg 197.

Site/Hole	Latitude	Longitude	Water depth (m)	Number of cores	Interval cored (m)	Core recovered (m)	Recovery (%)	Interval drilled (m)	Total penetration (m)	Time on hole (hr)
1203A	50°56.9976'N	167°44.3969'E	2604.4	68	614.60	333.91	54.3	300.00	914.60	326.25
				Totals: 68	**614.60**	**333.91**	**54.3**	**300.00**	**914.60**	**326.25**
1204A	51°11.6784'N	167°46.3604'E	2382.0	14	118.40	55.86	47.2	761.90	880.30	71.50
1204B	51°11.6406'N	167°46.4217'E	2381.0	17	143.80	55.93	38.9	810.70	954.50	102.00
				Totals: 31	**262.20**	**111.79**	**42.6**	**1572.60**	**1834.80**	**17.50**
1205A	41°19.9986'N	170°22.6992'E	1321.0	45	326.00	165.62	50.8	0.00	326.00	191.50
				Totals: 45	**326.00**	**165.62**	**50.8**	**0.00**	**326.00**	**191.50**
1206A	34°55.5485'N	172°08.7536'E	1557.0	44	278.20	141.43	50.8	57.00	335.20	169.25
				Totals: 44	**278.20**	**141.43**	**50.8**	**57.00**	**335.20**	**169.25**
			Leg 197 Totals:	188	1481.00	752.75	50.8	1929.60	3410.60	860.50

Table T1

Table 2. Operations summary, Leg 197.

Proposed site	Site/Hole	Operations activity	Time (local)	Date (2001)	Time on hole (hr)	Time on site (hr)	Comments
HE-3A	1203A	Position on GPS	17:15	11-Jul			Spud at 1630 hr, 12 Jul
		Depart site	7:30	25-Jul	326.25	326.25	Depth objective exceeded
					Total:	**326.25**	
HE-3	1204A	Position on GPS	15:30	25-Jul			Spud at 2030 hr, 25 Jul
		Clear rotary table	15:00	28-Jul	71.50	71.50	Terminated due to plugged bit
	1204B	Clear rotary table	15:00	28-Jul			Spud at 2015 hr, 28 Jul
		Depart site	21:00	1-Aug	102.00	102.00	Time expired at 138.5 m basement penetration
					Total:	**173.50**	
HE-4A	1205A	Position on GPS	6:30	4-Aug			Spud at 1230 hr, 4 Aug
		Depart site	6:00	12-Aug	191.50	191.50	Time expired at 283.3 m basement penetration
					Total:	**191.50**	
HE-6A	1206A	Position on GPS	21:15	13-Aug			Spud at 0215 hr, 14 Aug
		Depart site	22:30	20-Aug	169.25	169.25	No logging; TD = 278.2 m basement penetration
					Total:	**169.25**	
				Total hours:	**860.50**		
				Total days:	**35.85**		

Table T2

Figure F1

Figure F2

A

Inclination (°)

Predicted inclination
from Pacific APWP

B

Paleolatitude (°)

Present-day latitude of Hawaii

C

S (°)

1.

2.

Estimated VGP scatter for:
1. 45–80 Ma
2. 80–110 Ma

Inclination groups

D

33n

Detroit

82

81

Hawaii
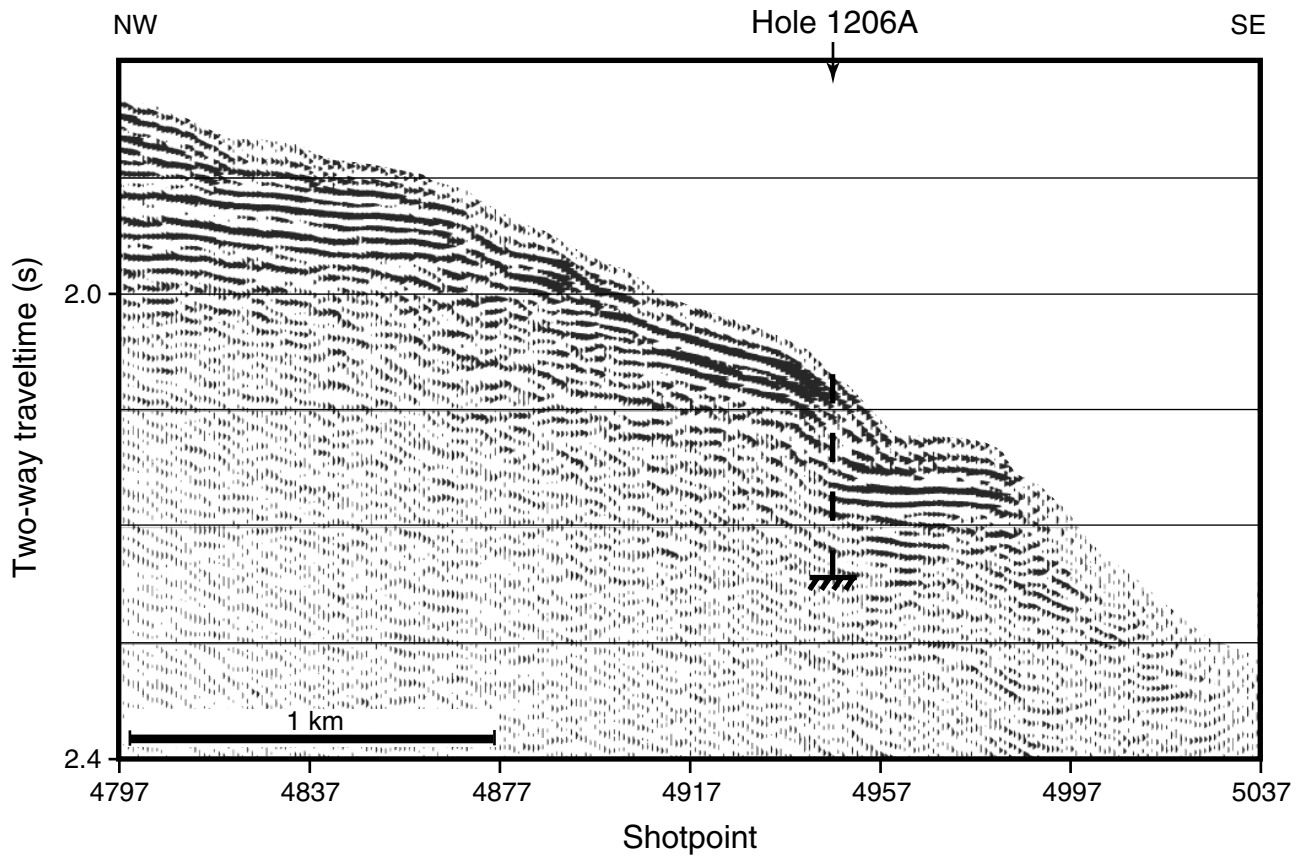
Primary
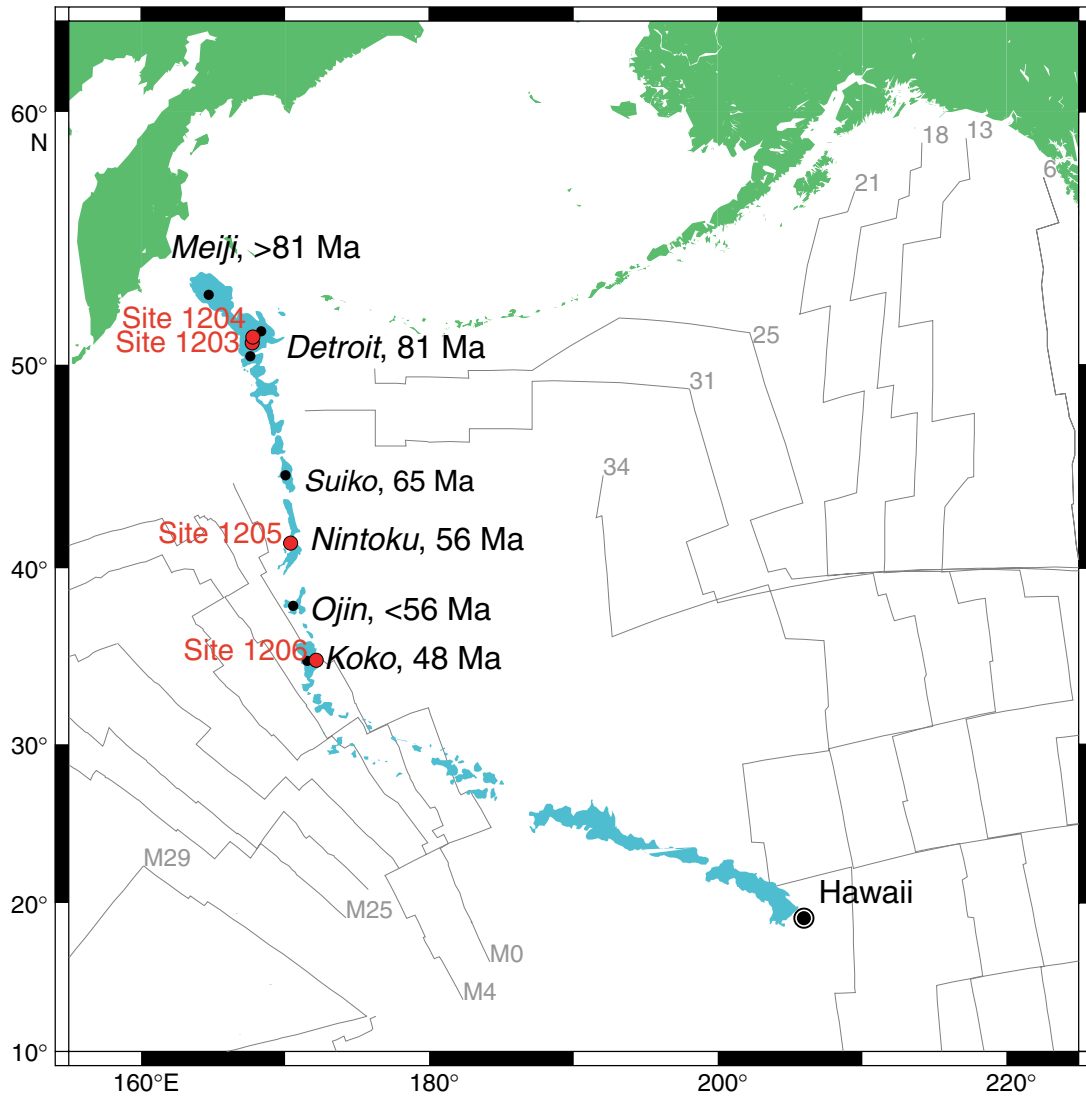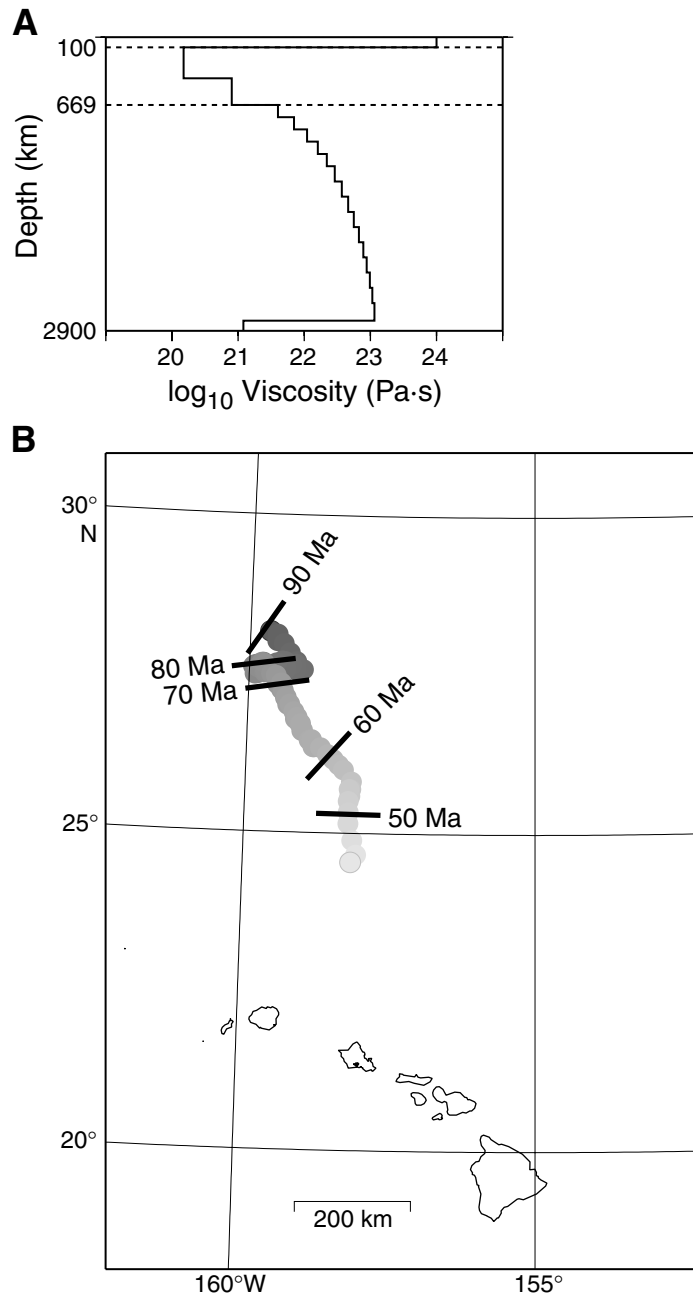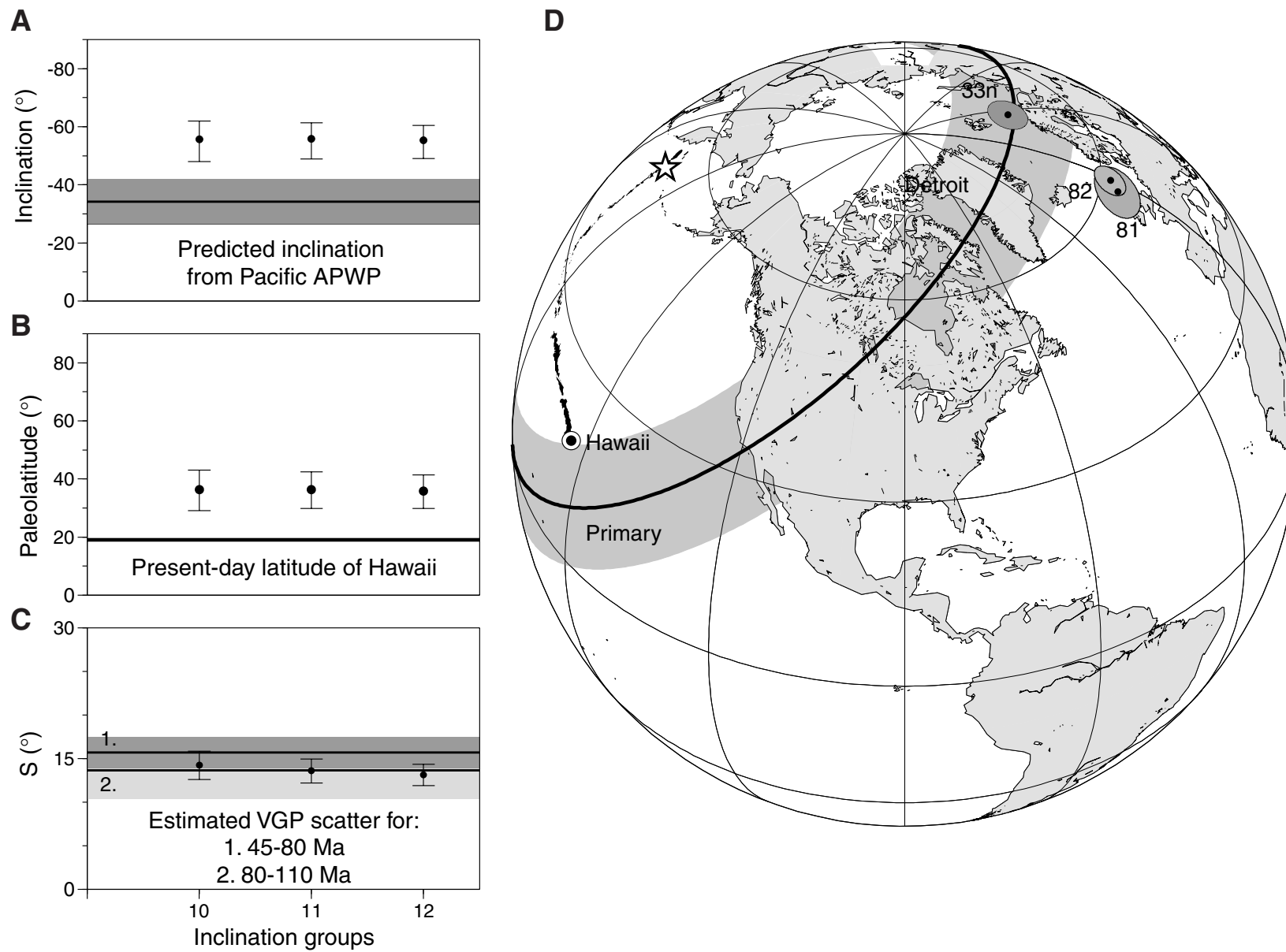
Figure F3
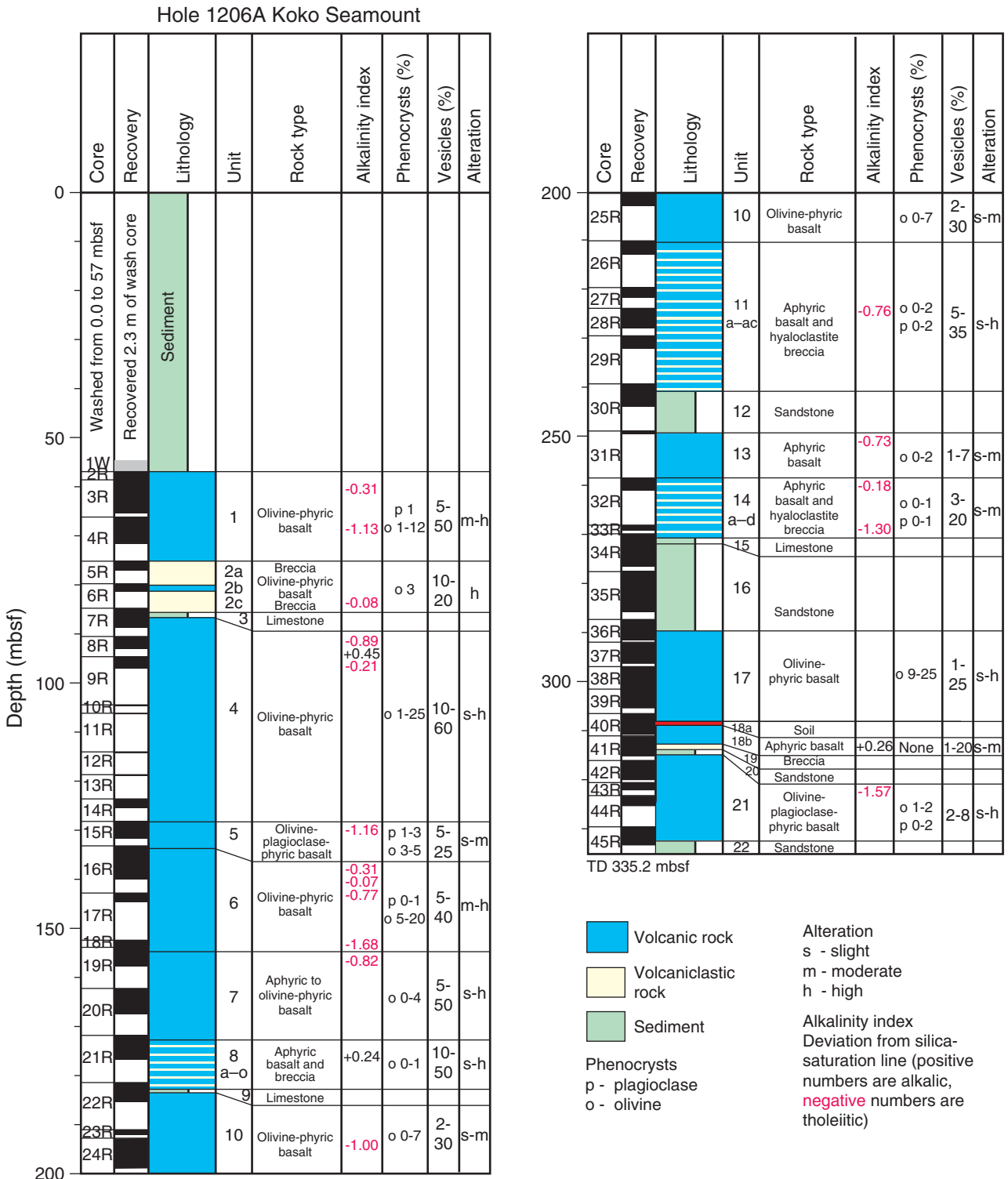
Figure F4
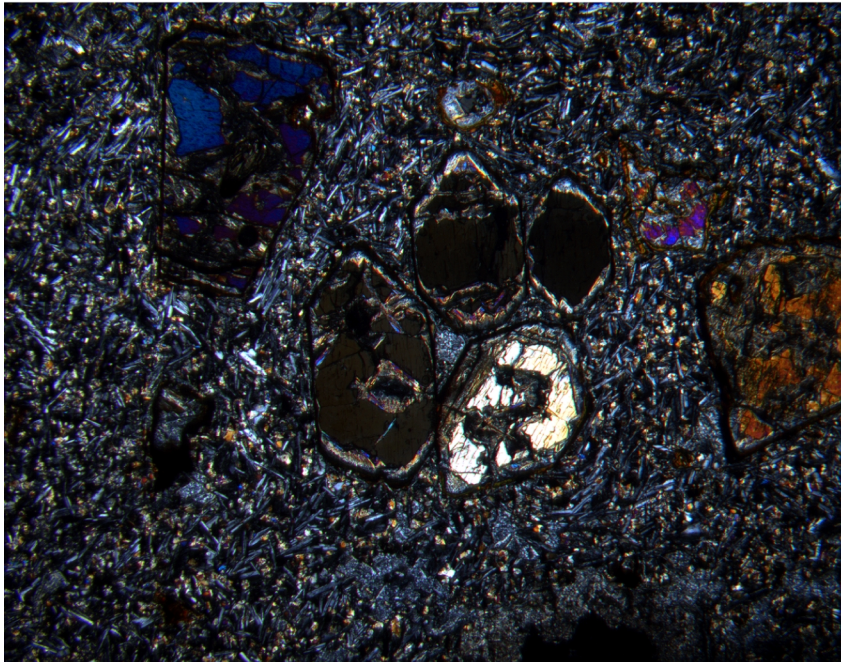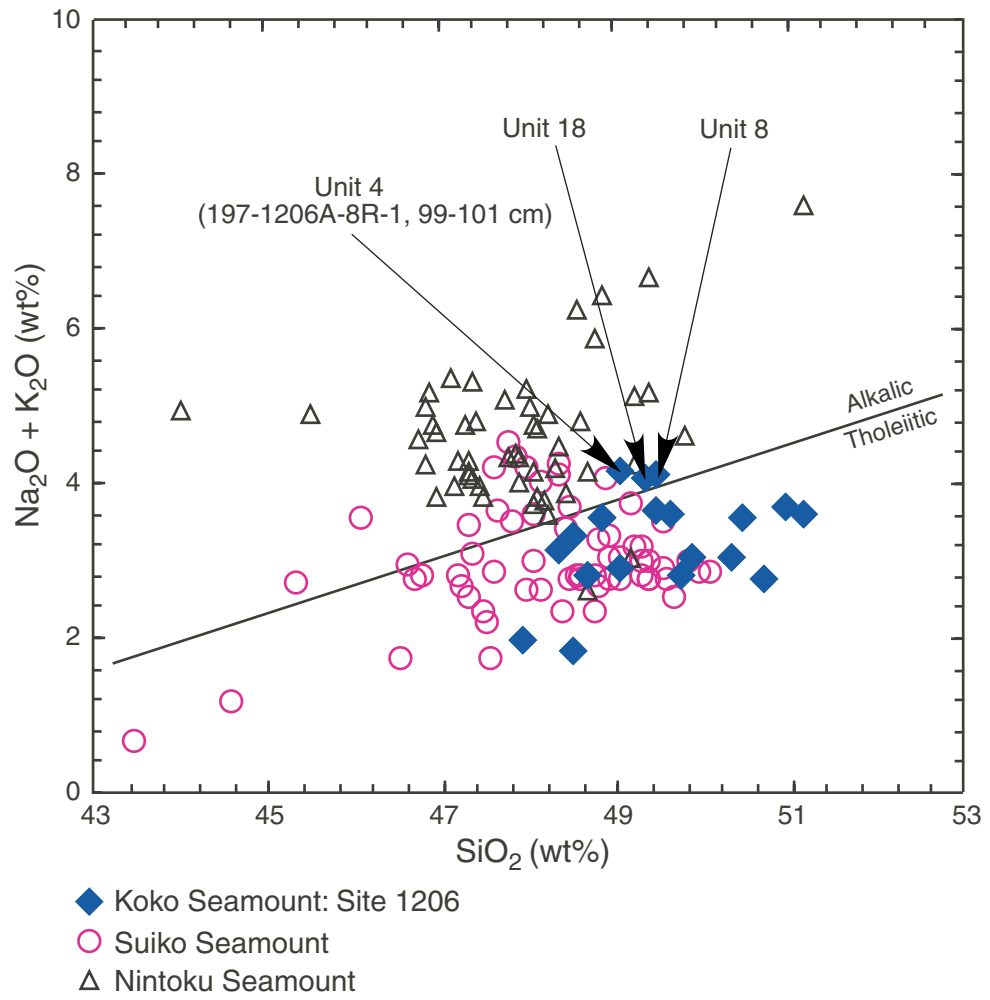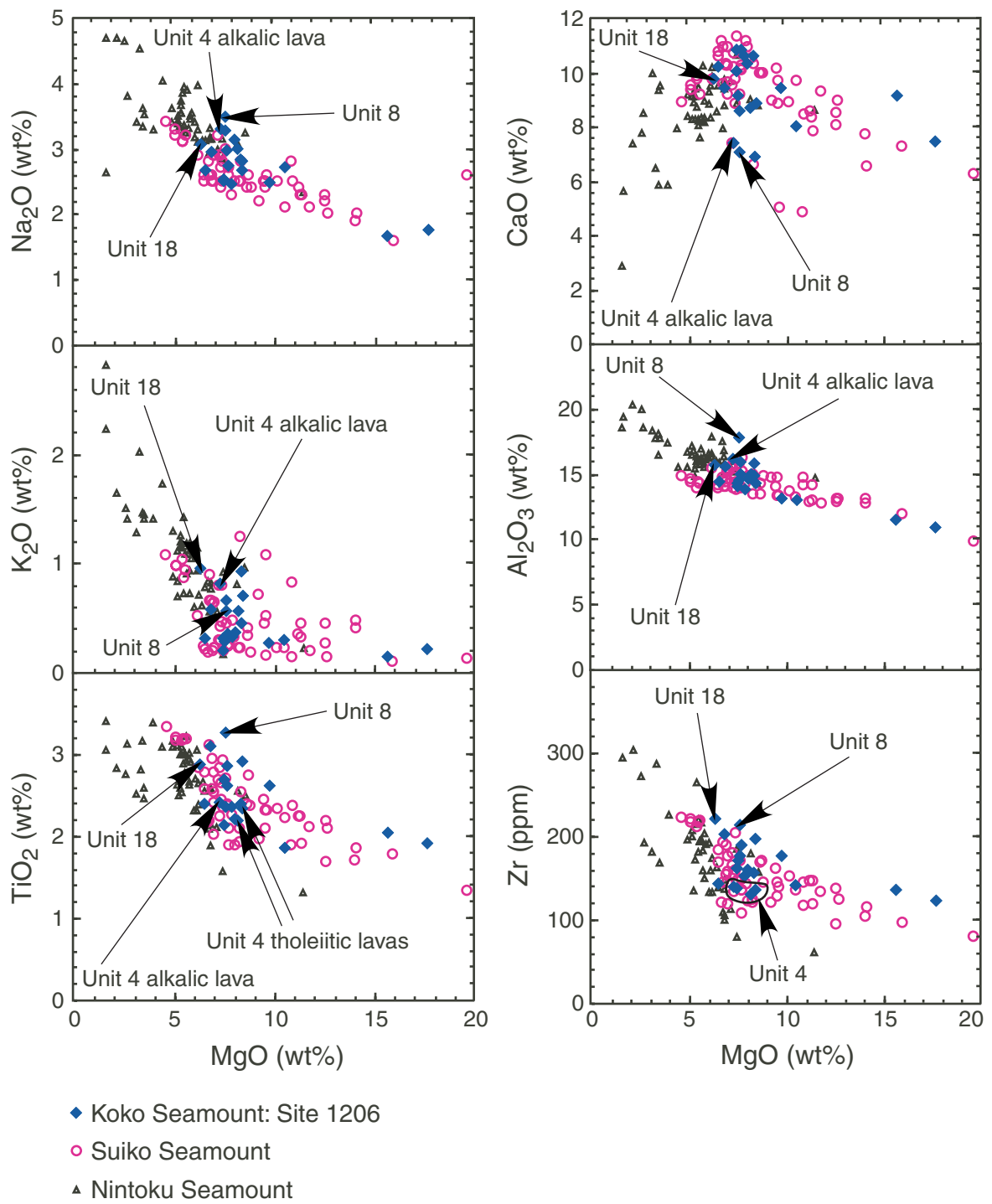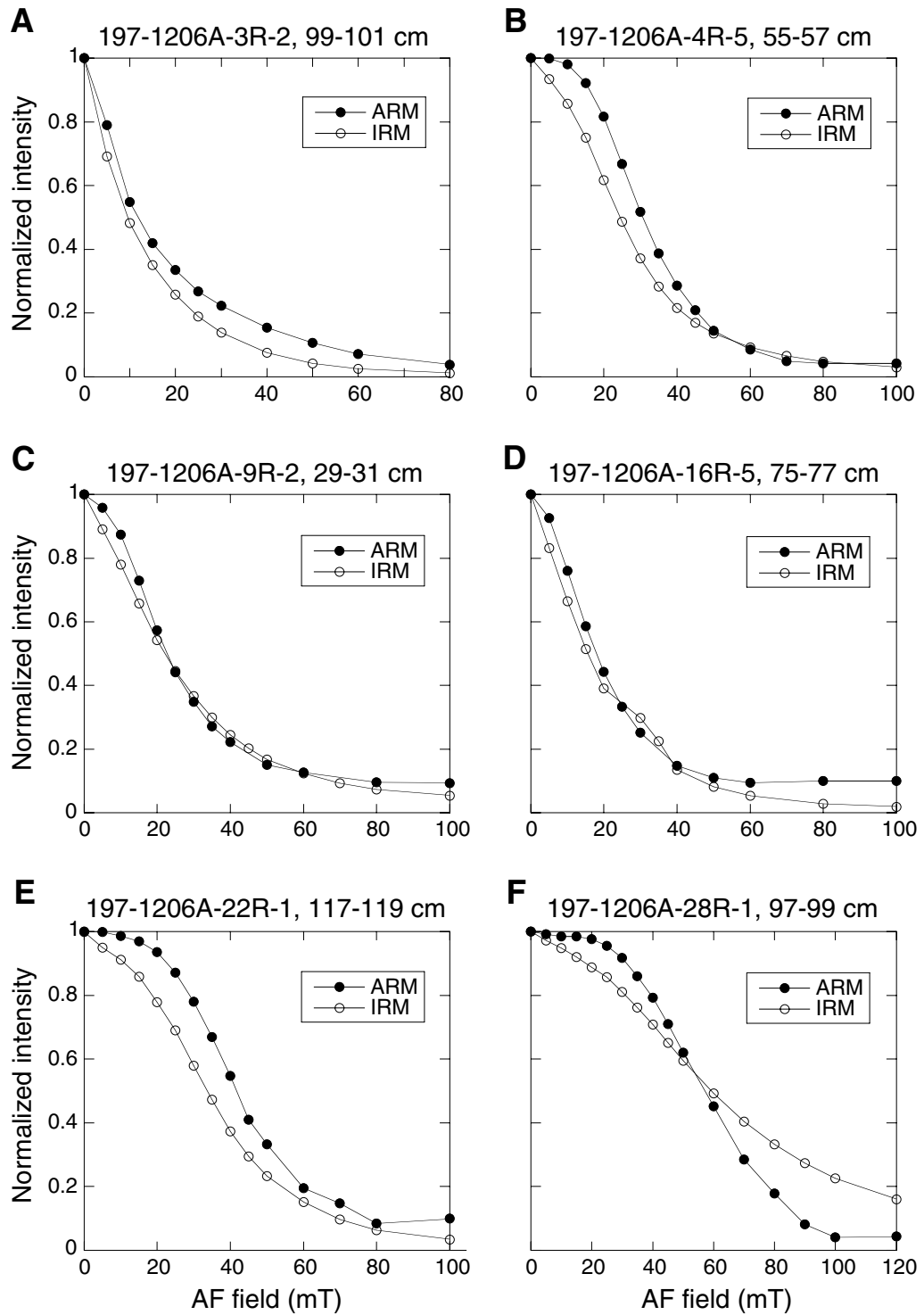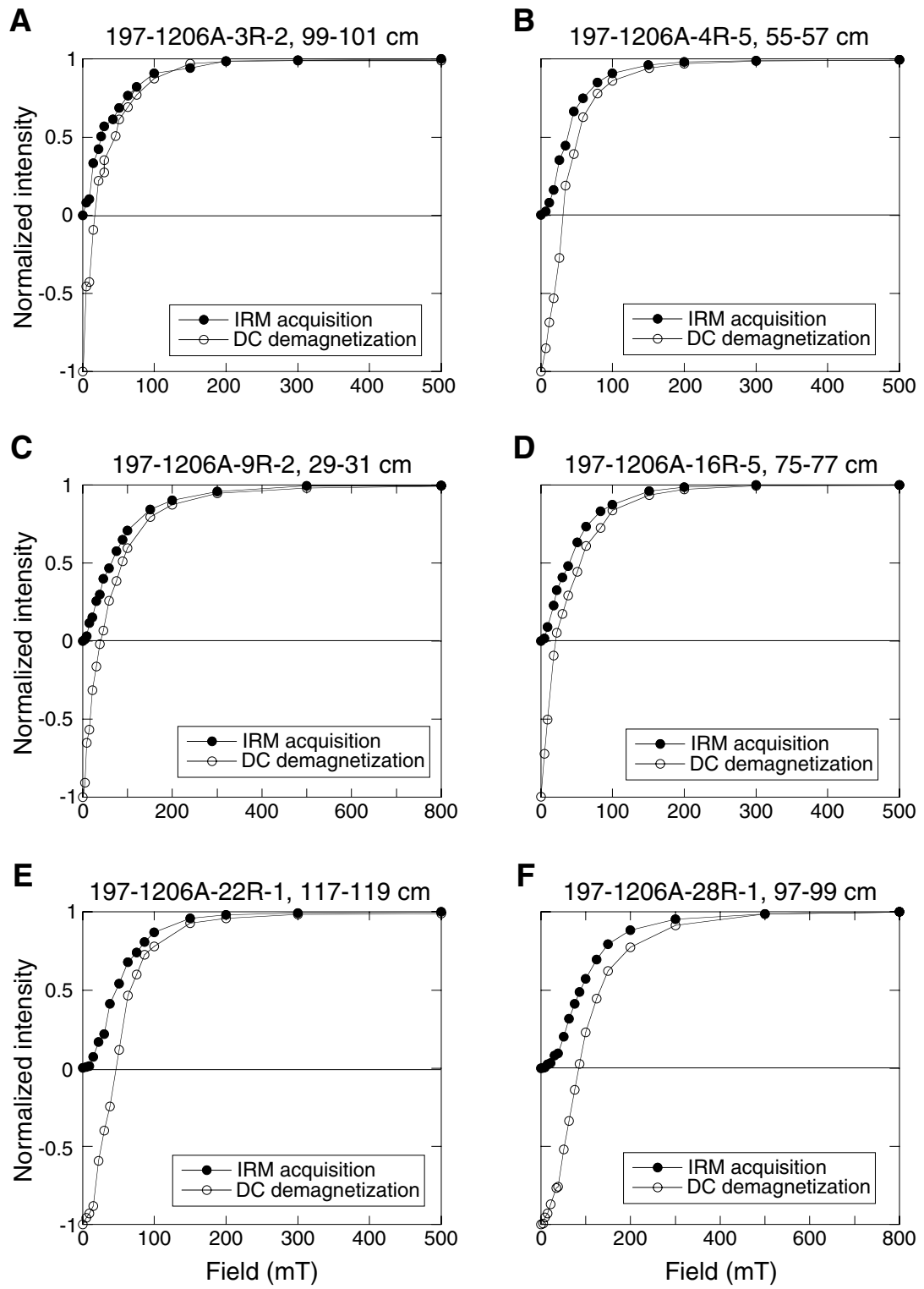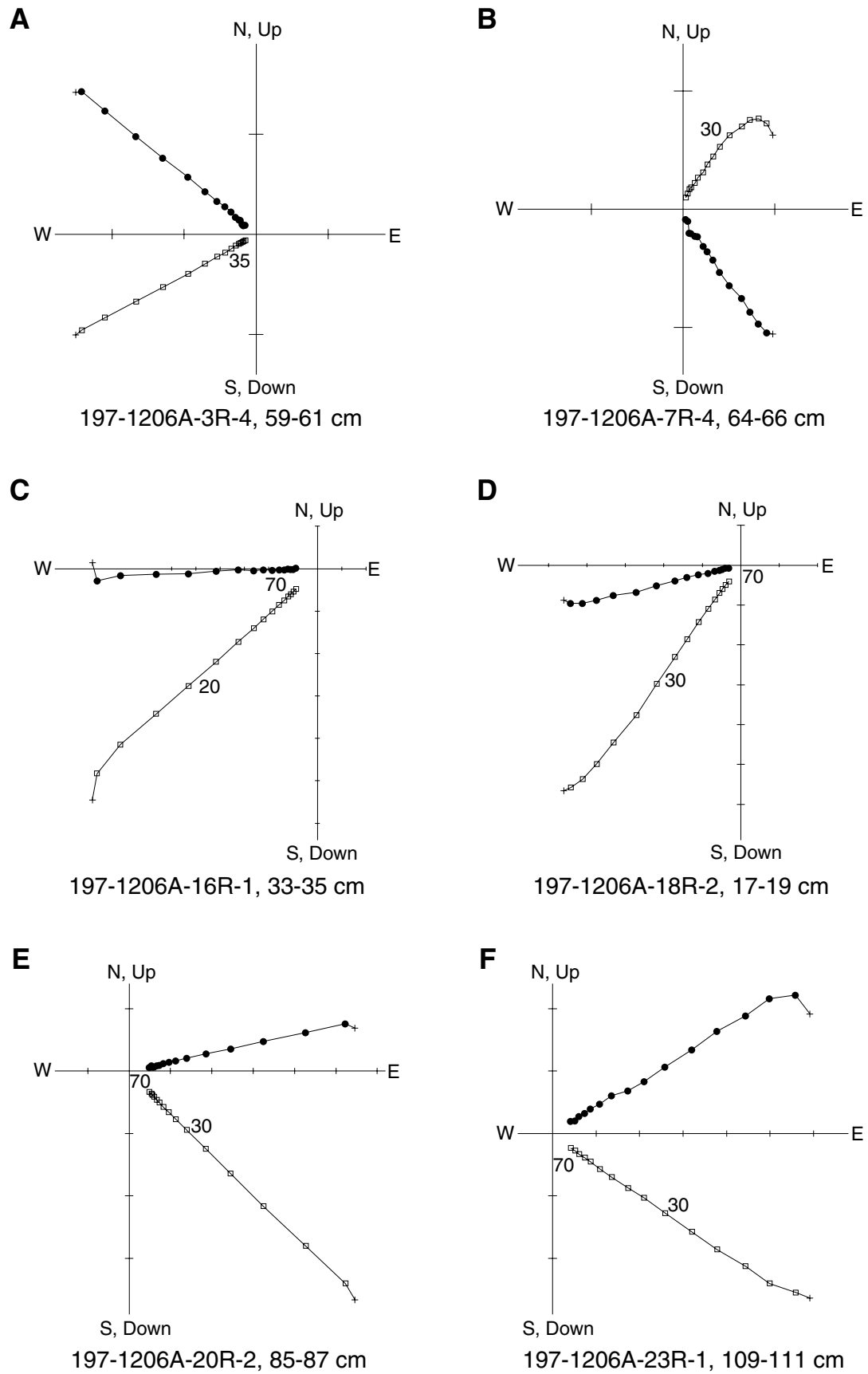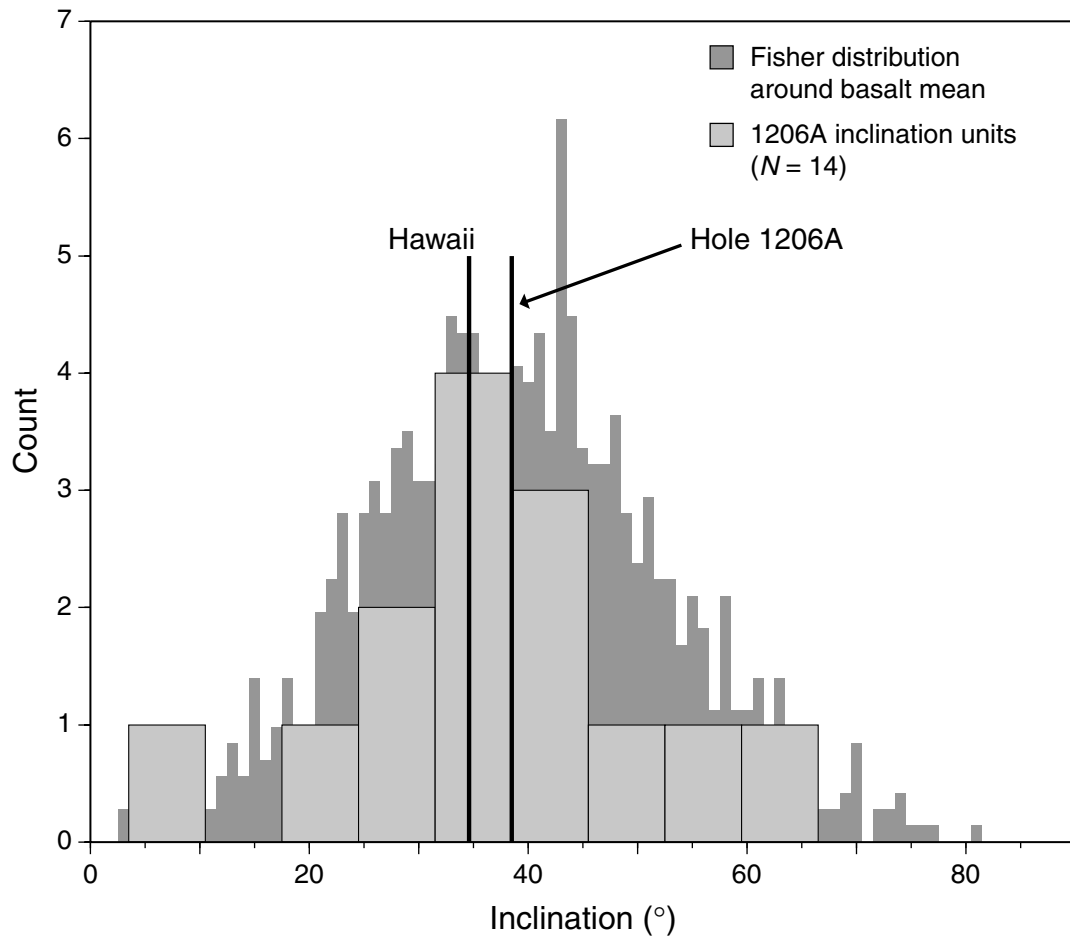
A

B
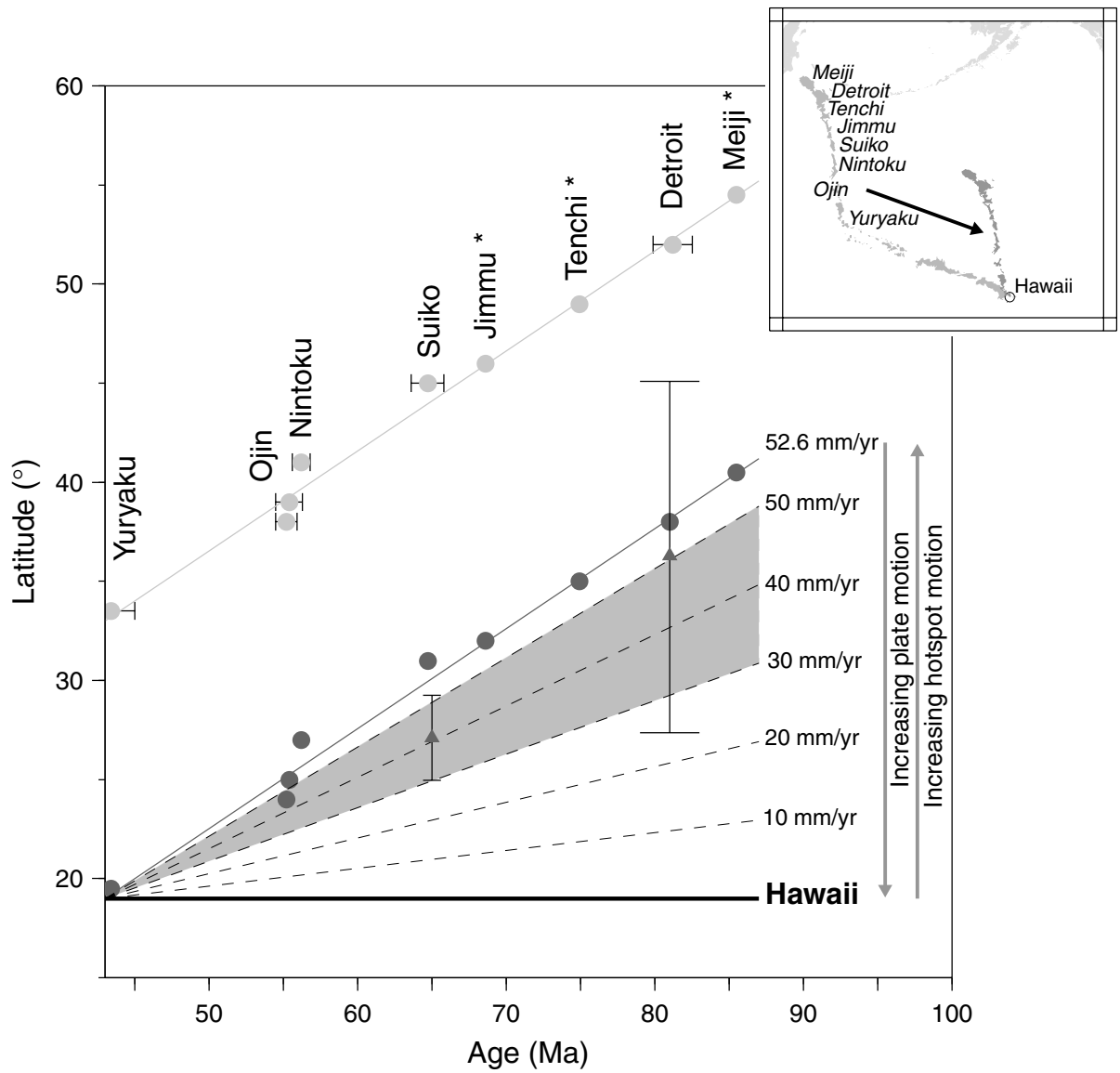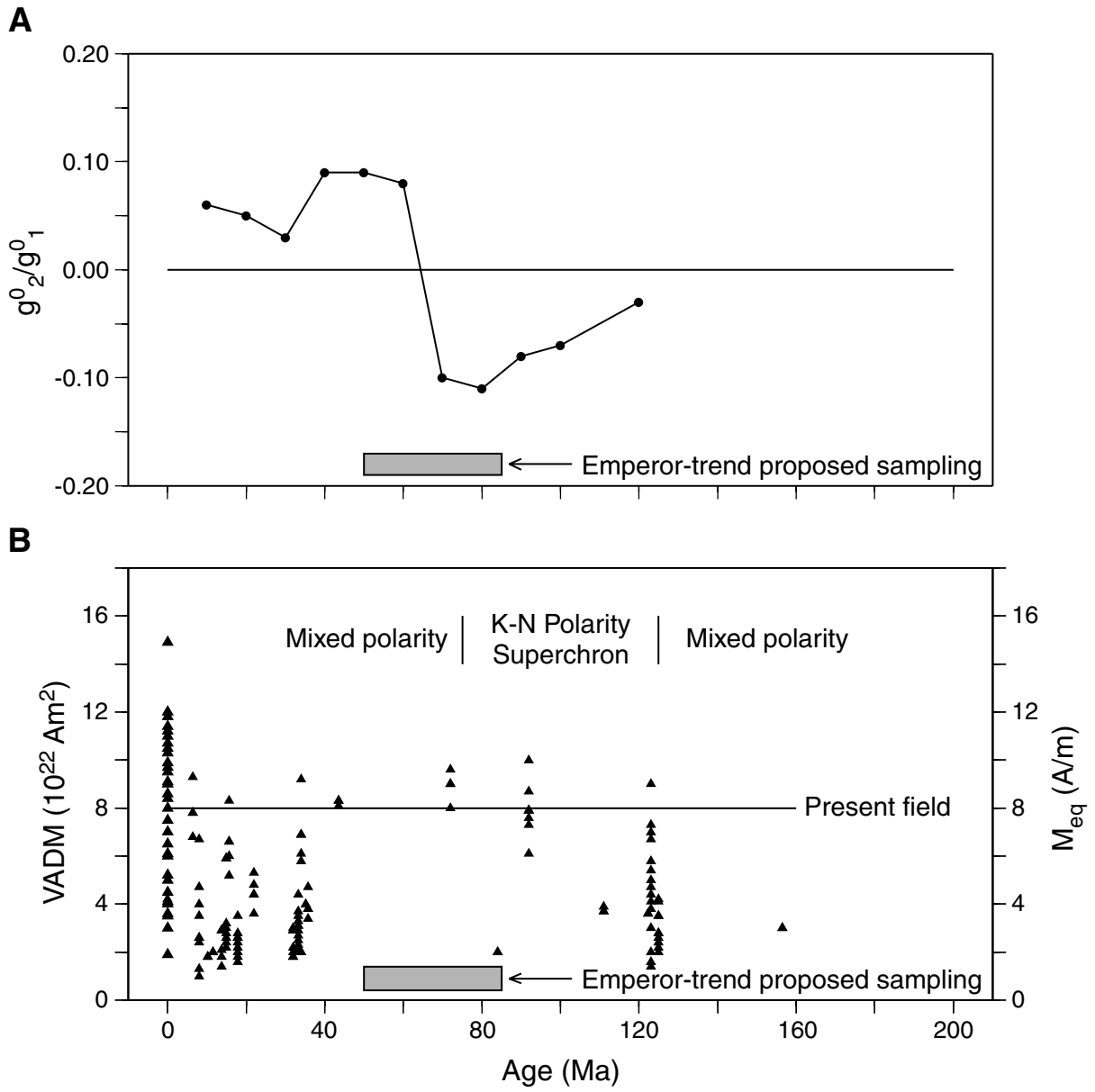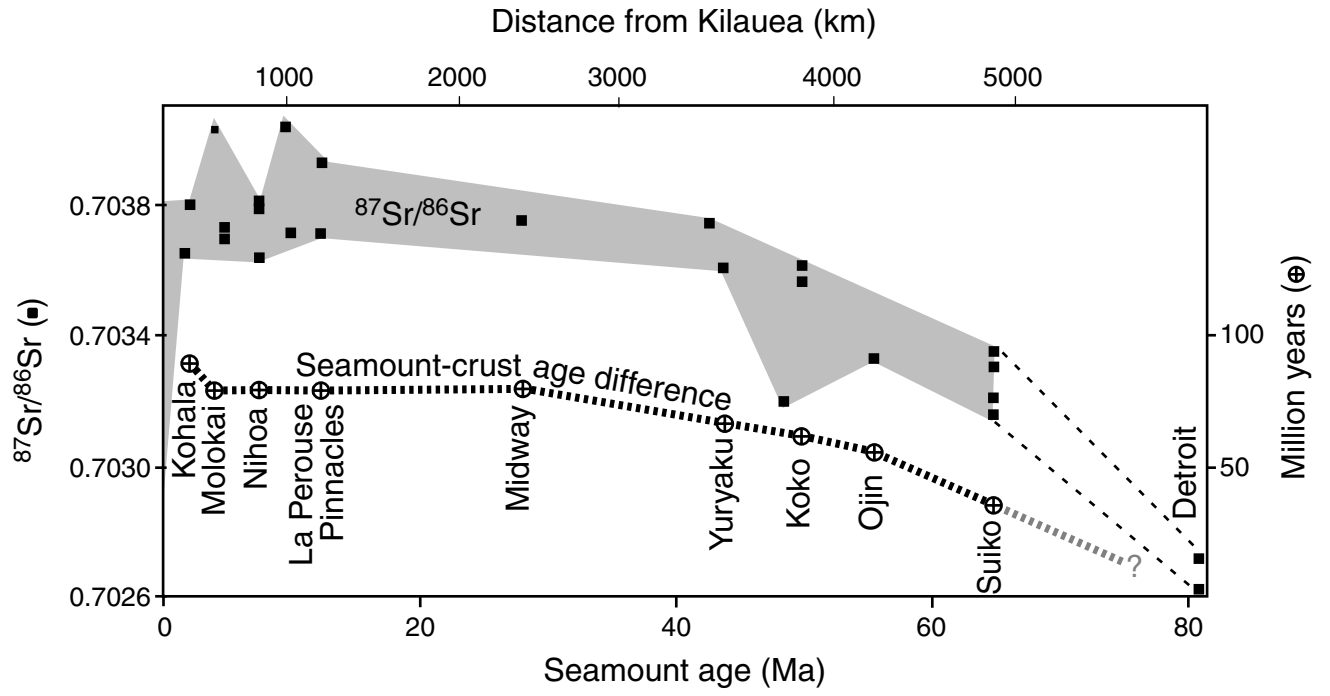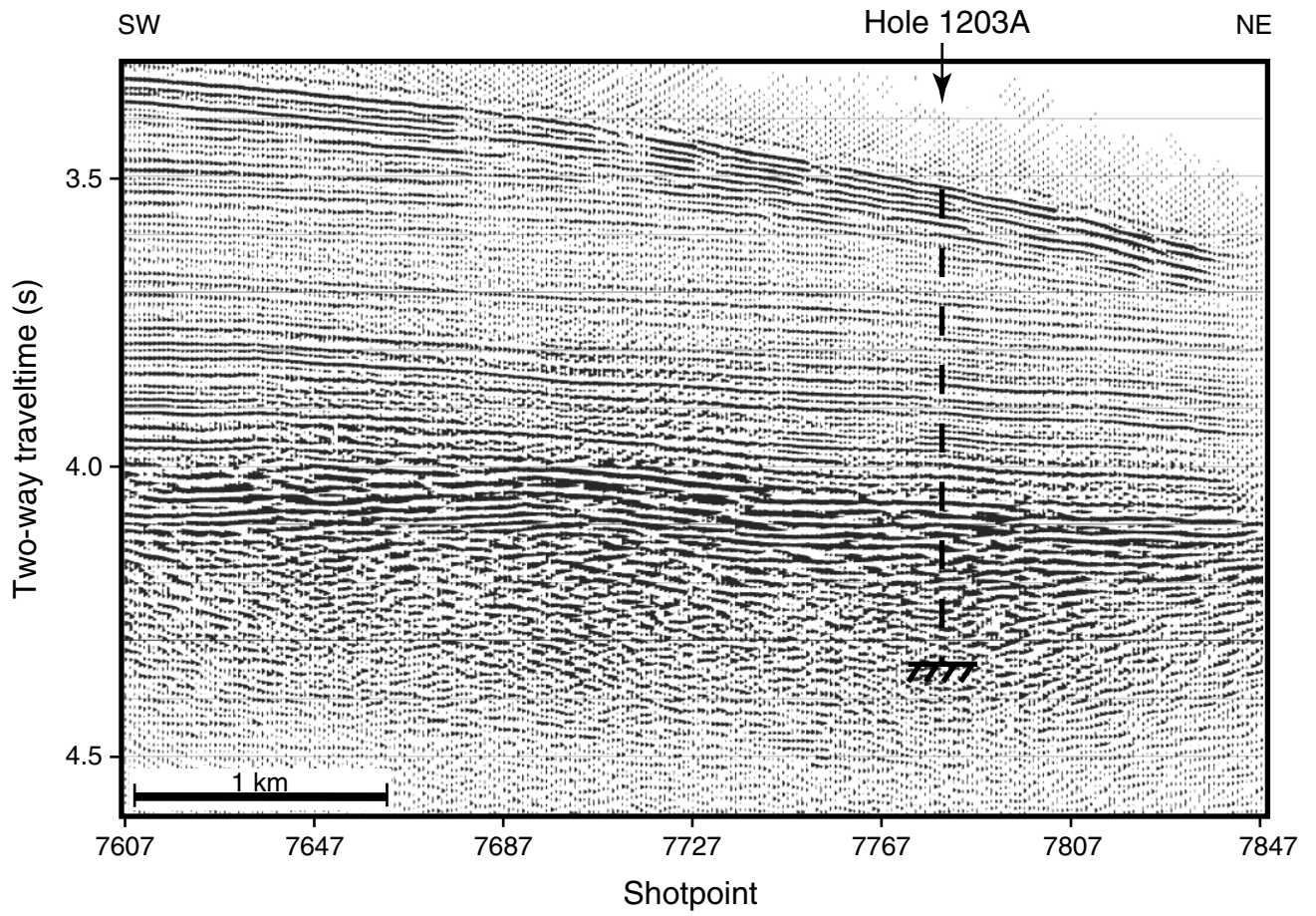
Figure F5

Figure F6

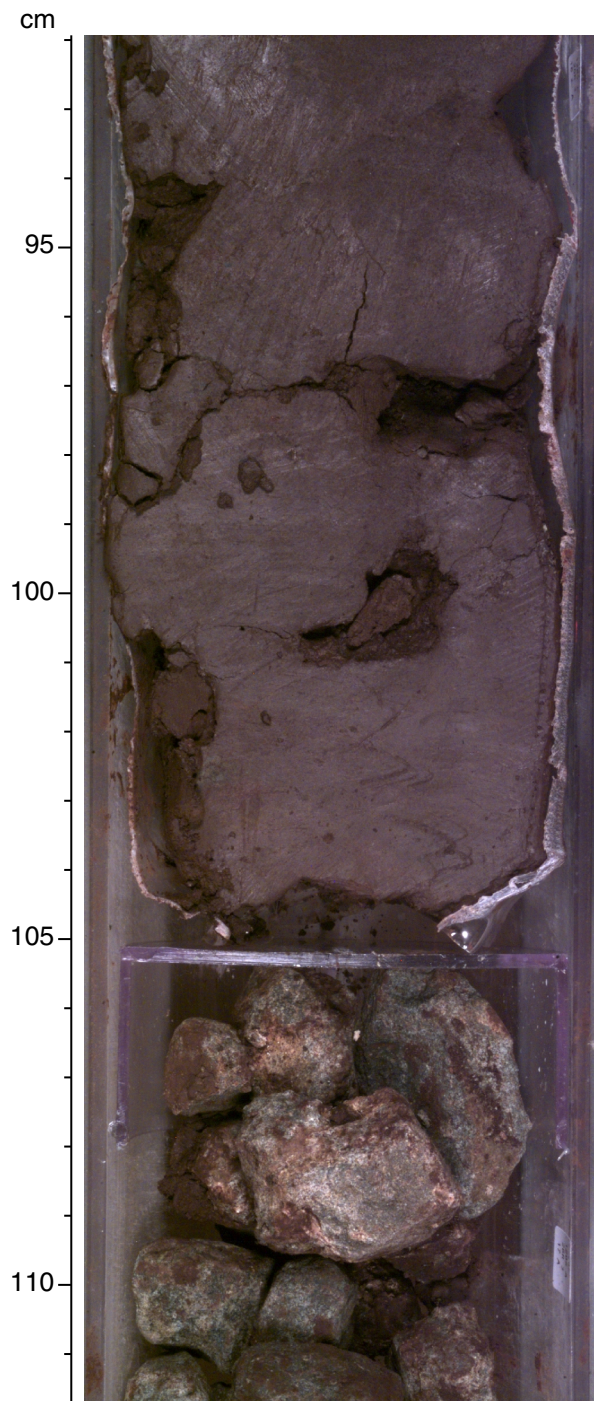Figure F7
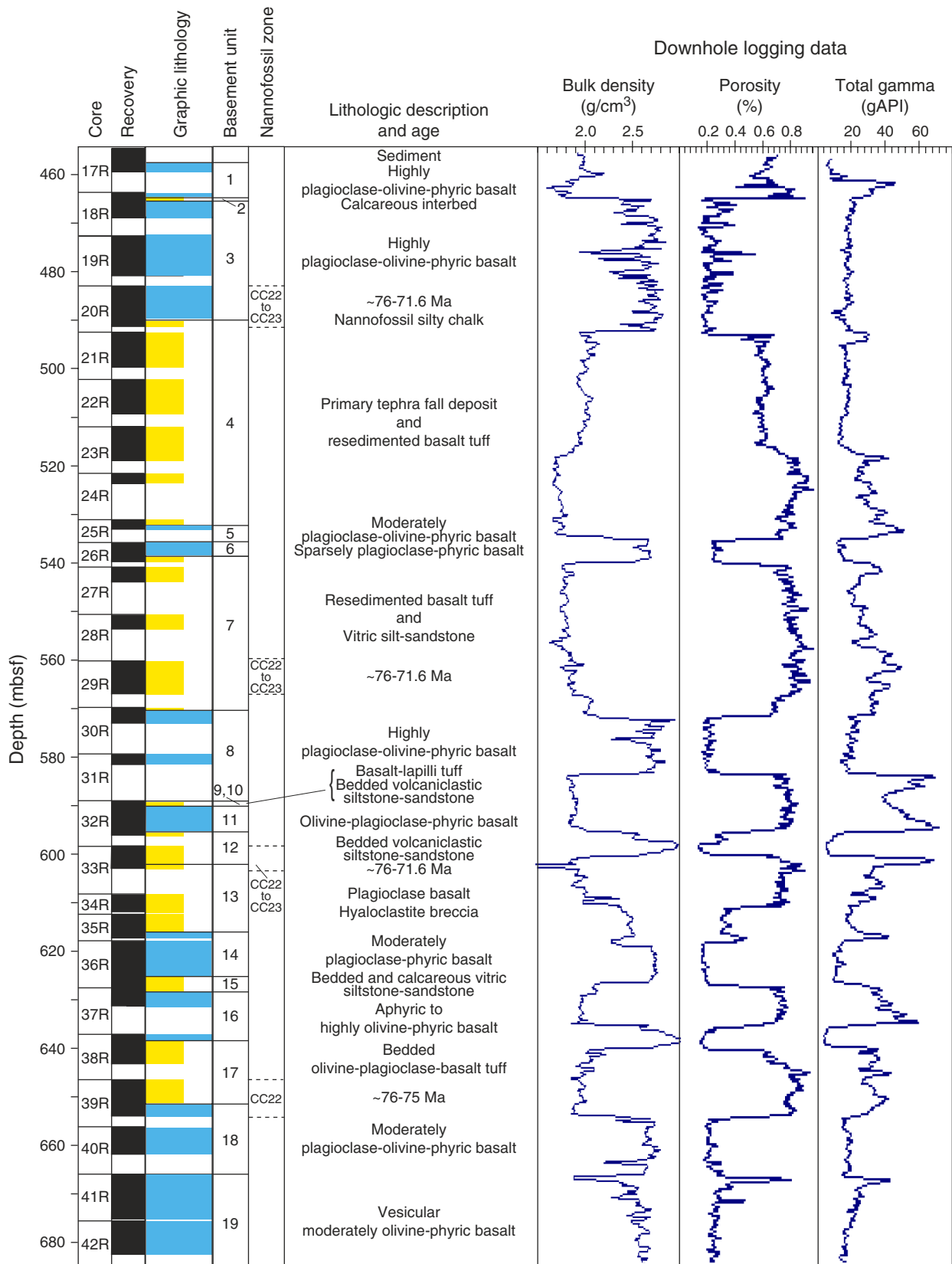
Figure F8
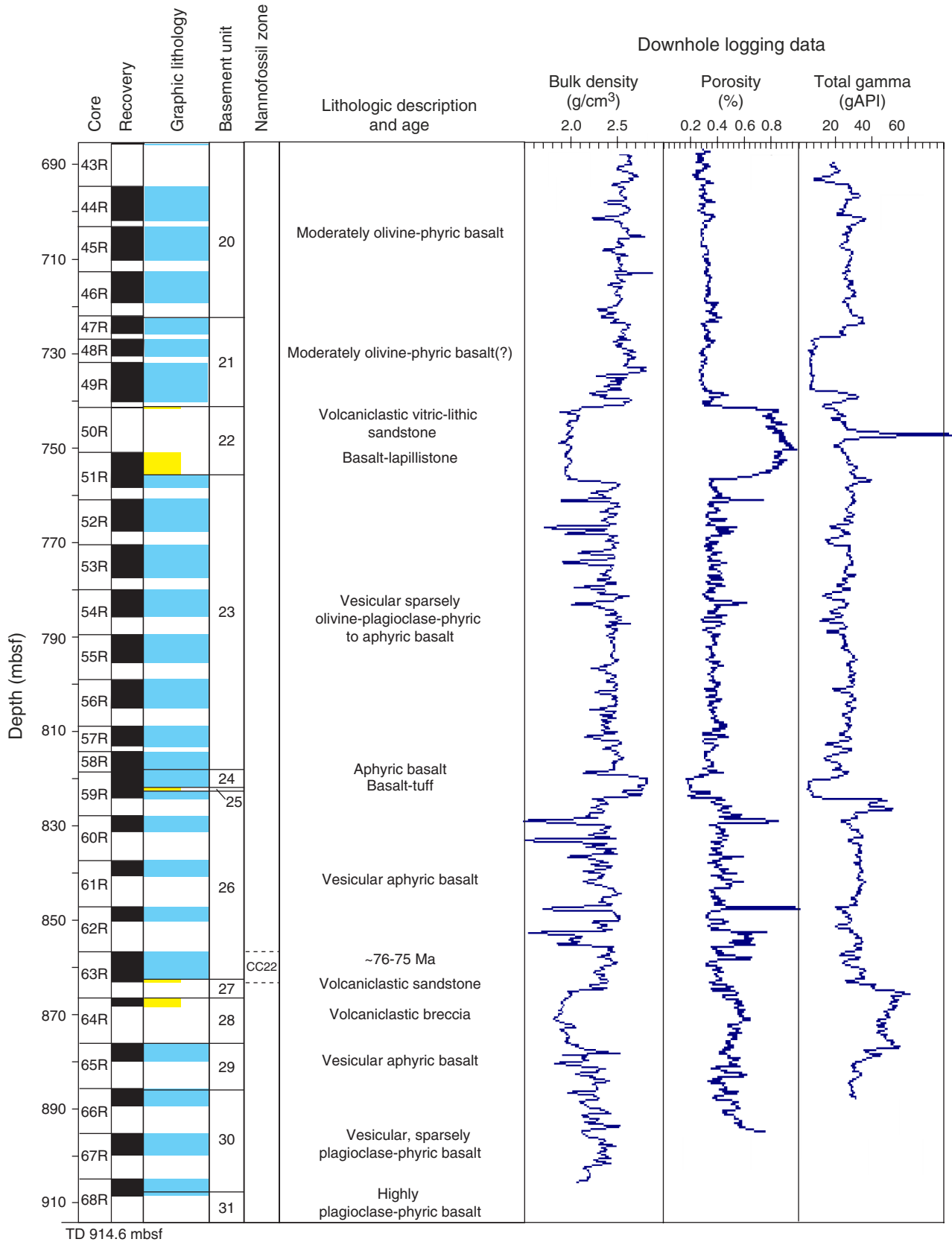
Figure F8 (continued)
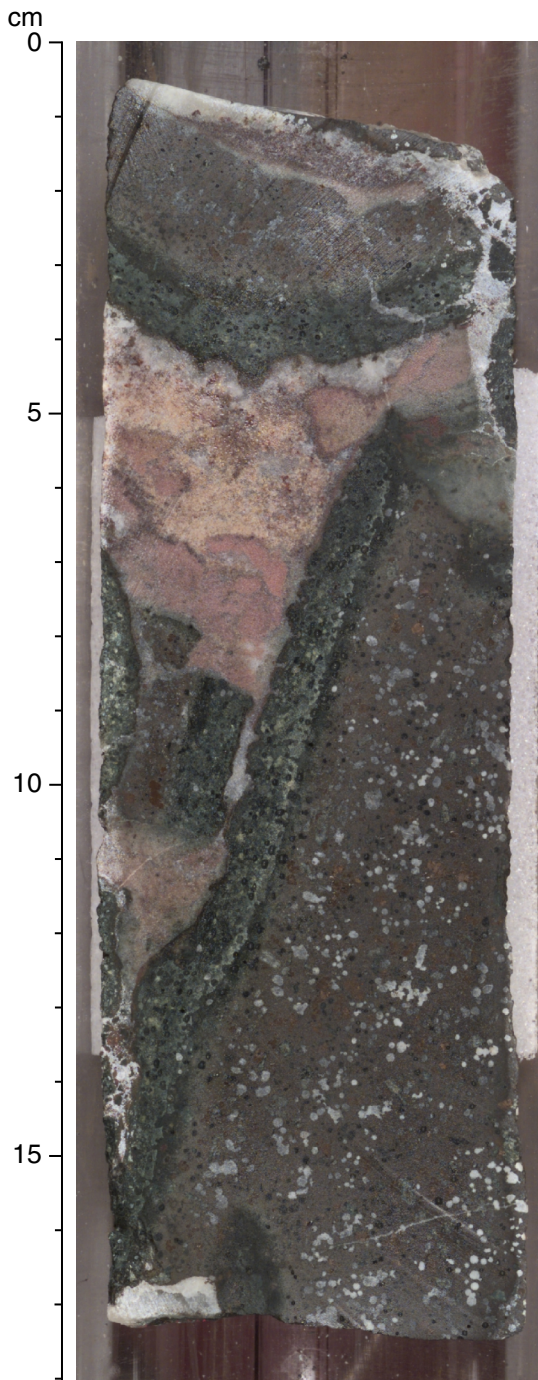
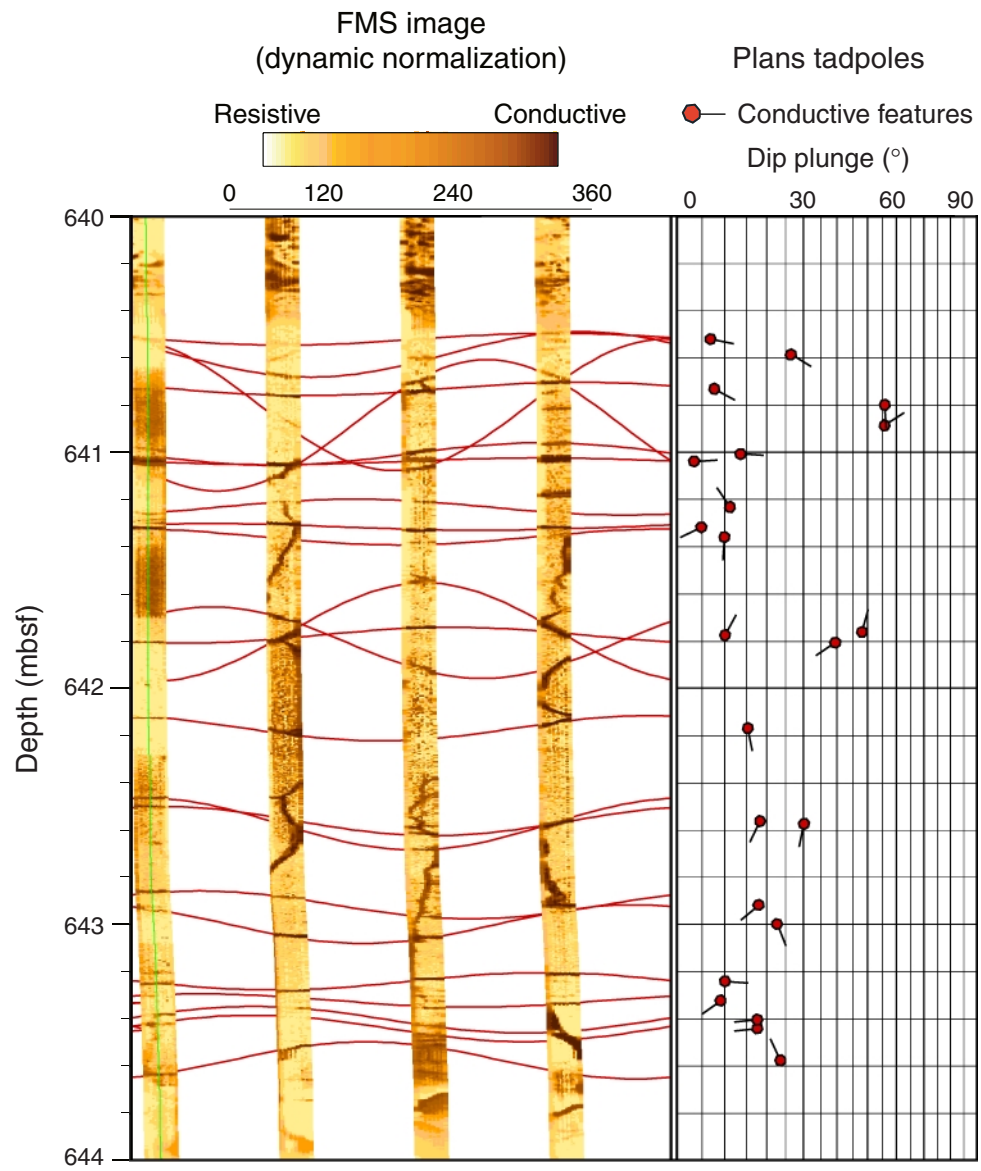Figure F9

A
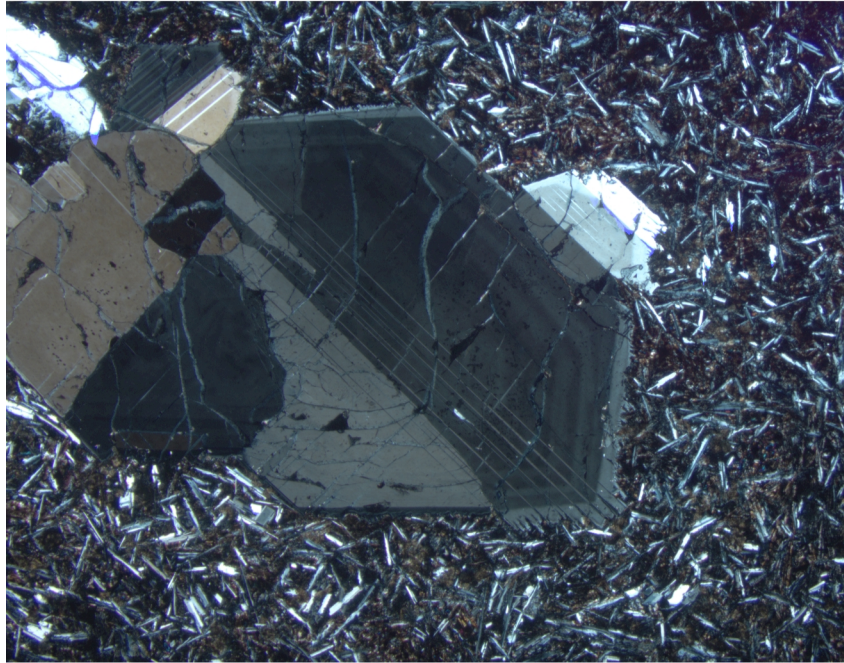
B

Figure F10
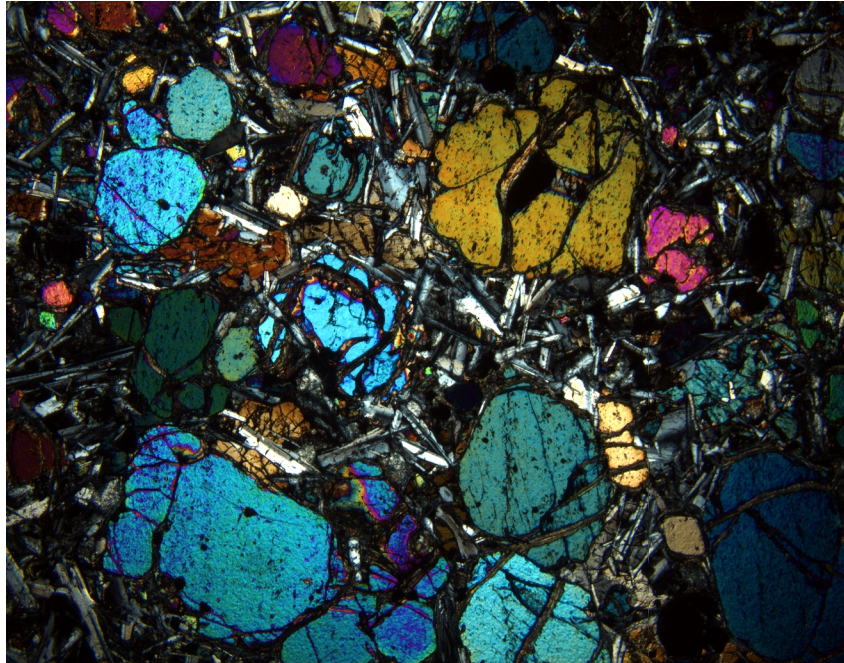
Figure F11
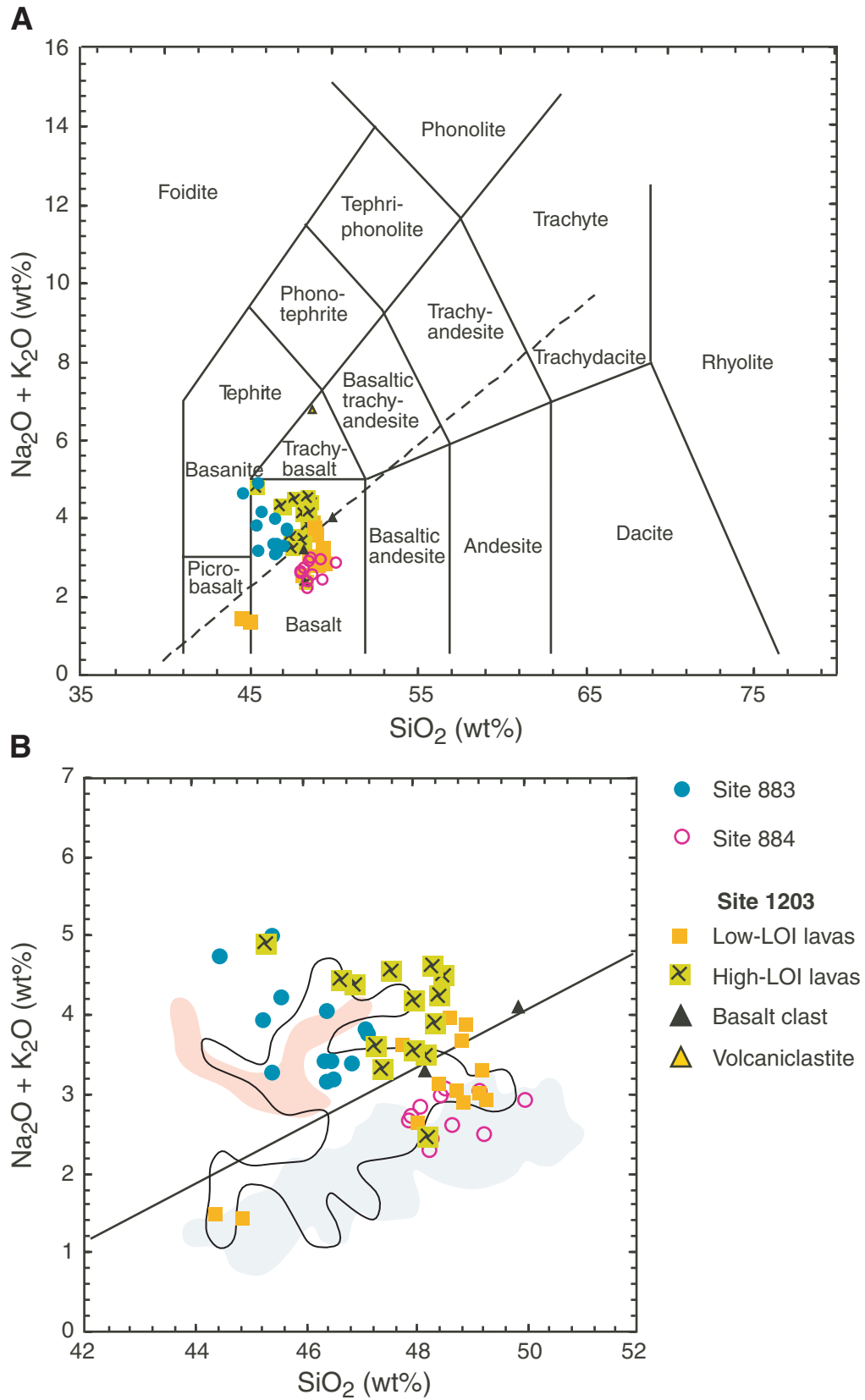
Figure F12
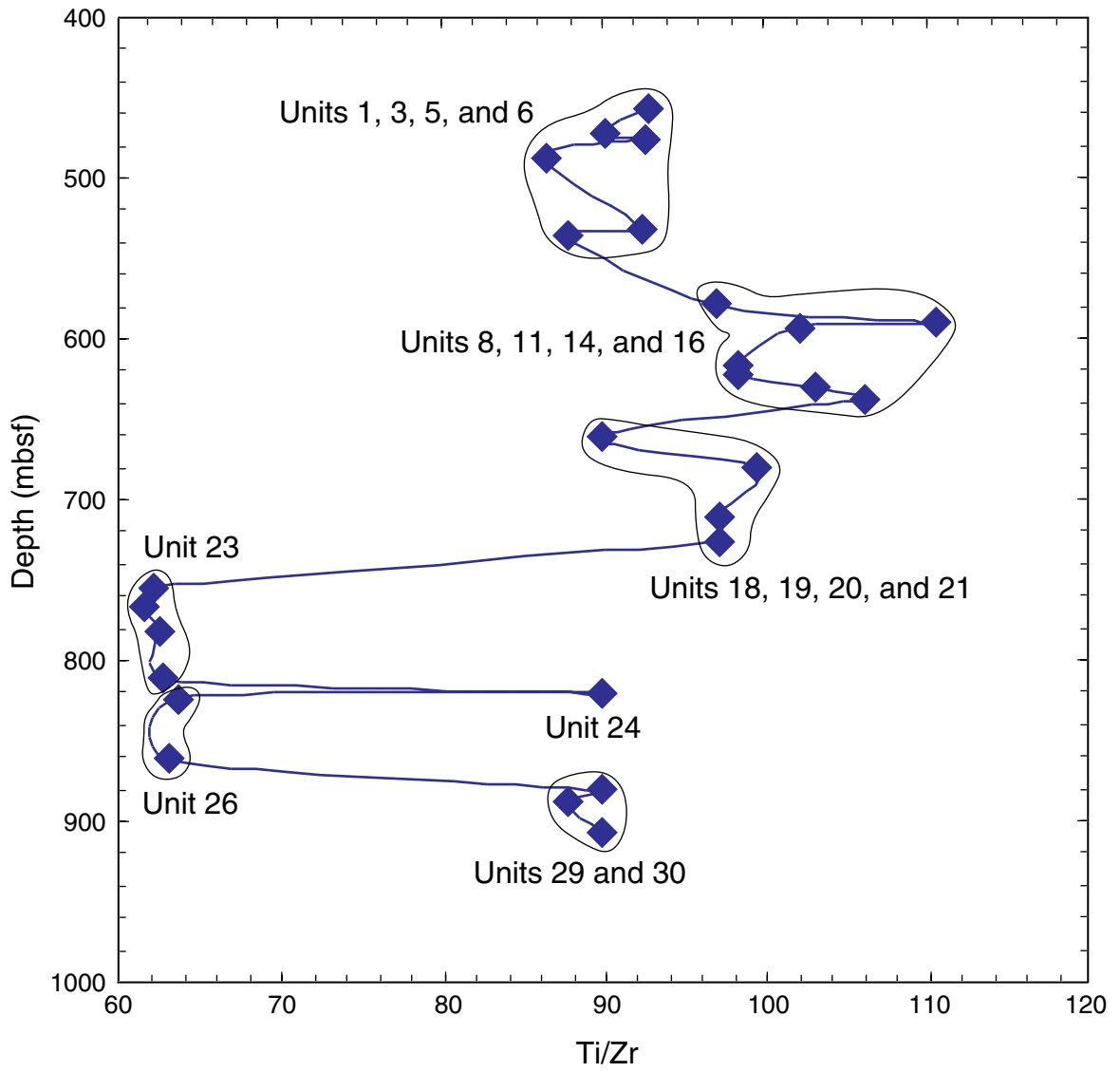
Figure F13
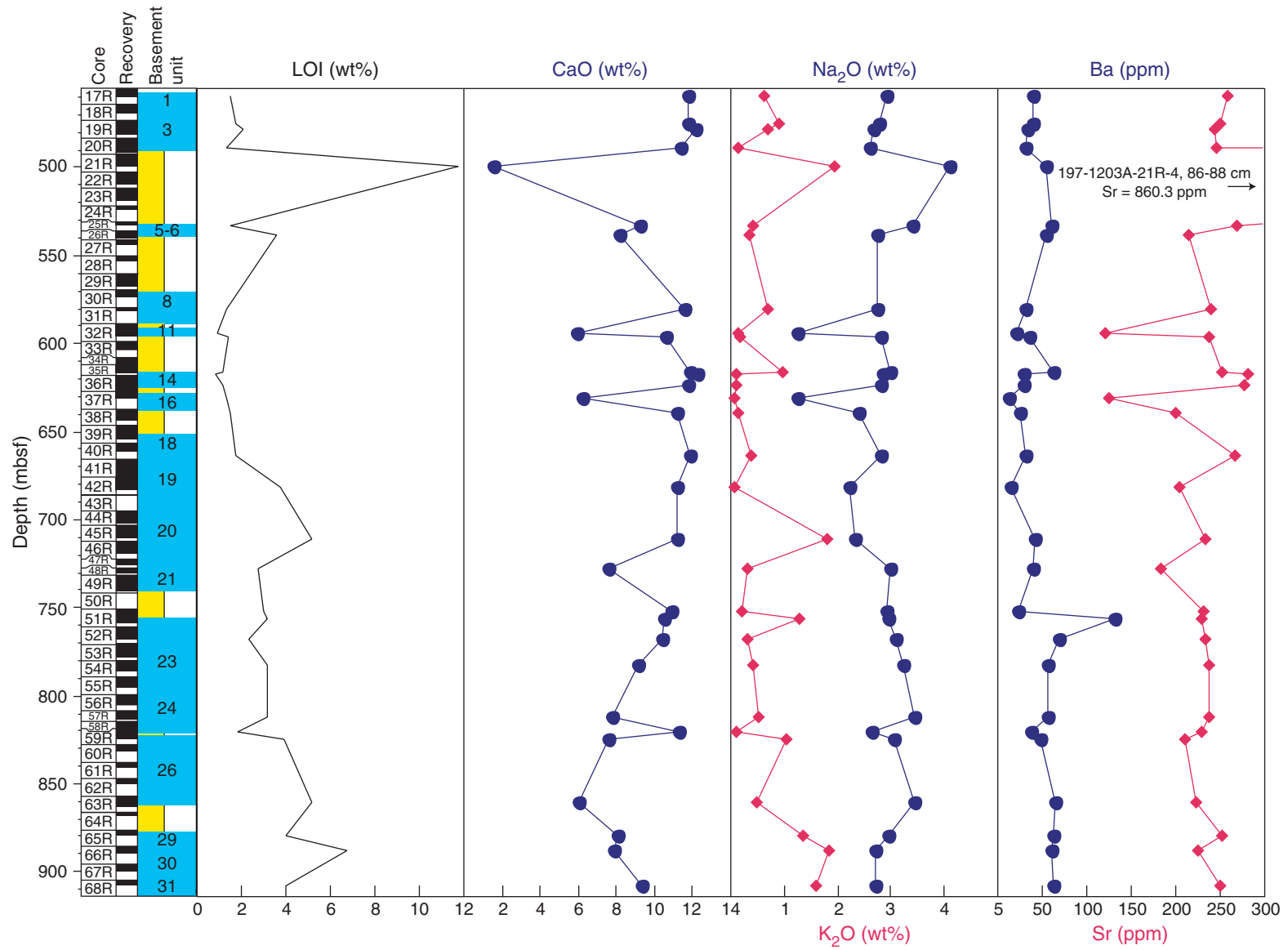
Figure F14
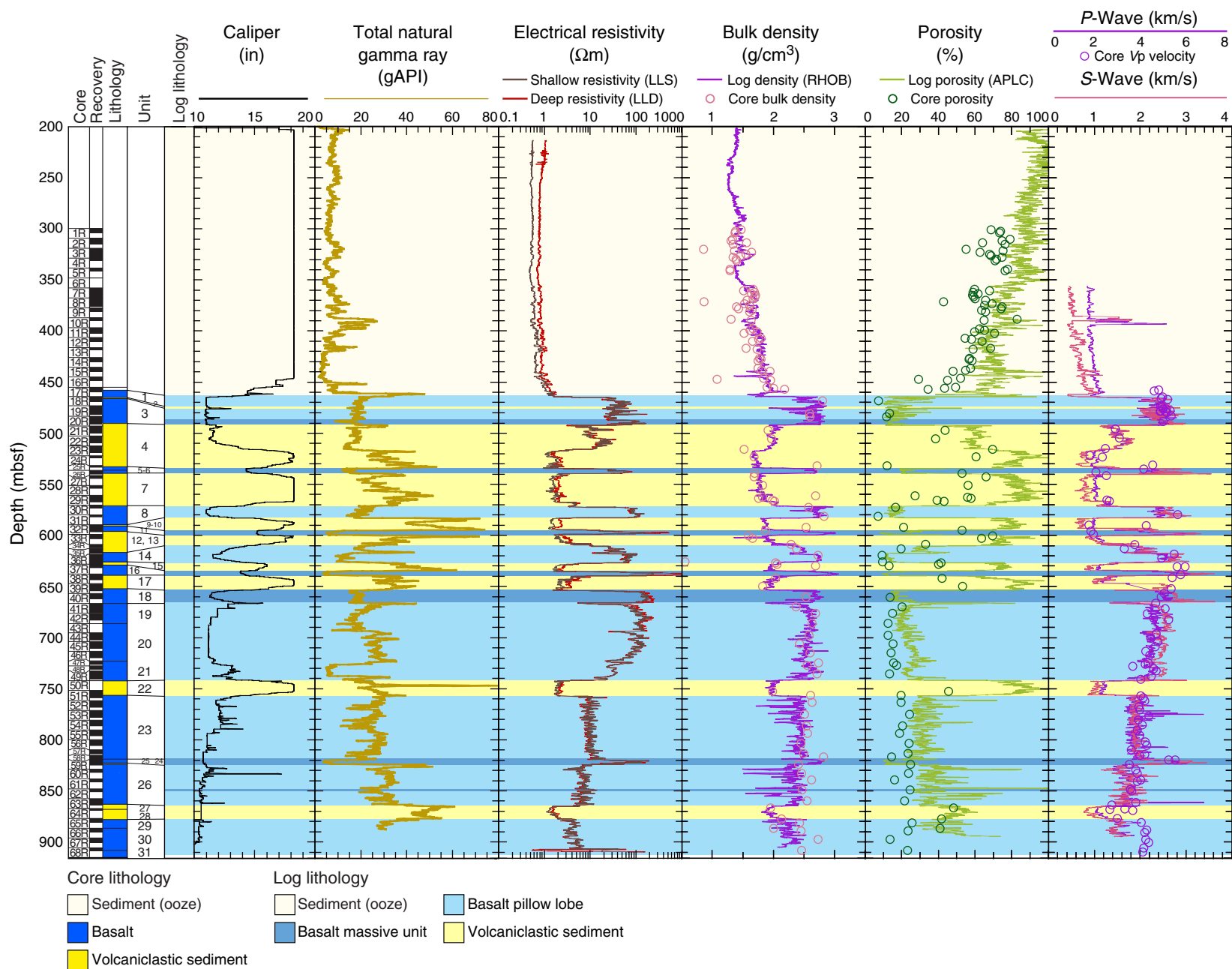
Figure F15
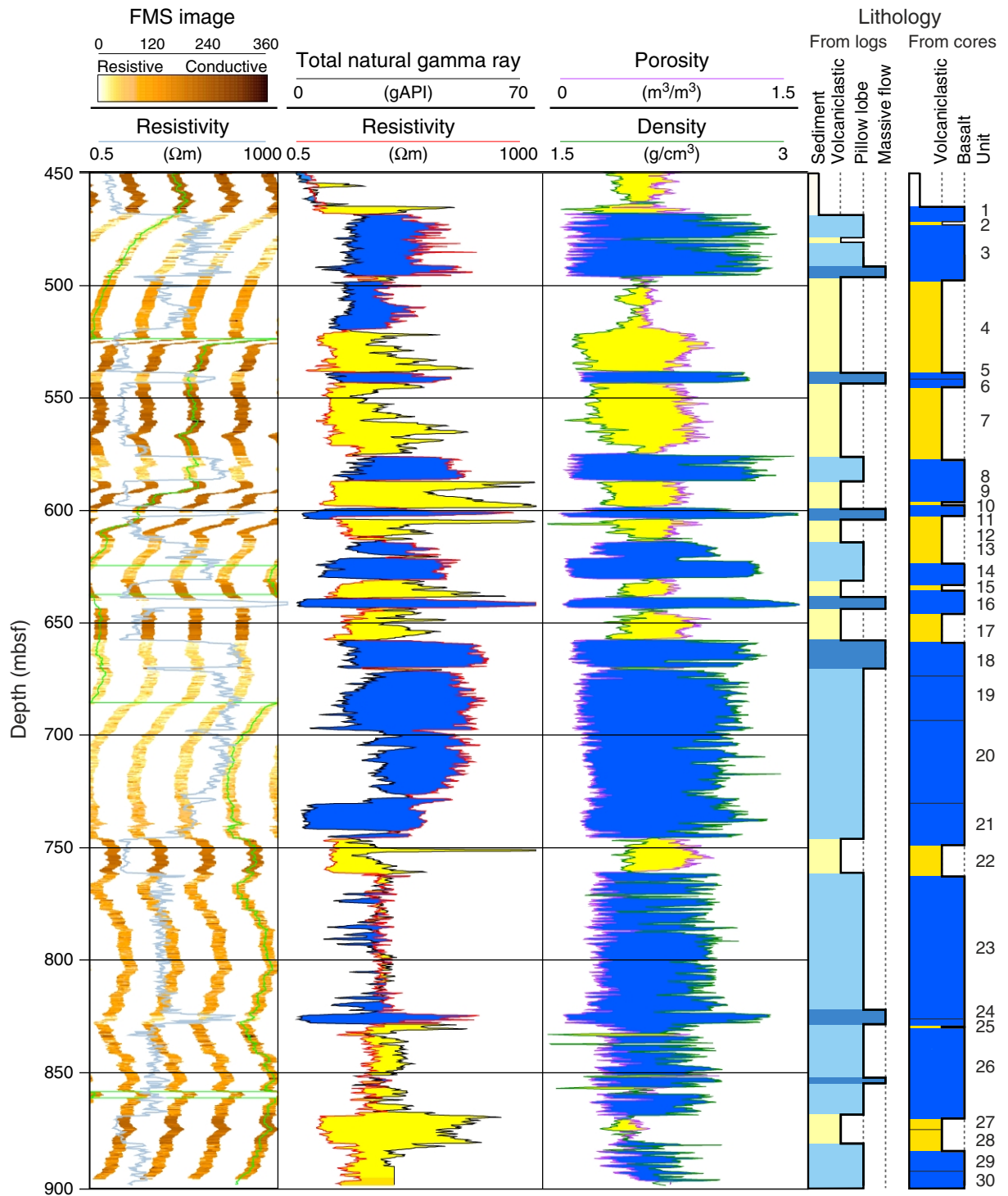
Figure F16
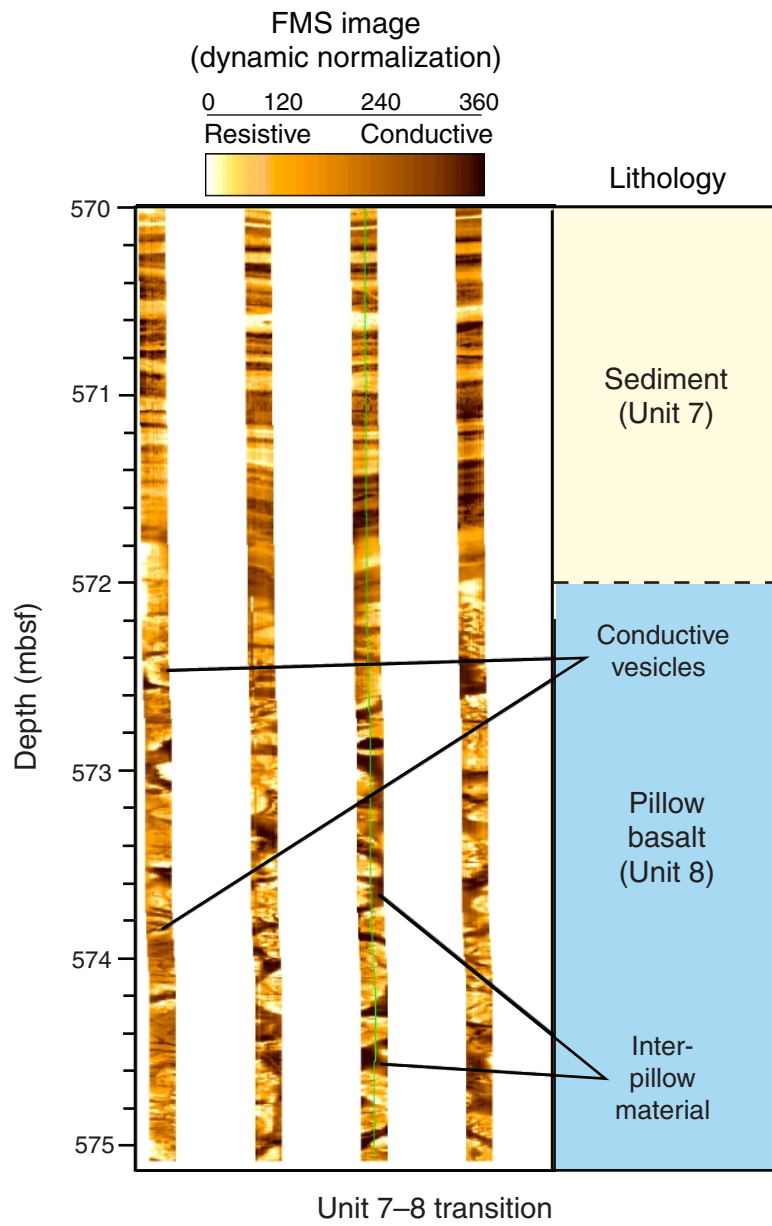
Figure F17
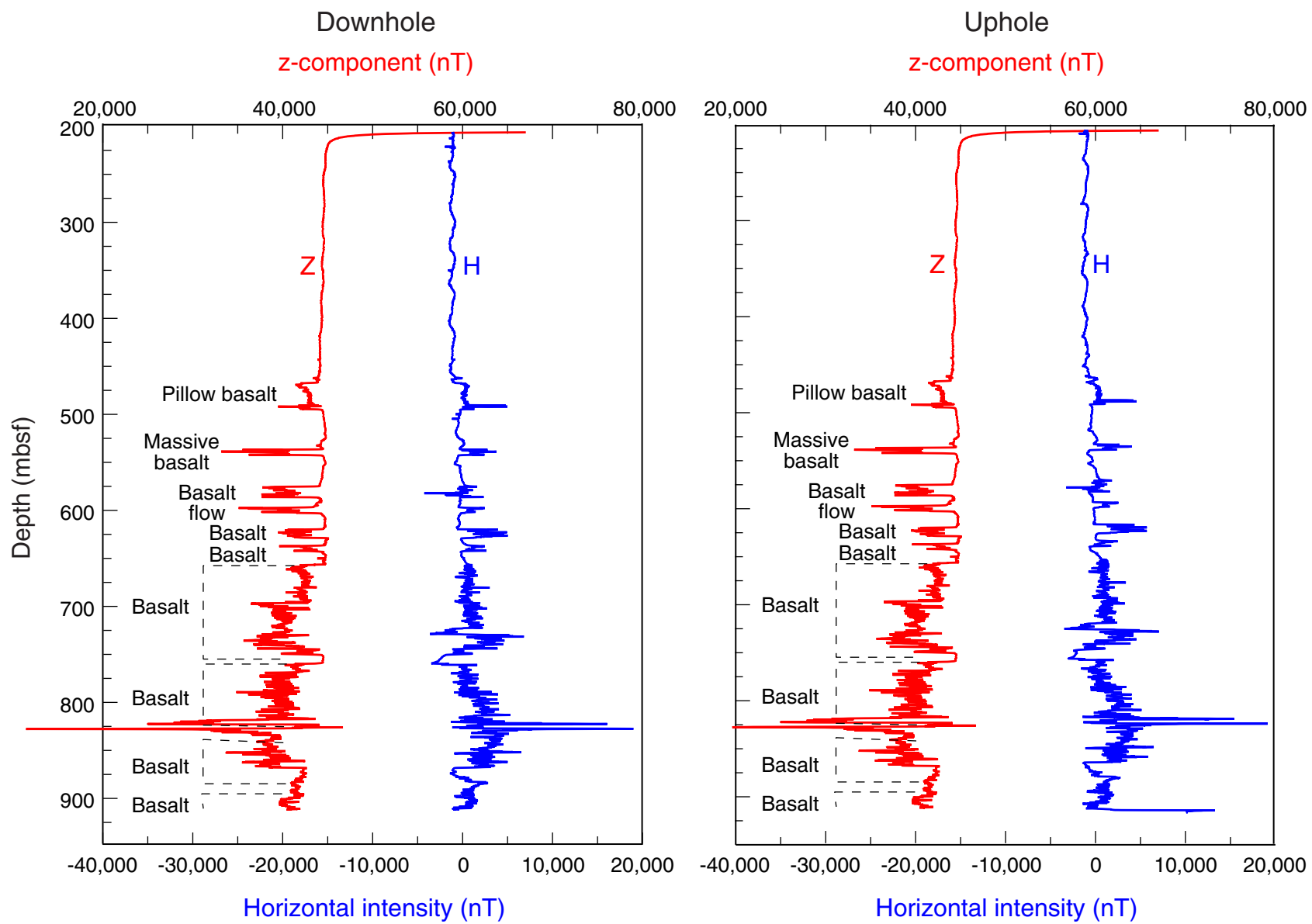
Figure F18
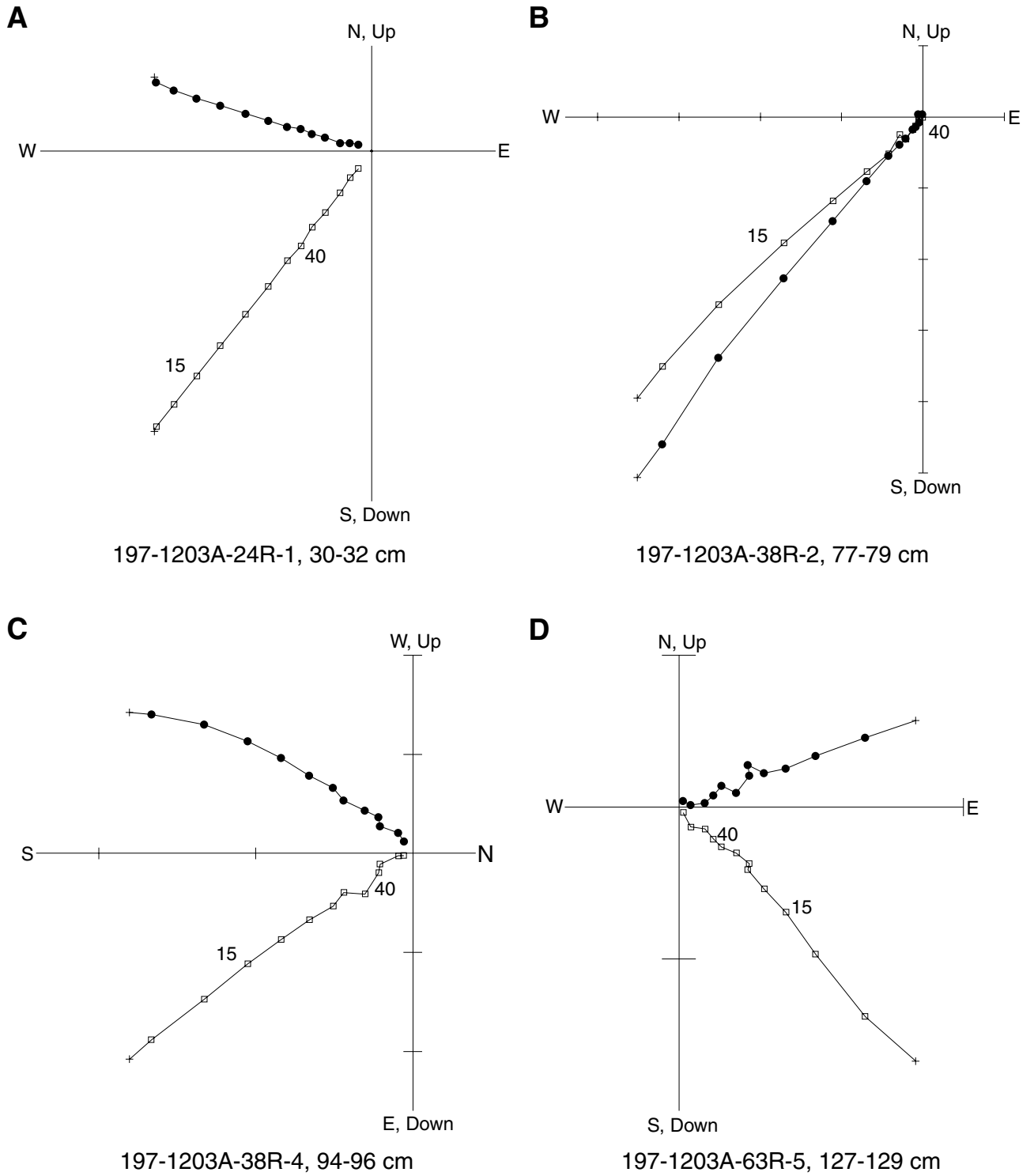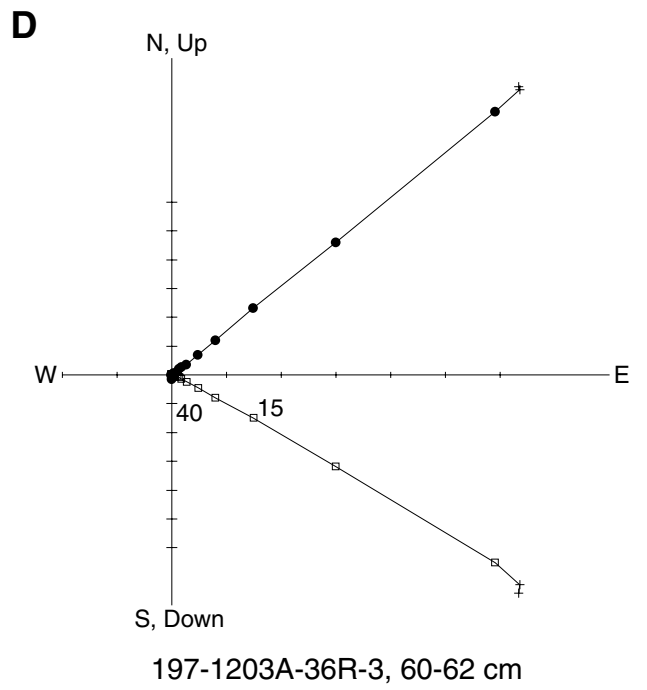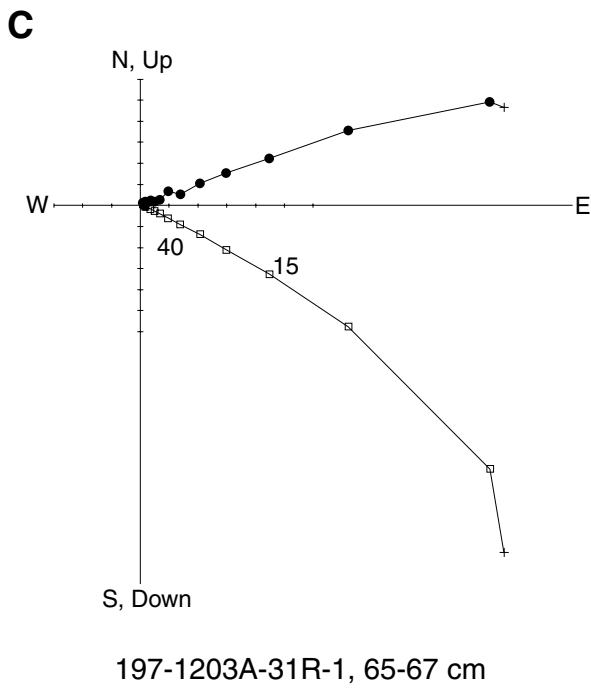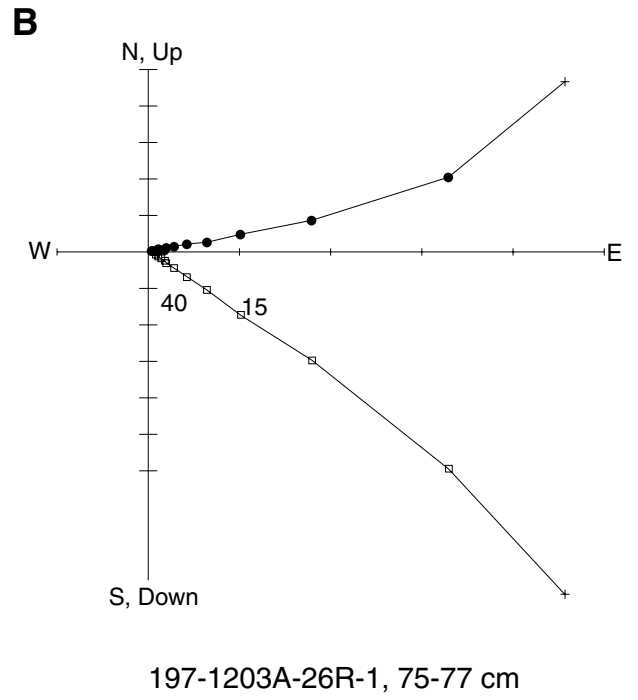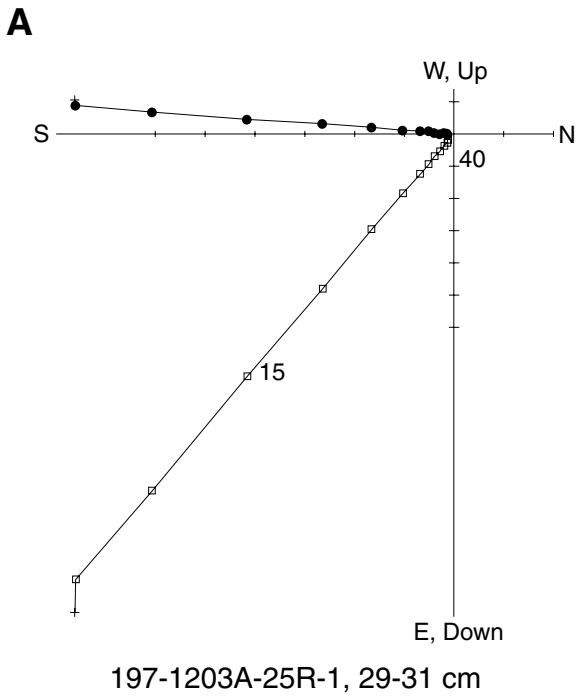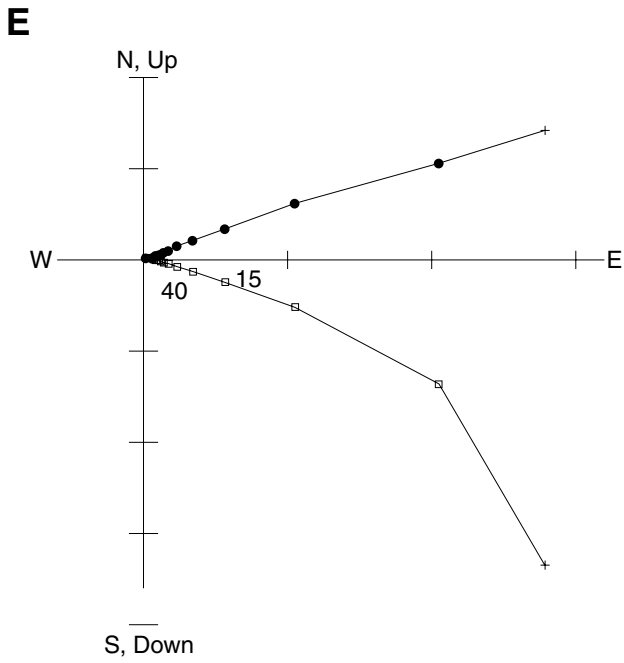
A

N, Up

W

E

40

15

S, Down

197-1203A-24R-1, 30-32 cm

B

N, Up

W

E

40

15

S, Down

197-1203A-38R-2, 77-79 cm

C

W, Up

S

N

40

15

E, Down

197-1203A-38R-4, 94-96 cm

D

N, Up

W

E

40

15

S, Down

197-1203A-63R-5, 127-129 cm

Figure F19

A

B

C

D

197-1203A-25R-1, 29-31 cm

197-1203A-26R-1, 75-77 cm

197-1203A-31R-1, 65-67 cm

197-1203A-36R-3, 60-62 cm

Figure F20

E

197-1203A-37R-3, 113-115 cm

F

197-1203A-47R-4, 18-20 cm

G

197-1203A-55R-5, 17-19 cm

H
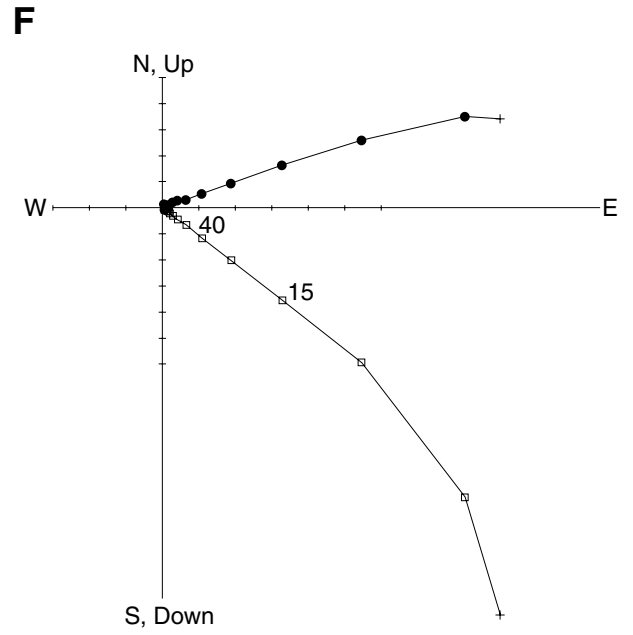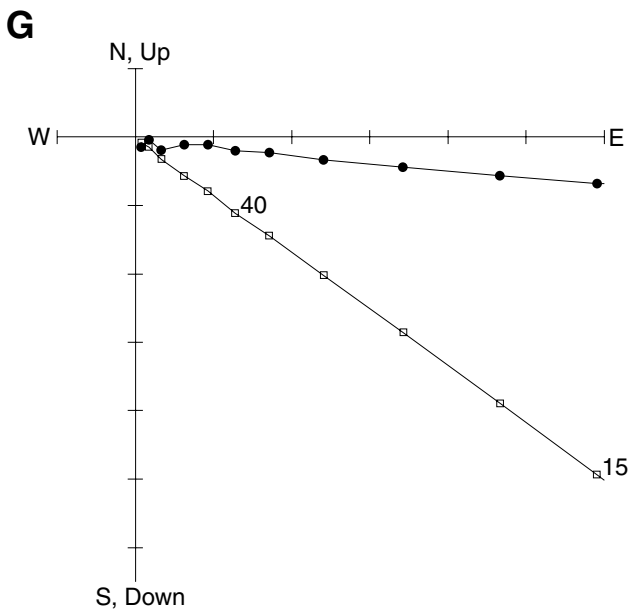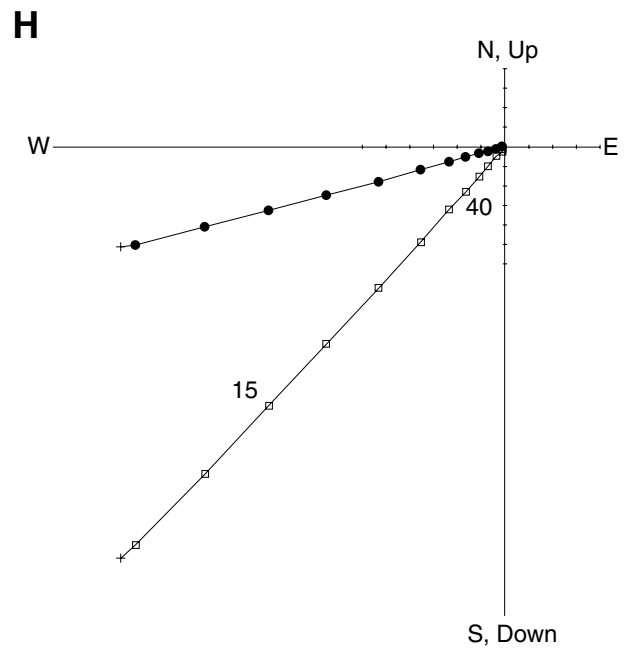
197-1203A-59R-4, 124-126 cm
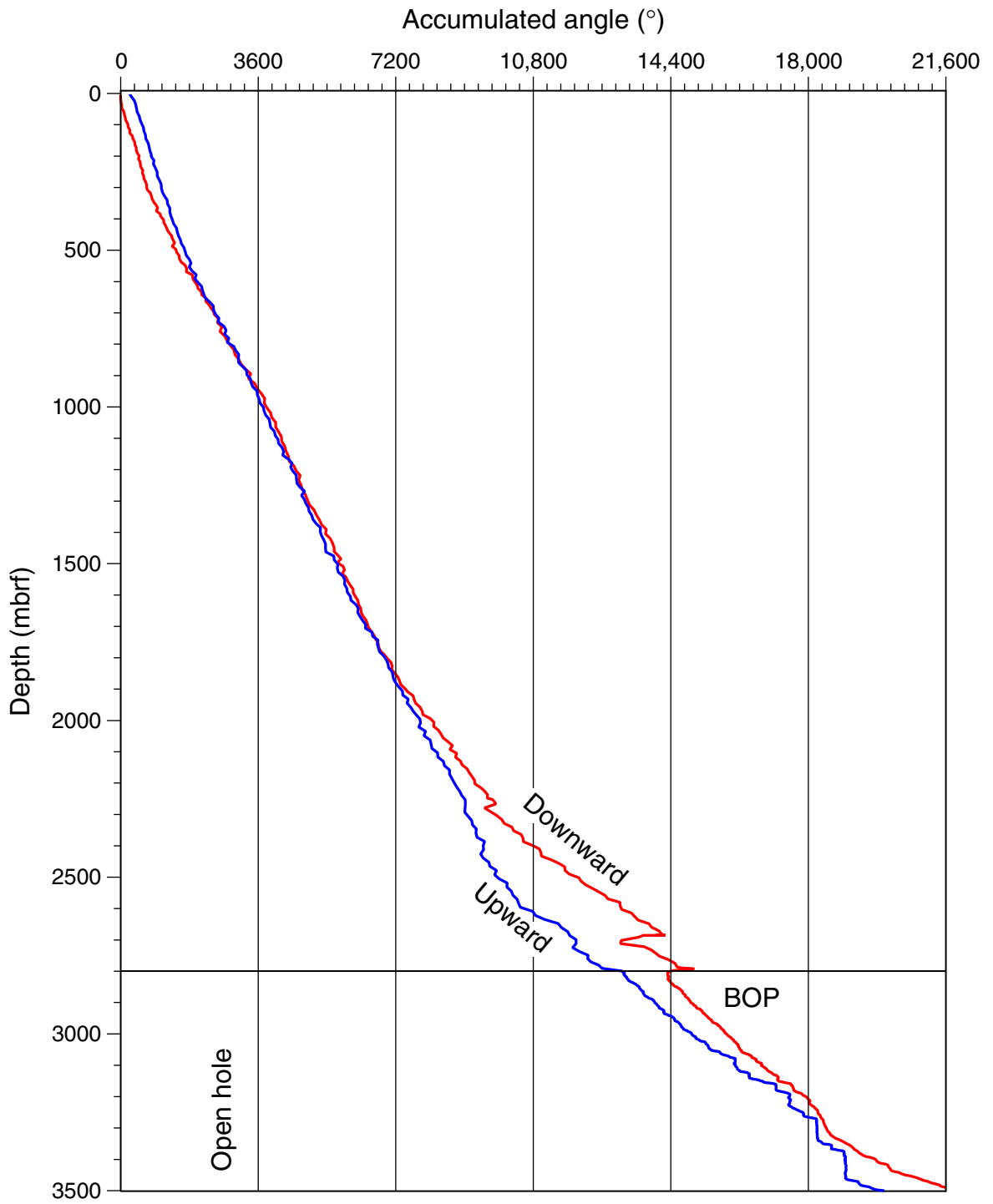
Figure F20 (continued)
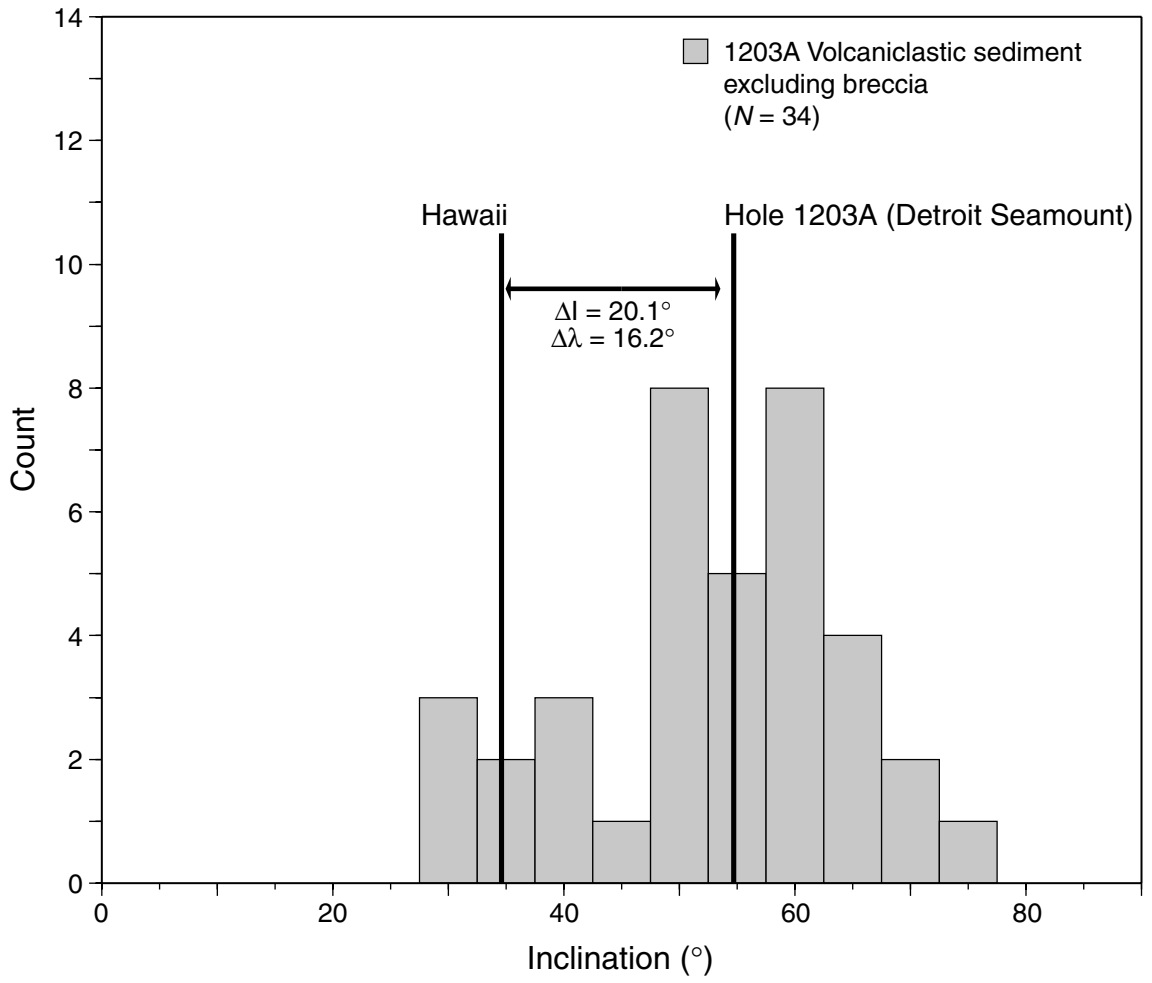
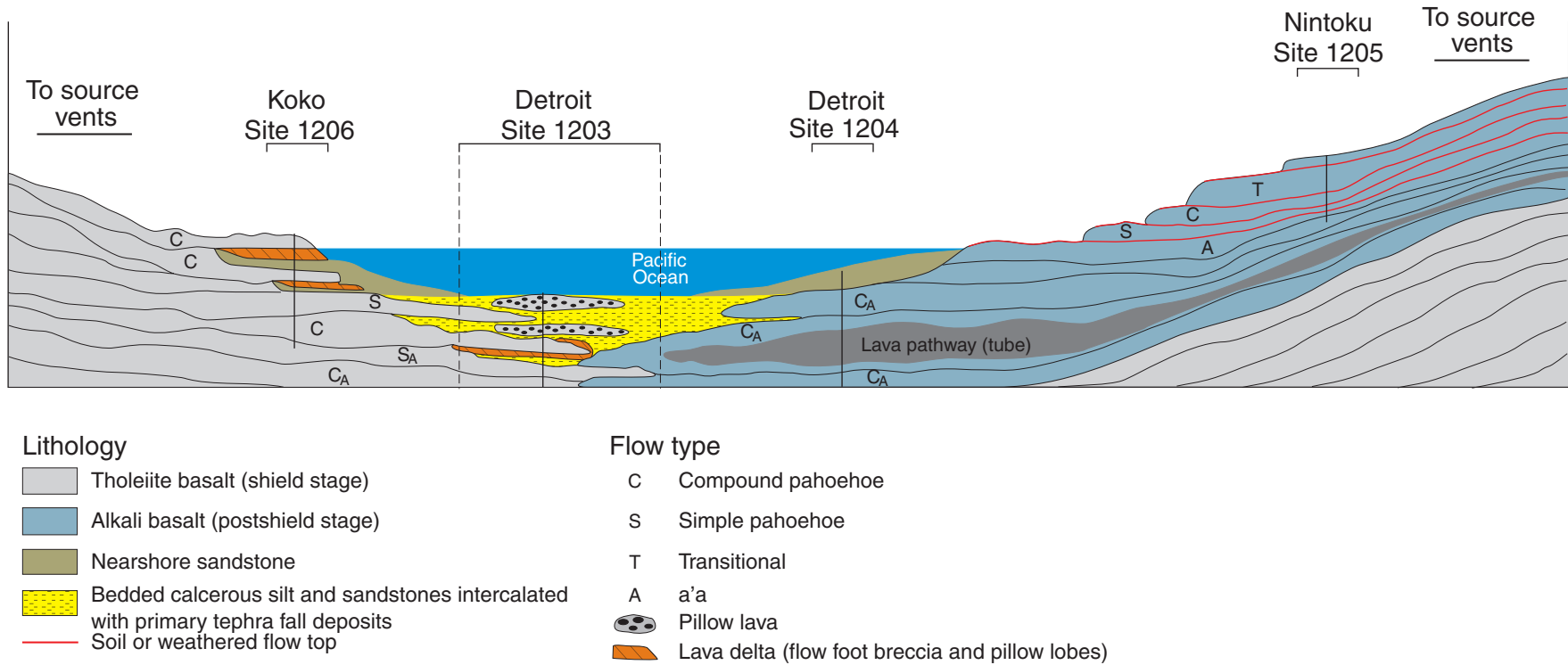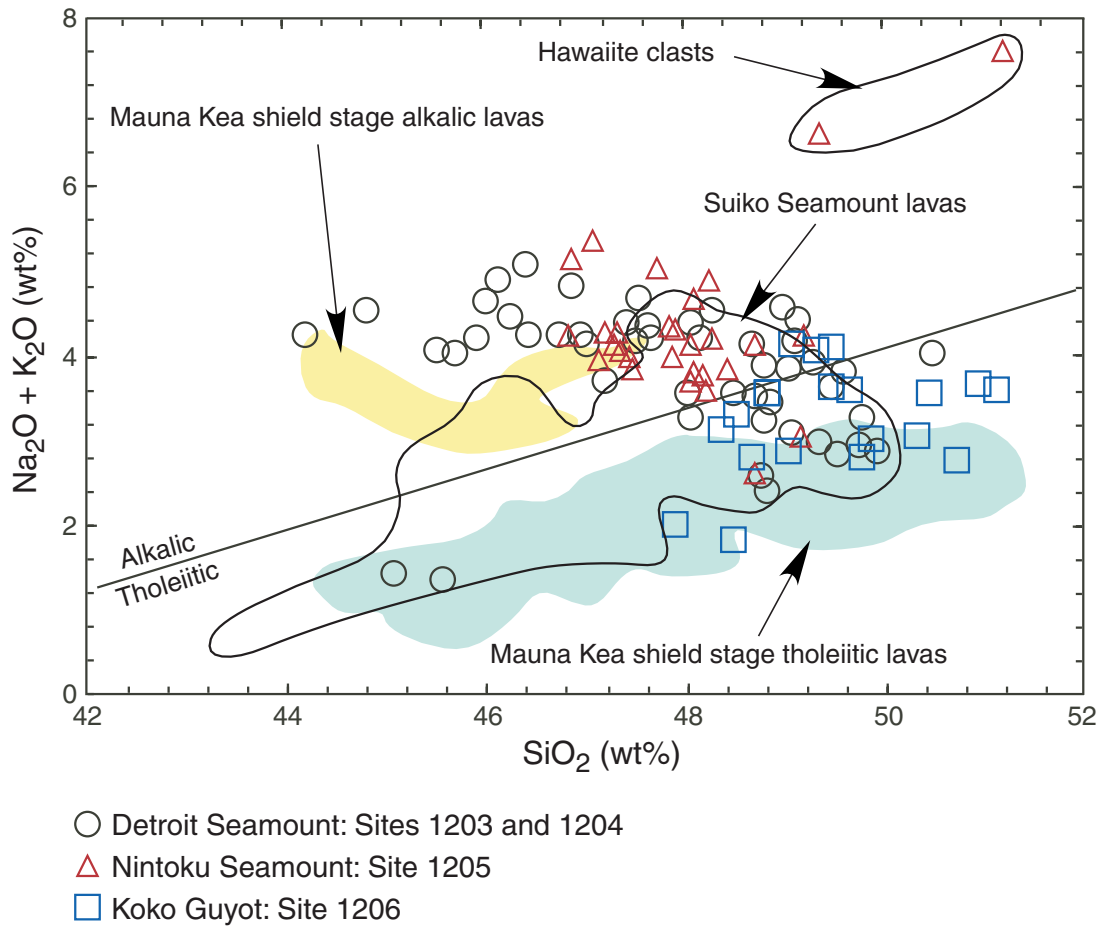Figure F21
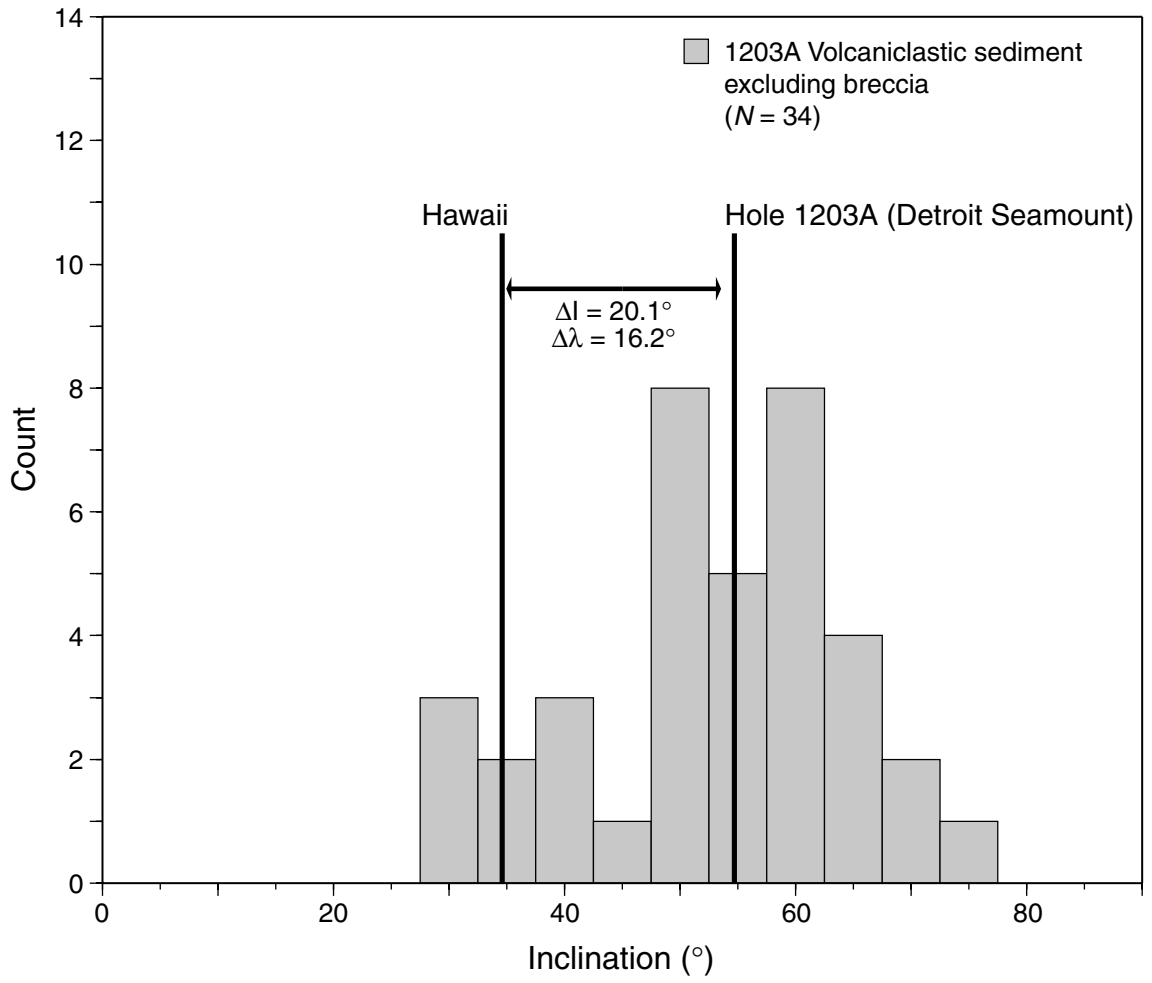
Figure F22
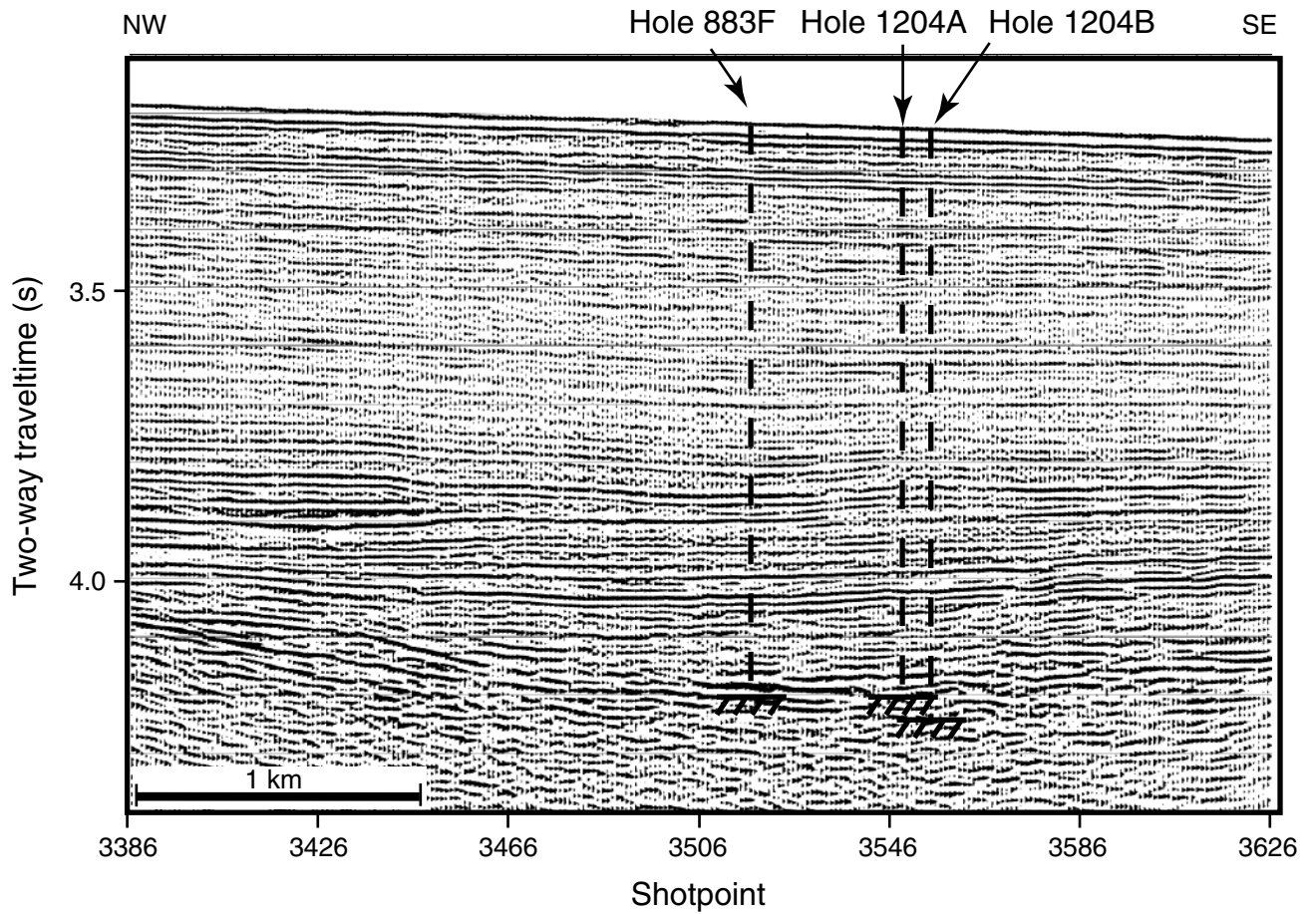
Figure F23
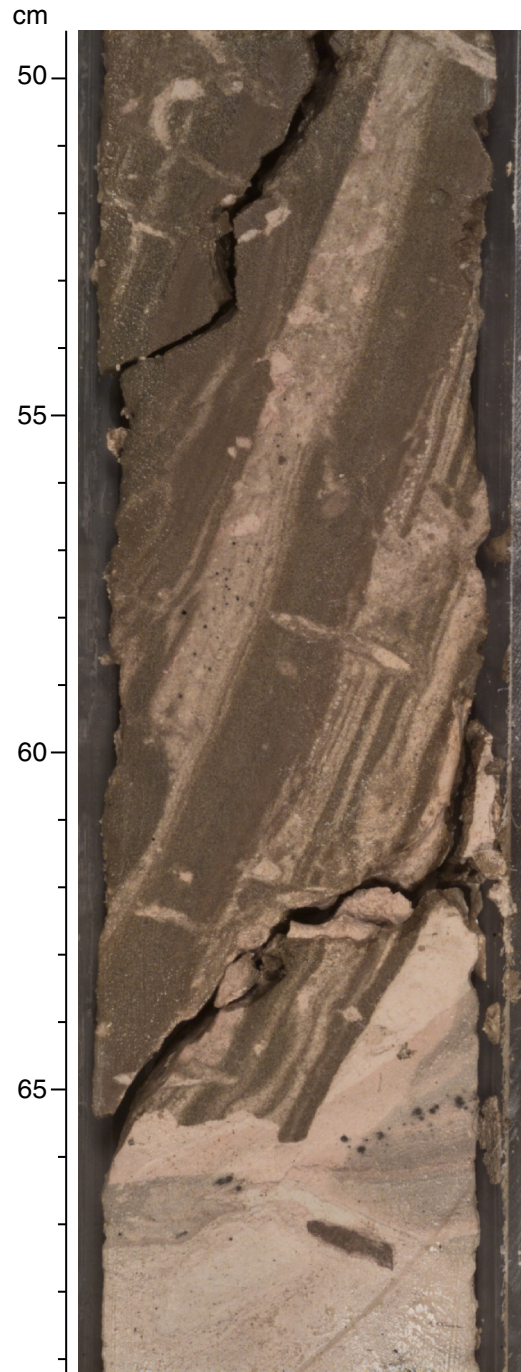
Figure F24
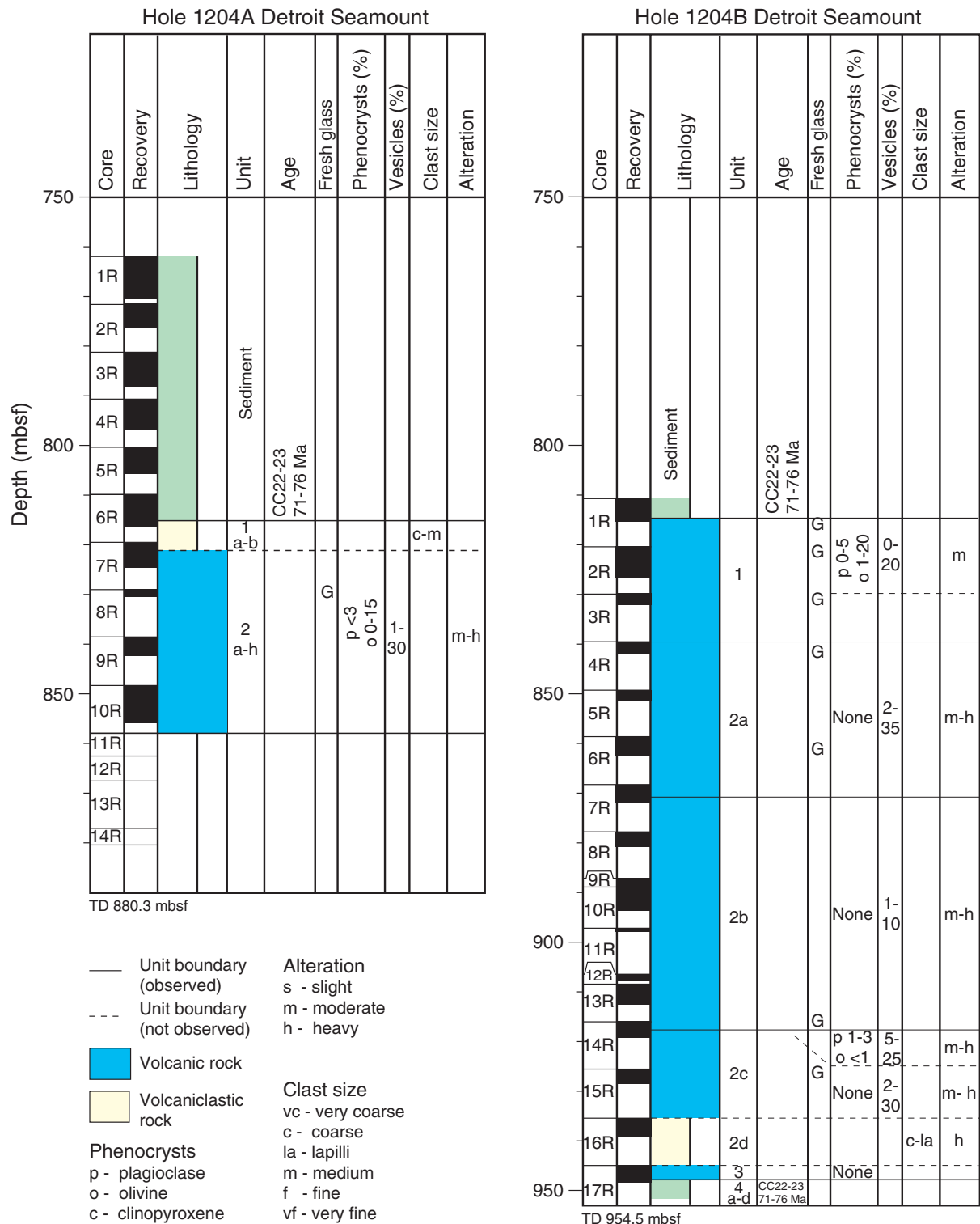
Figure F25
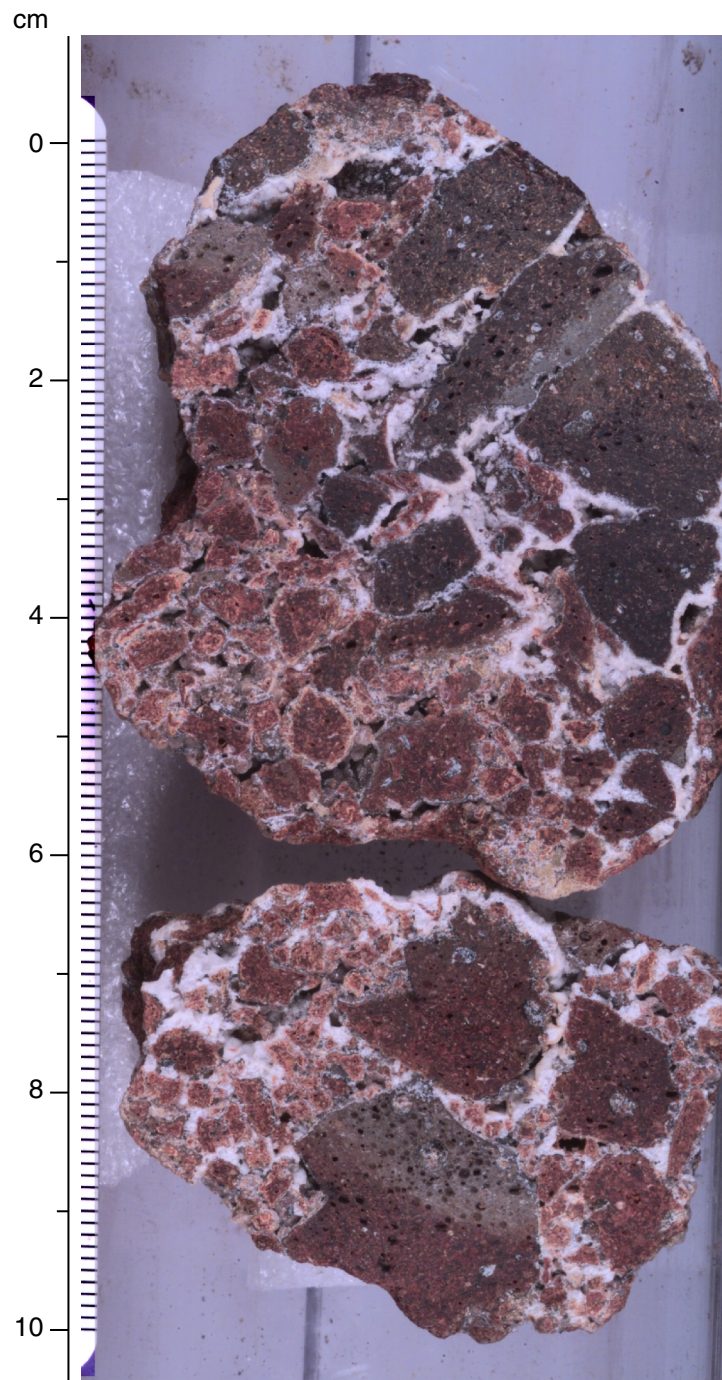
Figure F26
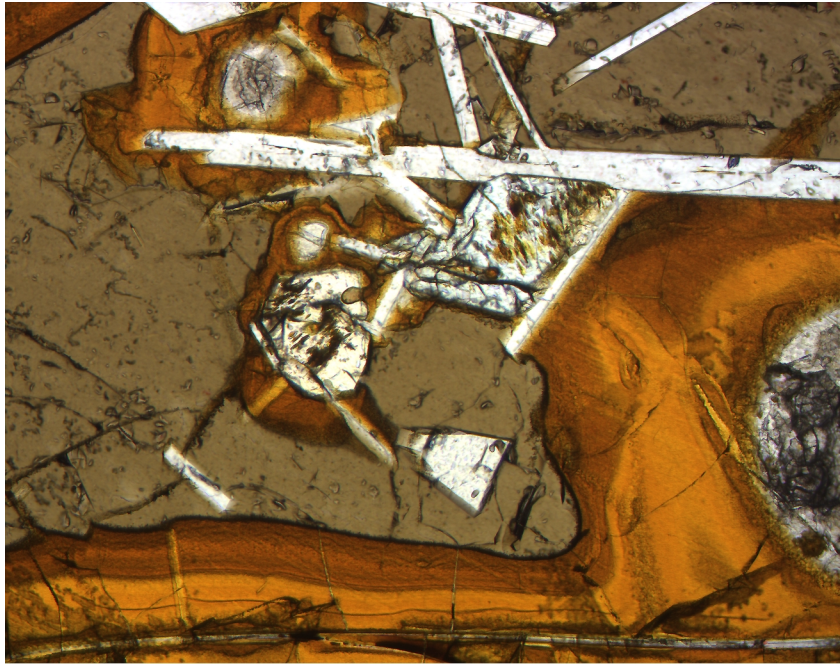
Figure F27

Figure F28

Figure F29

A — 197-1204B-2R-2, 14-16 cm

B — 197-1204B-14R-1, 14-16 cm

C — 197-1204B-13R-4, 82-84 cm

D — 197-1204B-17R-2, 104-106 cm

E — 197-1204B-10R-1, 6-9 cm

F — 197-1204B-15R-1, 11-13 cm

Figure F30

A 197-1204B-7R-3, 139-141 cm

B 197-1204B-9R-2, 8-10 cm

C 197-1204B-8R-2, 21-23 cm

D 197-1204B-10R-4, 40-42 cm

E 197-1204B-11R-2, 38-40 cm

F 197-1204B-13R-3, 33-35 cm
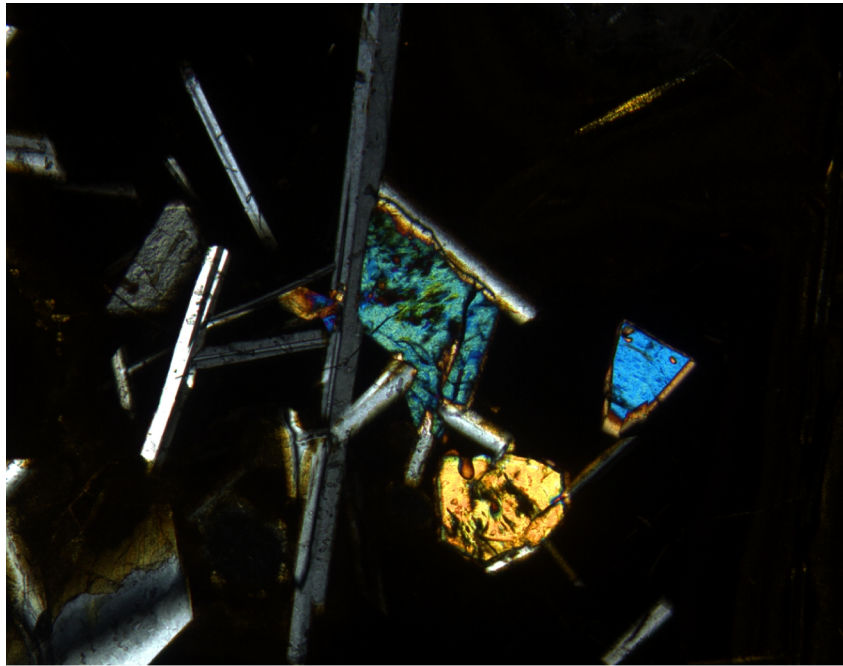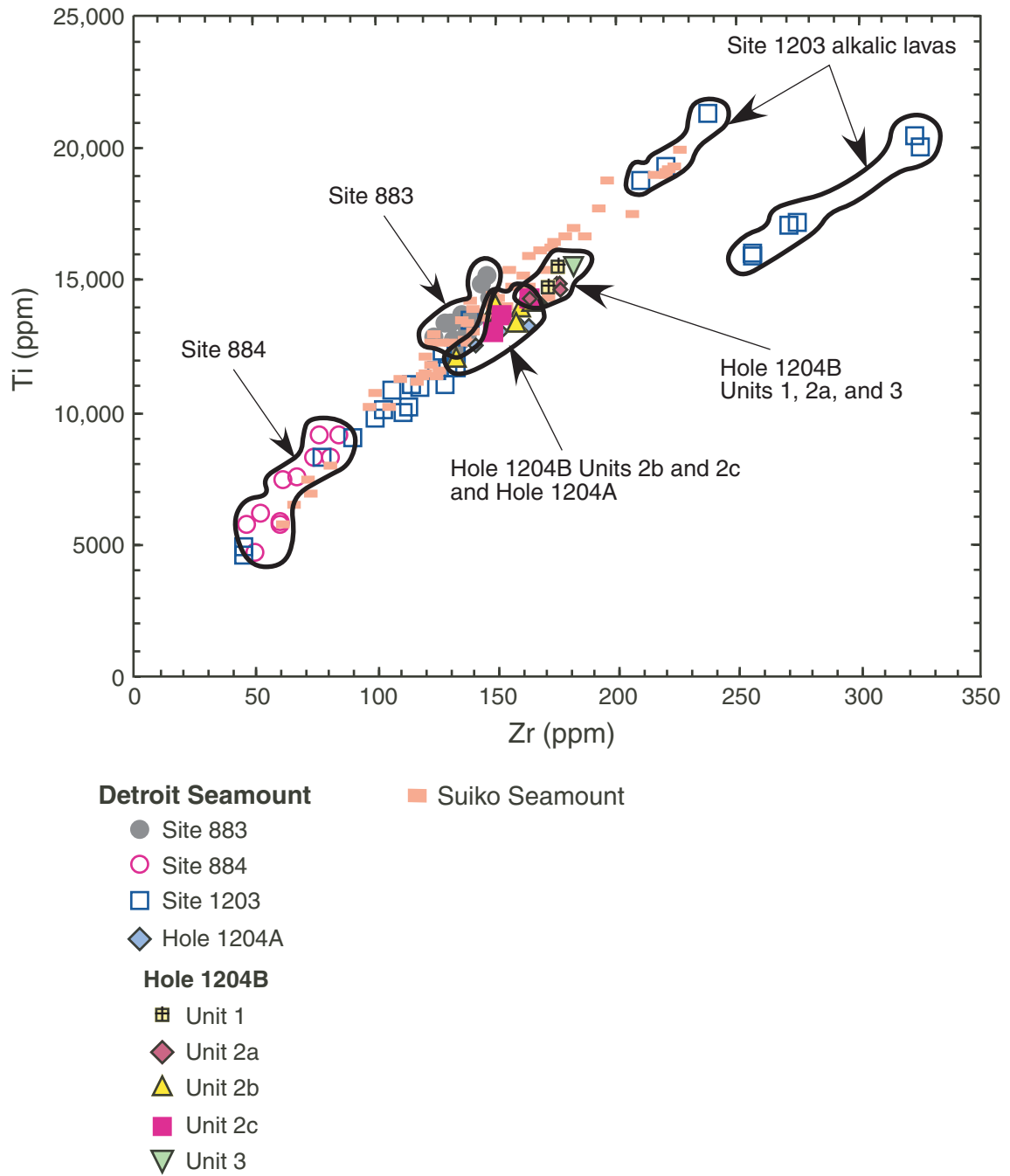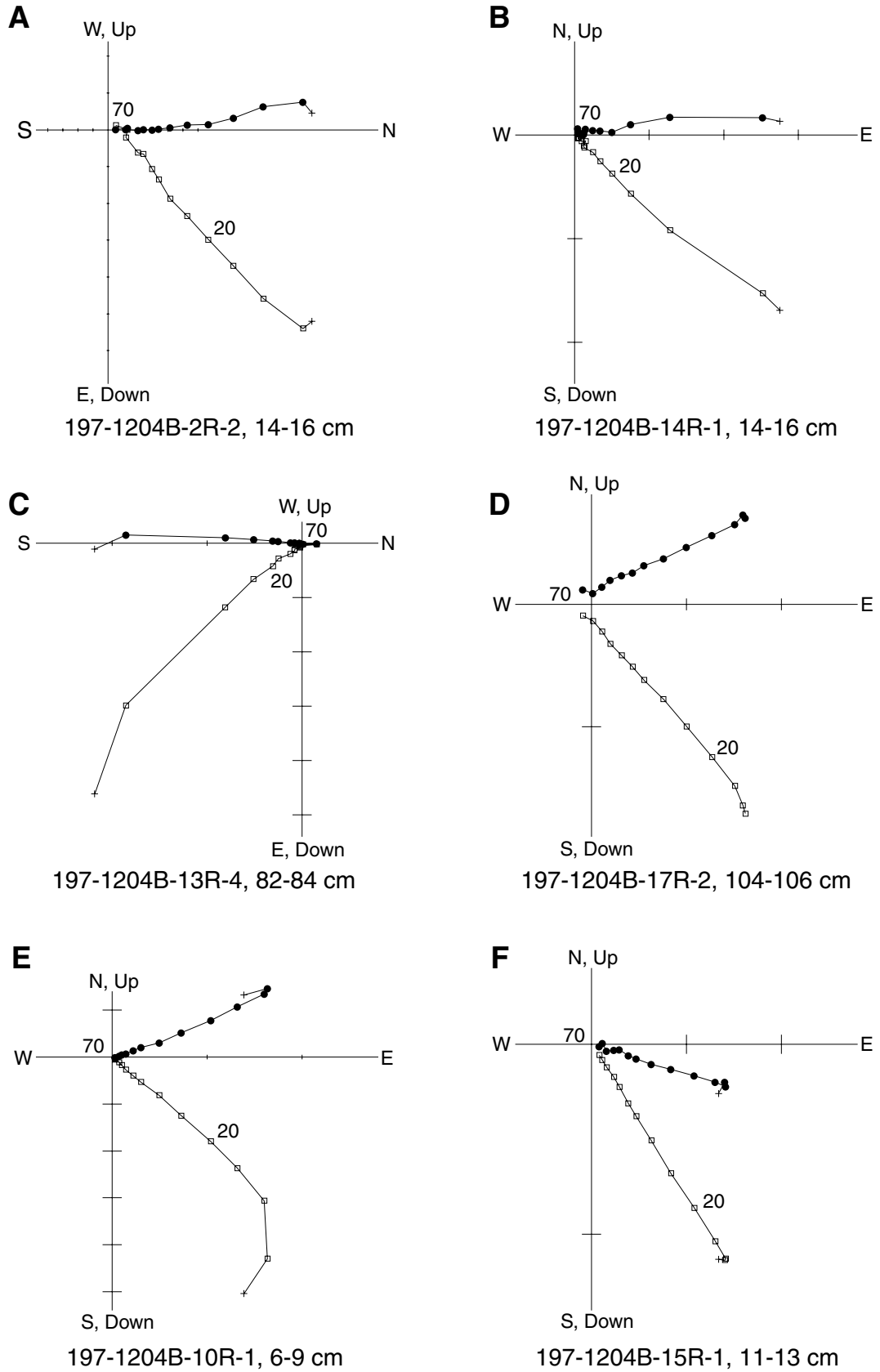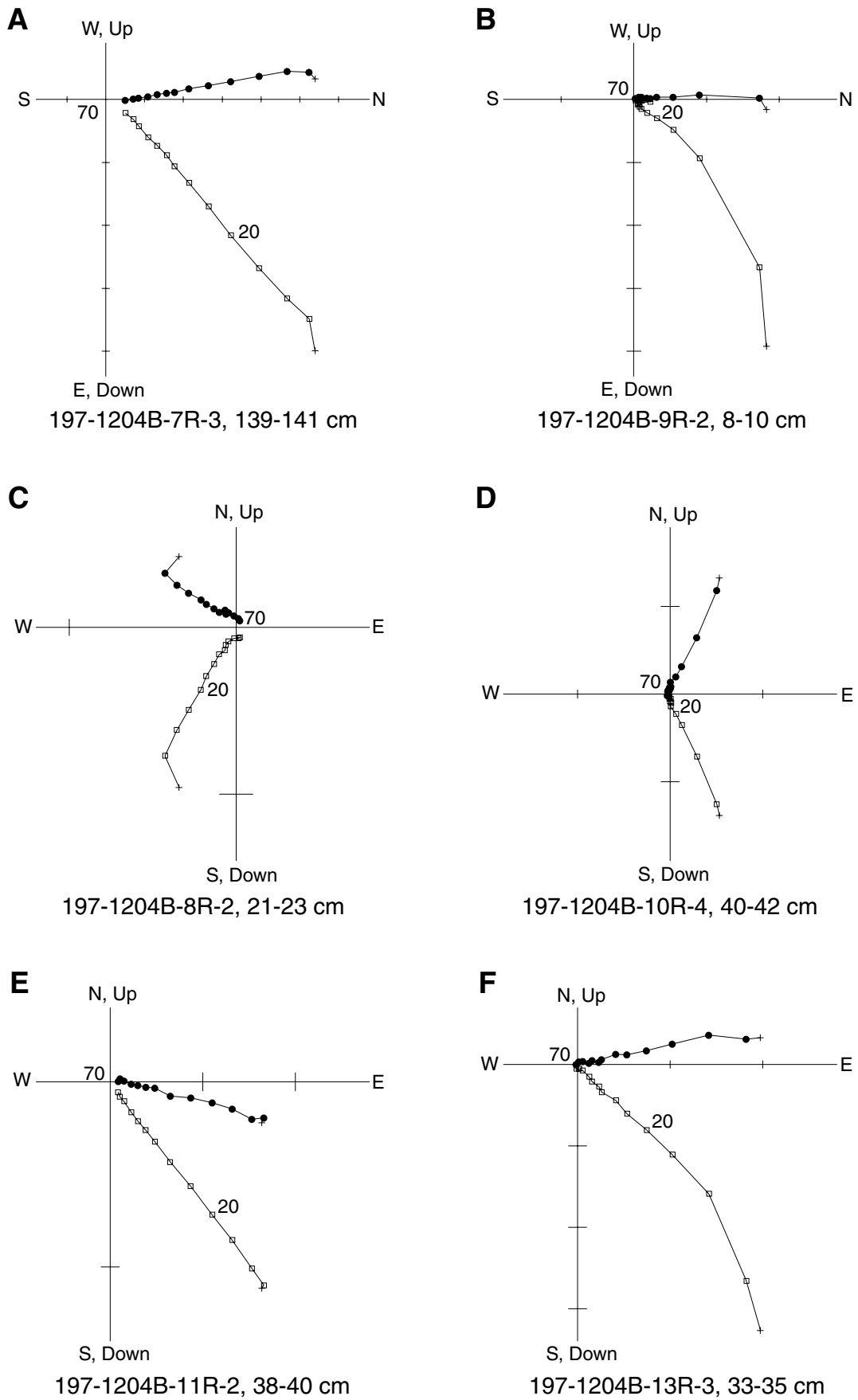
Figure F31

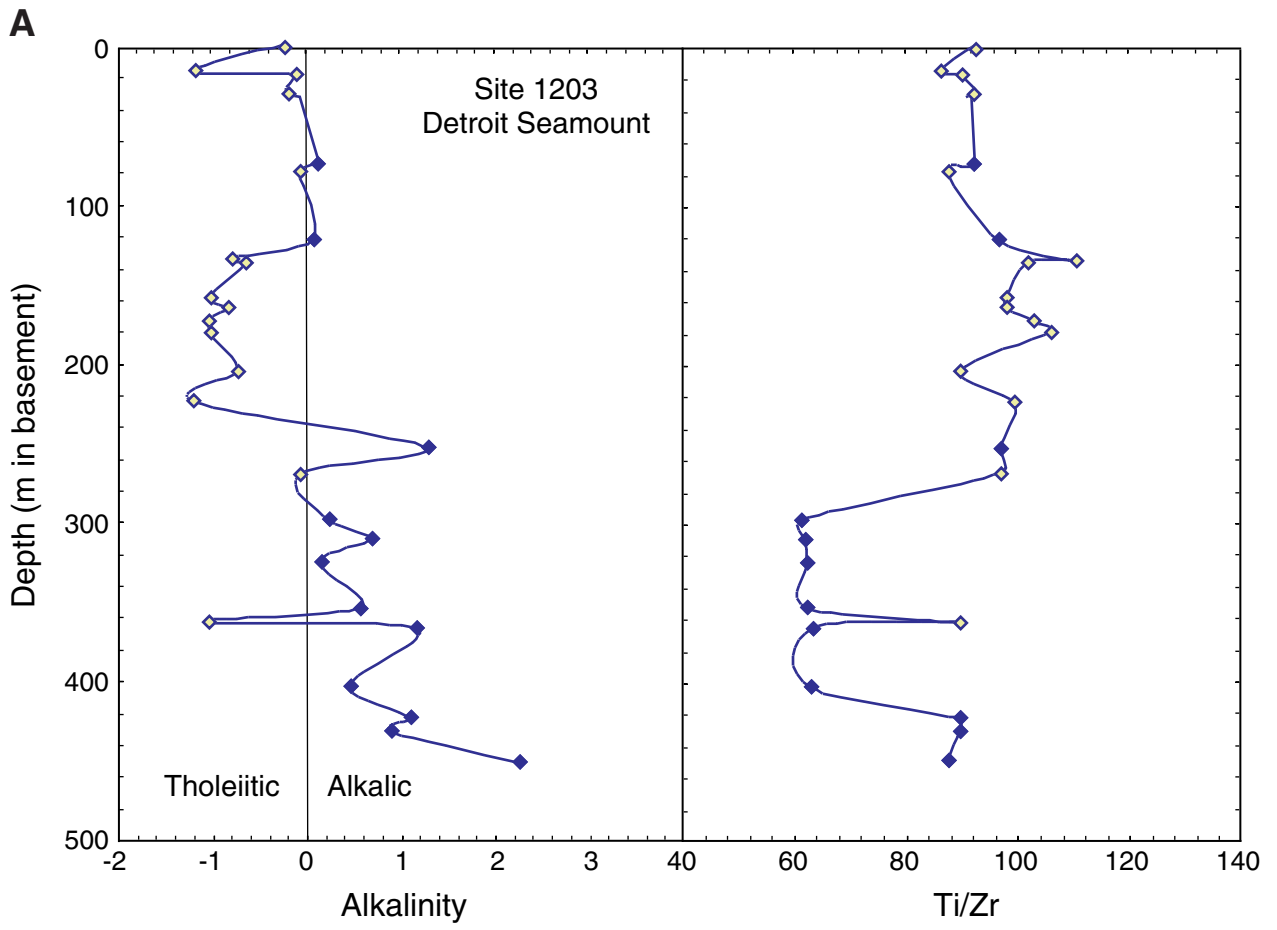Figure F32

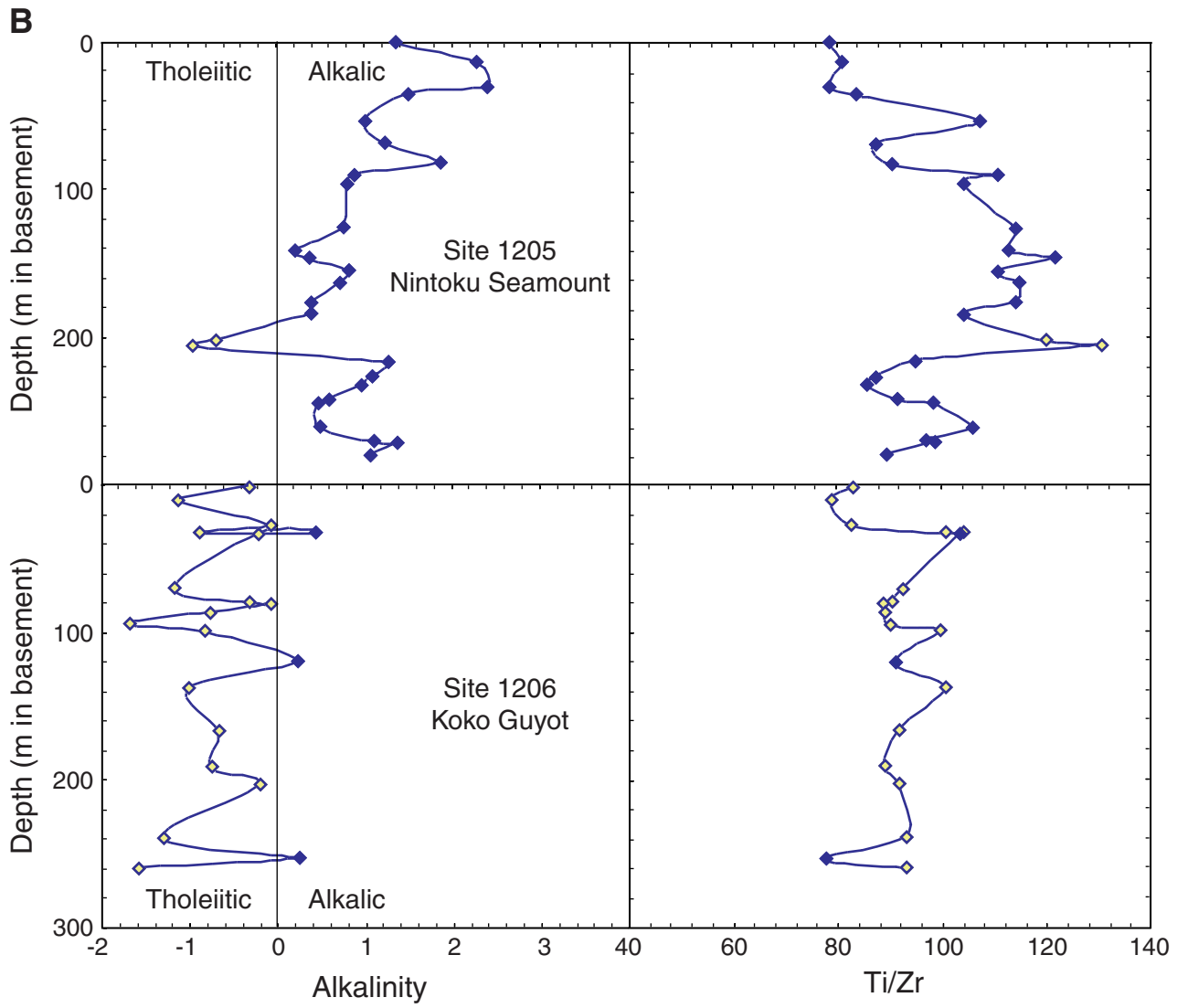Figure F33

Hole 1205A Nintoku Seamount
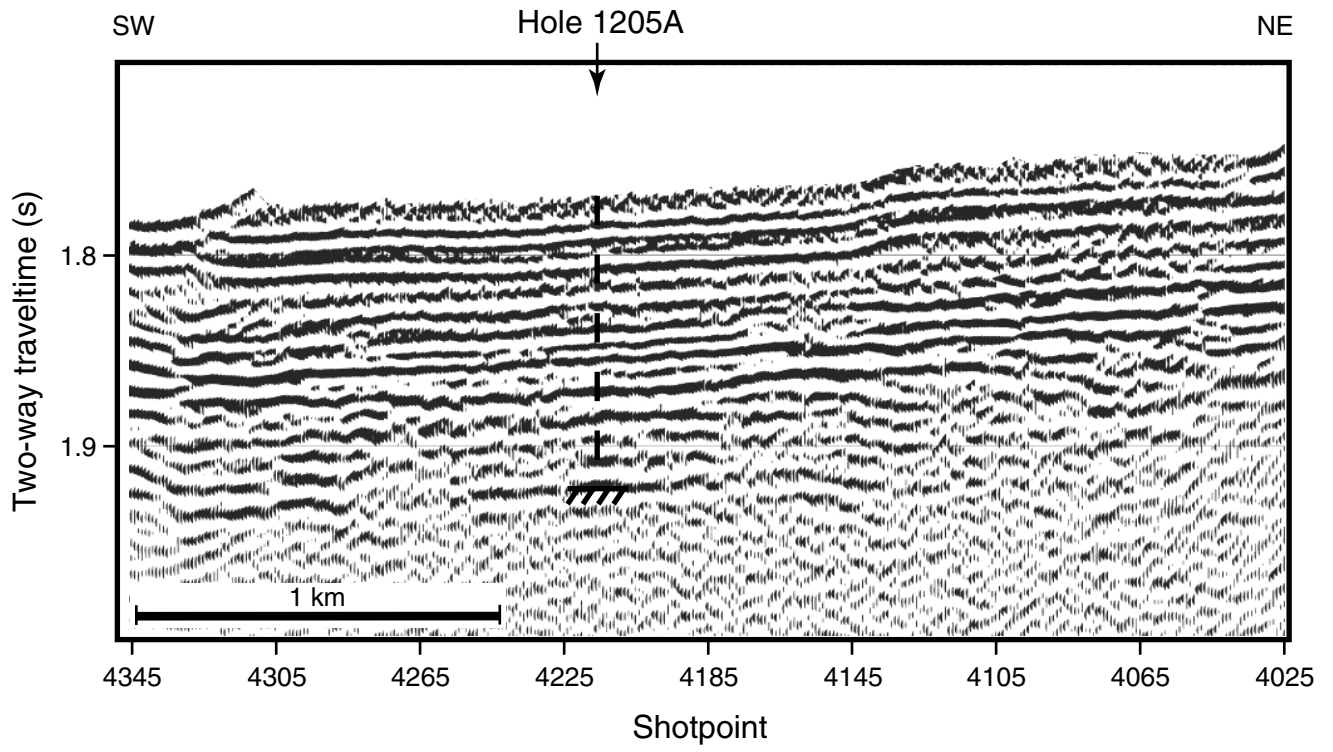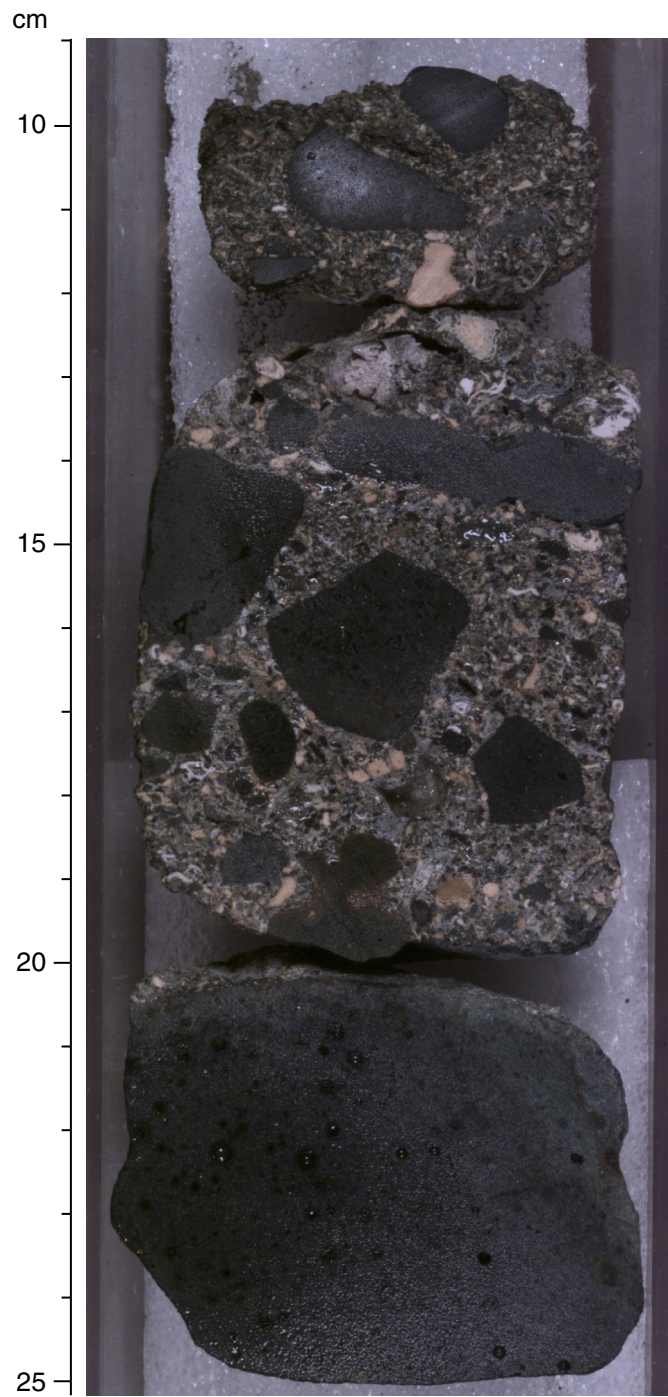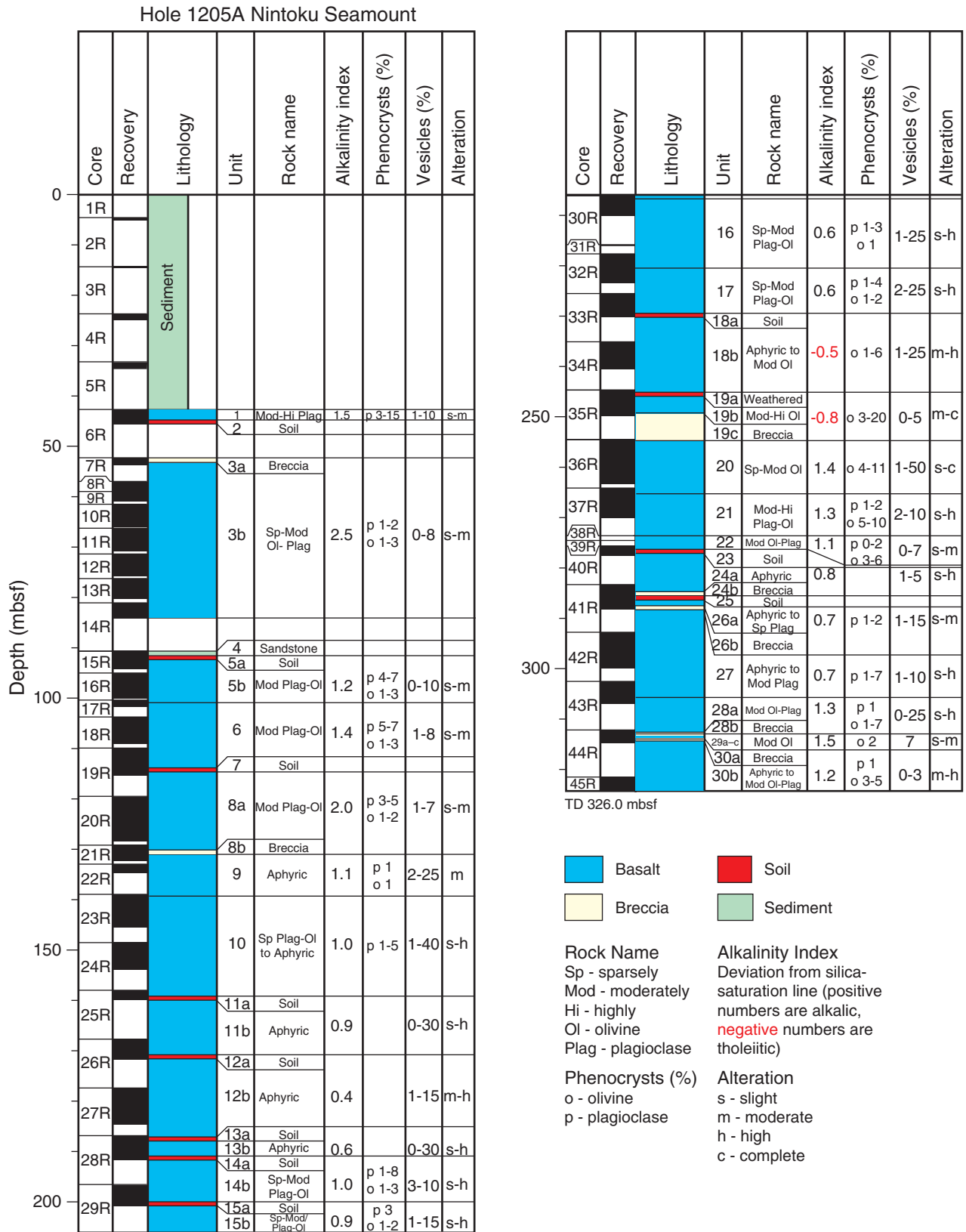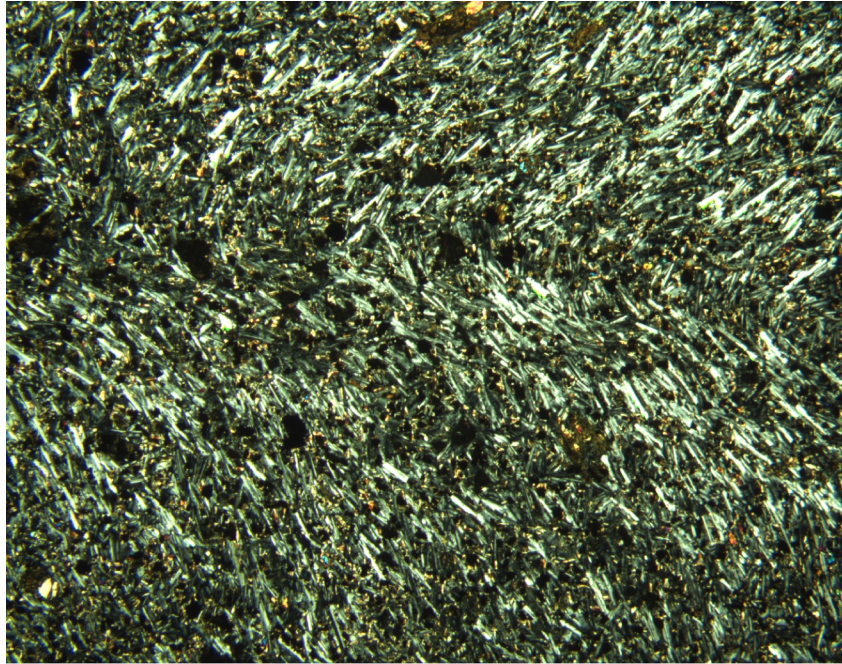
Figure F34
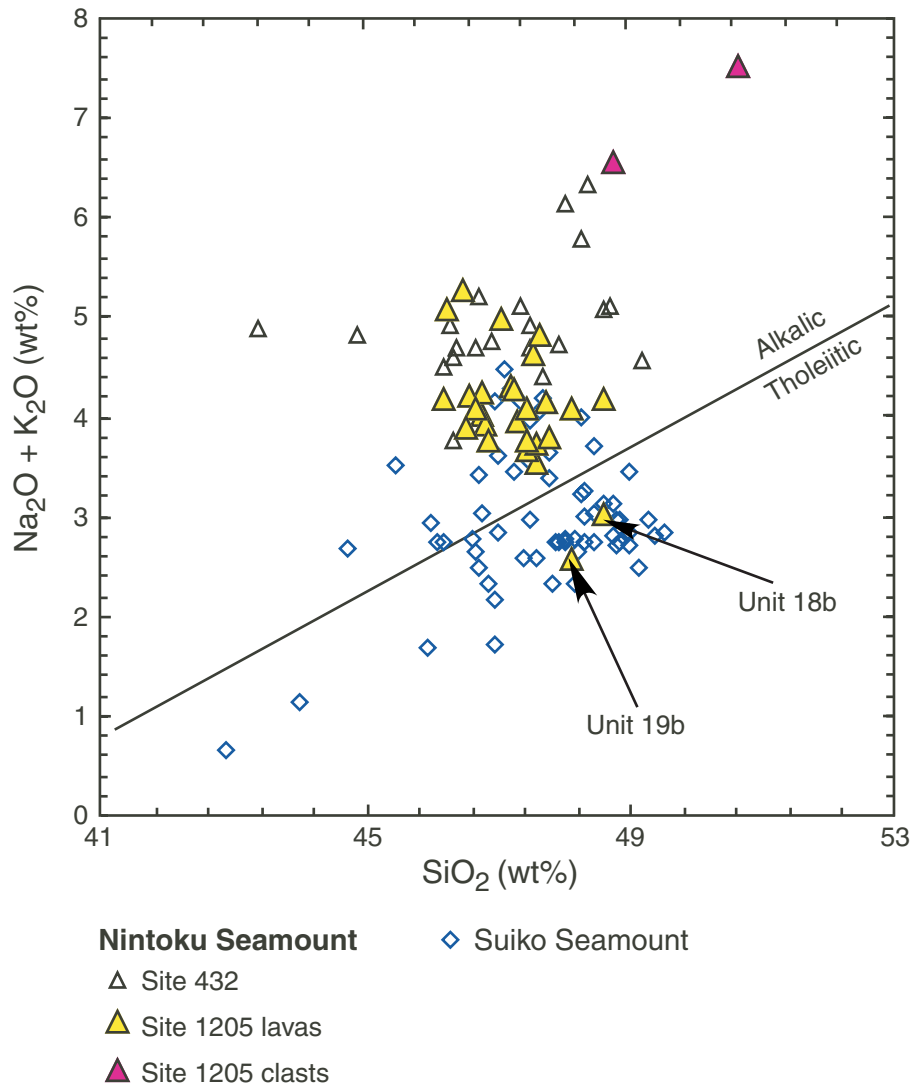
Figure F35

Figure F36
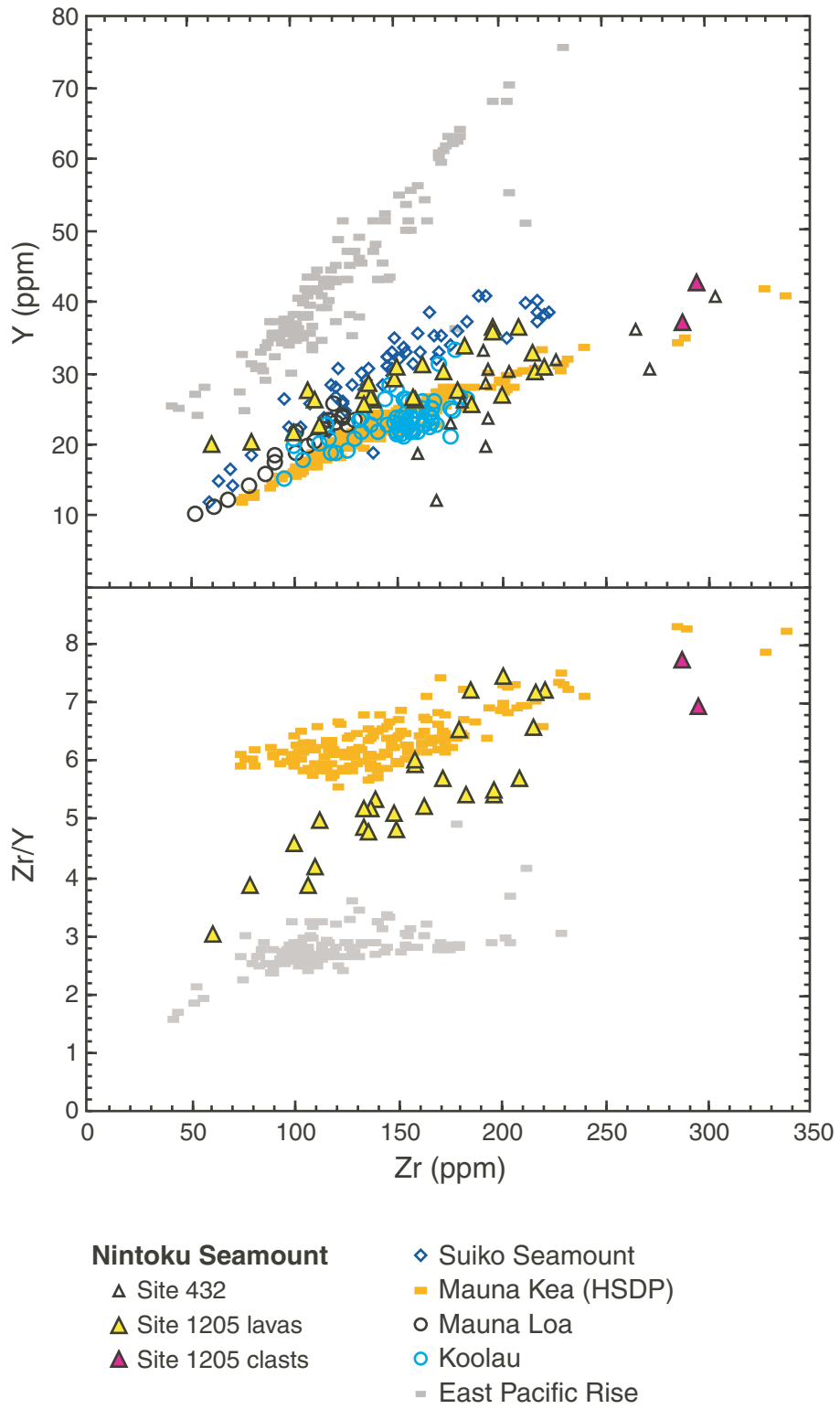
Figure F37

Figure F38

Figure F39

A

197-1205A-13R-2, 39-41 cm

B

197-1205A-25R-2, 17-19 cm

C

197-1205A-26R-1, 117-119 cm

D

197-1205A-28R-3, 4-6 cm

E

197-1205A-29R-4, 126-128 cm

F

197-1205A-44R-1, 68-70 cm
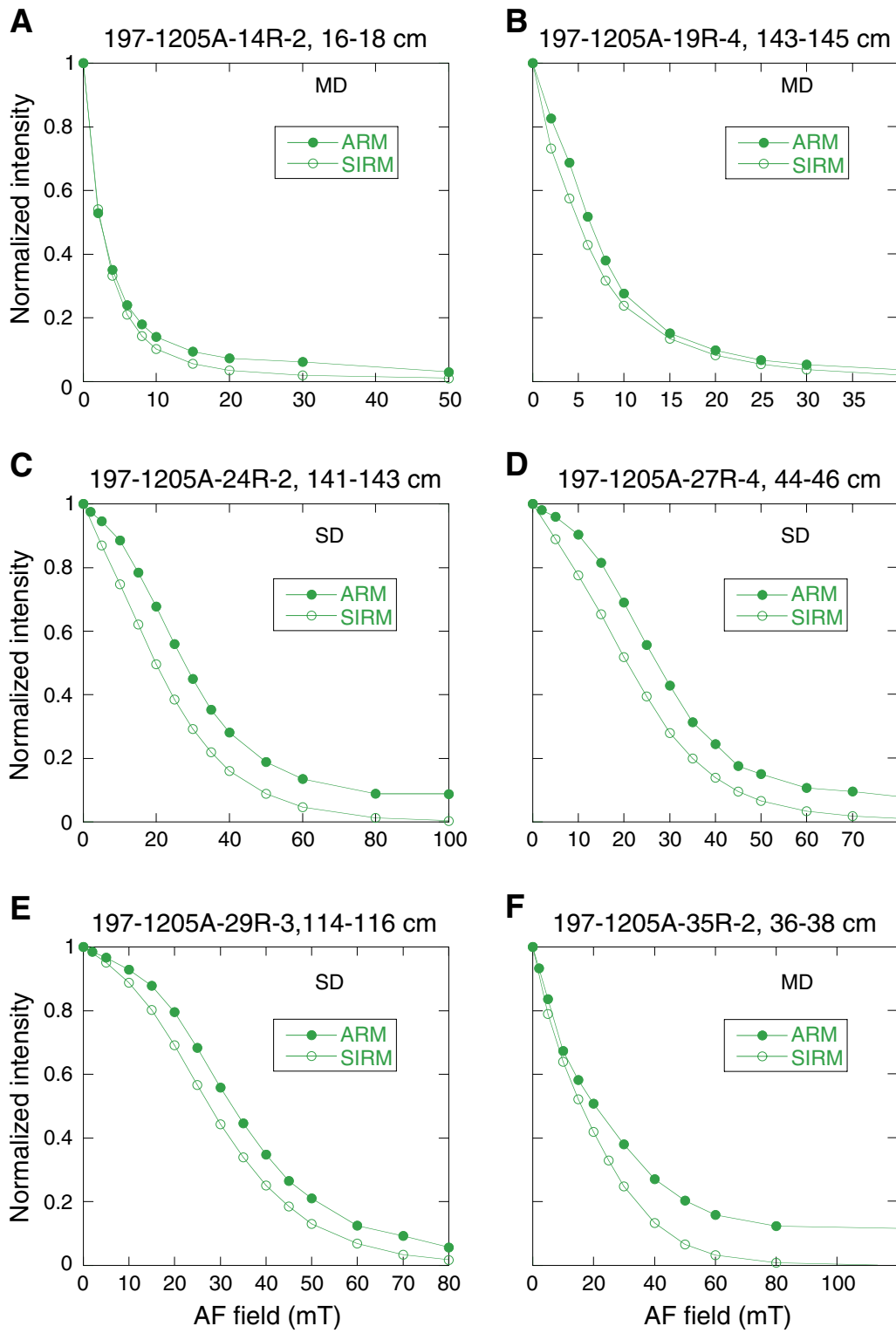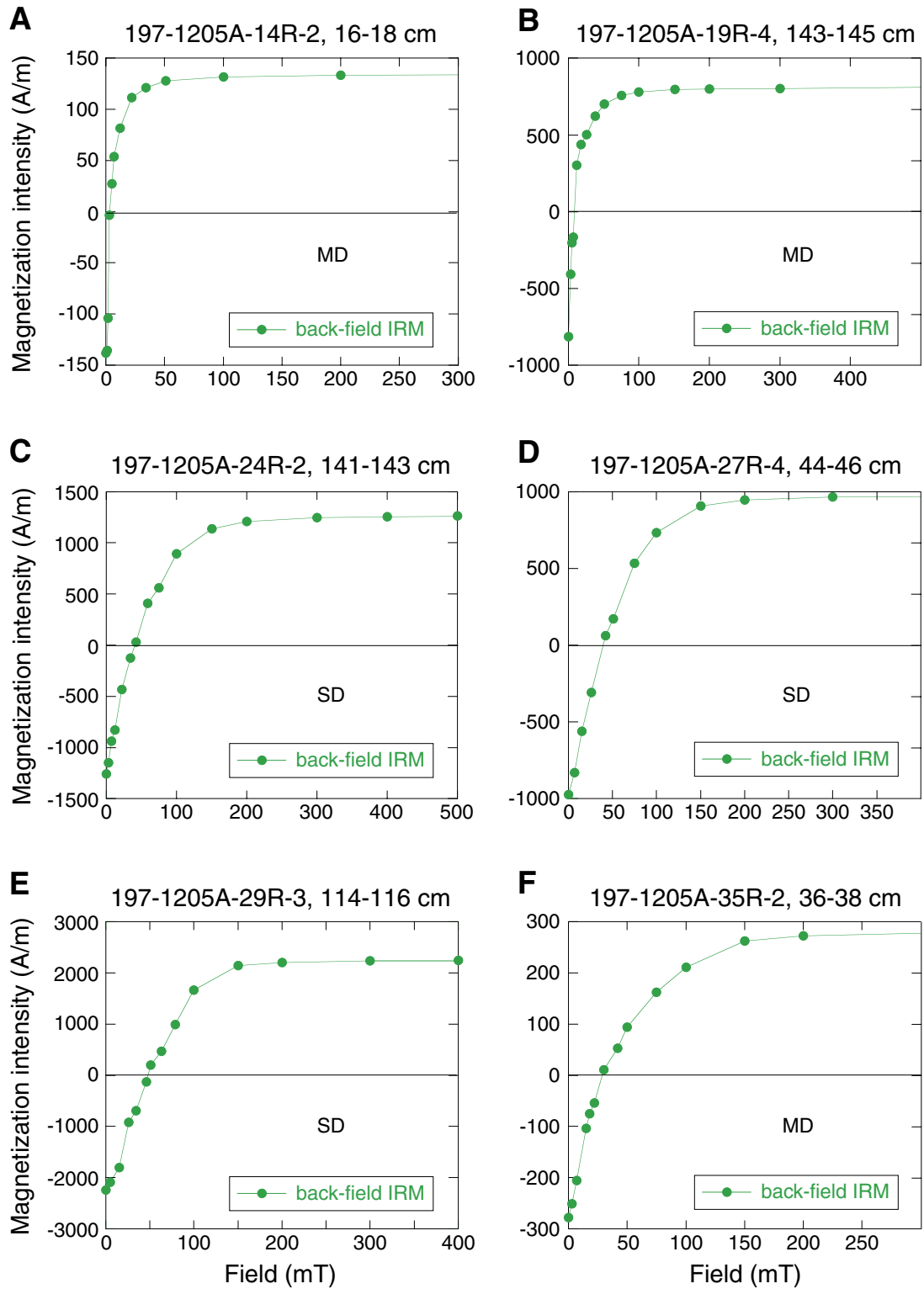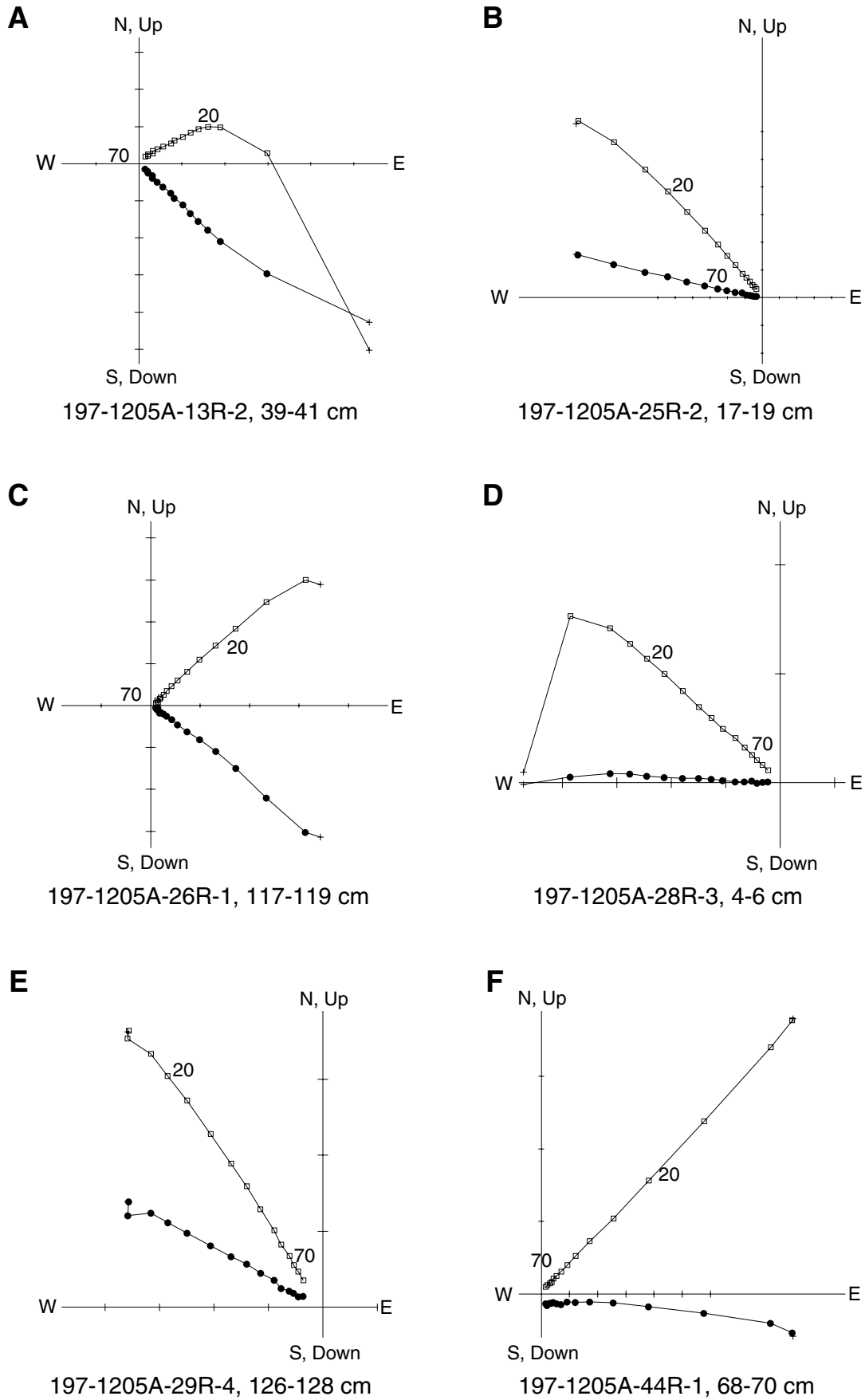
Figure F40

Figure F41

Figure F42

Hole 1206A Koko Seamount
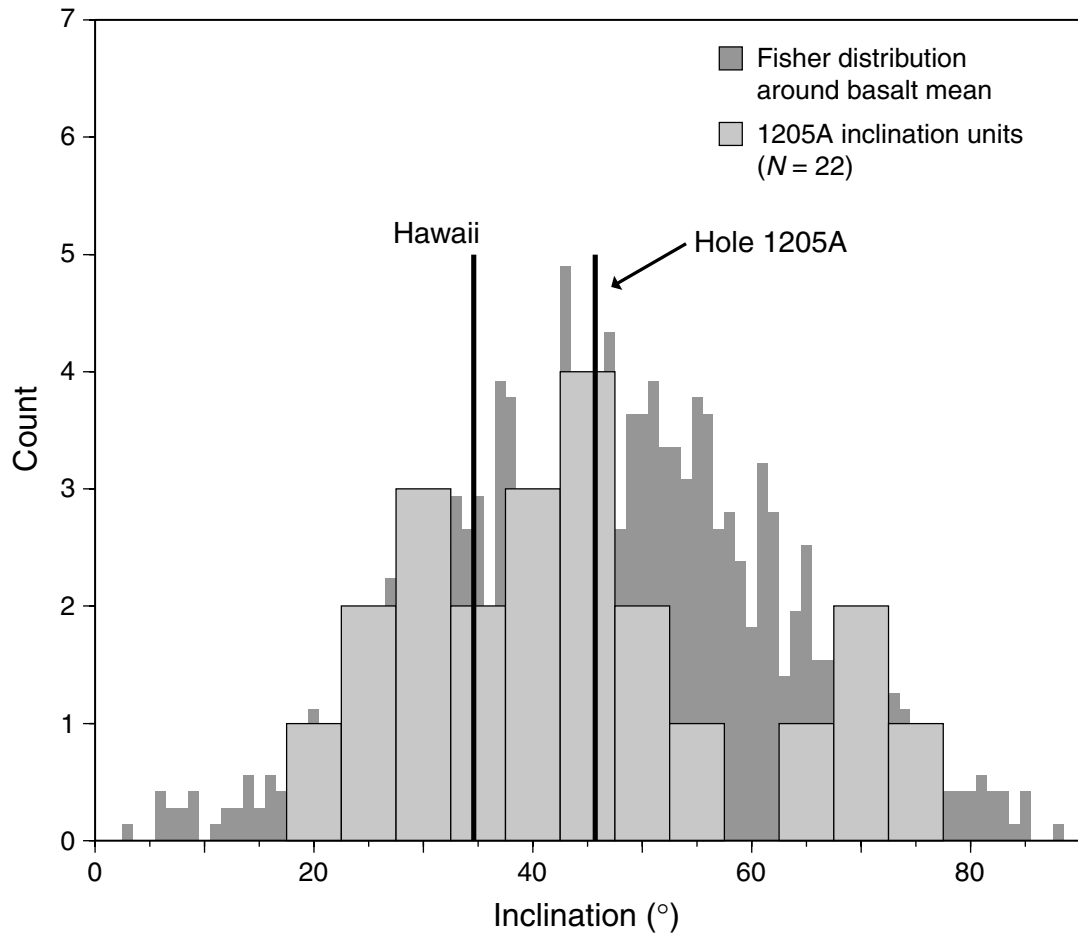
Figure F43

A
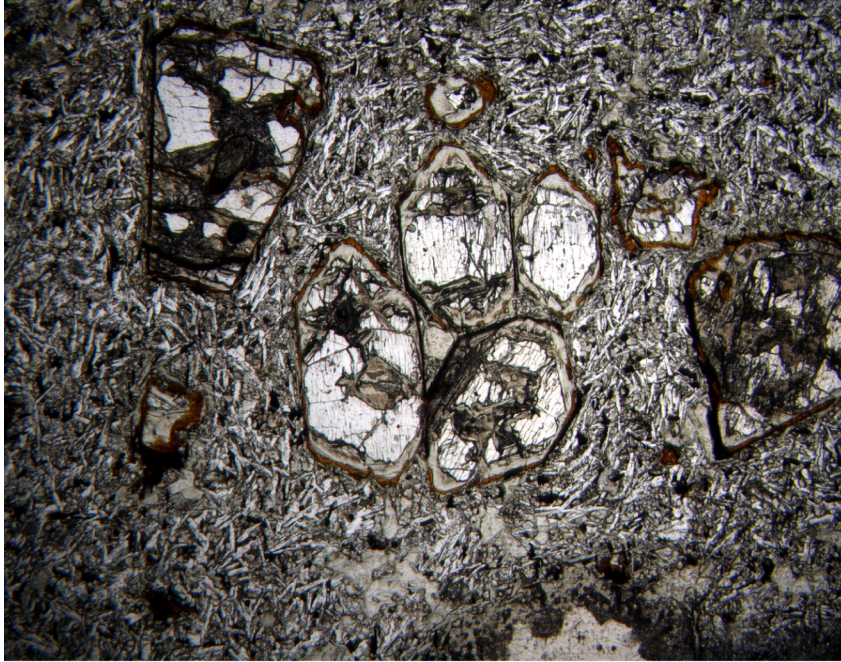
B

Figure F44

Figure F45

Figure F46

Figure F47

Figure F48

A. 197-1206A-3R-4, 59-61 cm

B. 197-1206A-7R-4, 64-66 cm

C. 197-1206A-16R-1, 33-35 cm

D. 197-1206A-18R-2, 17-19 cm
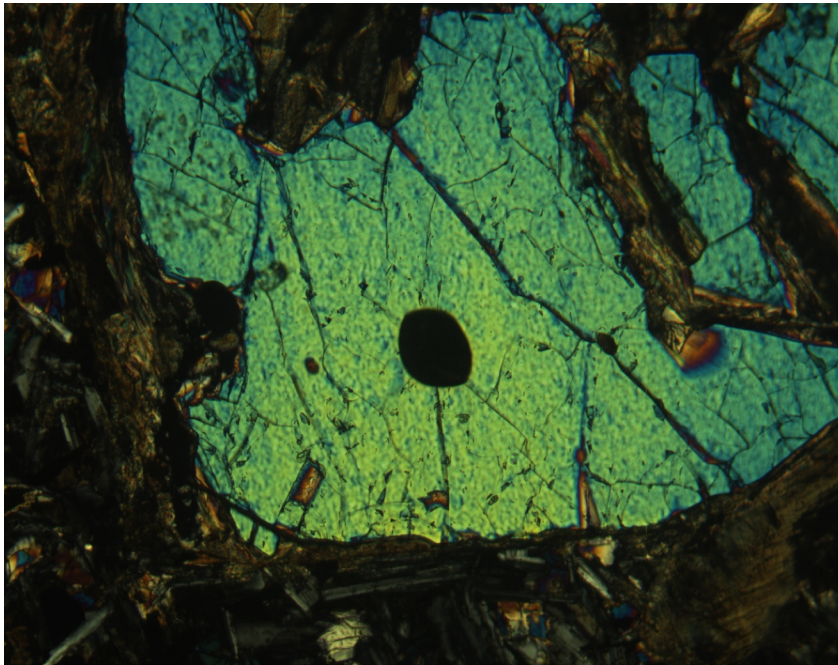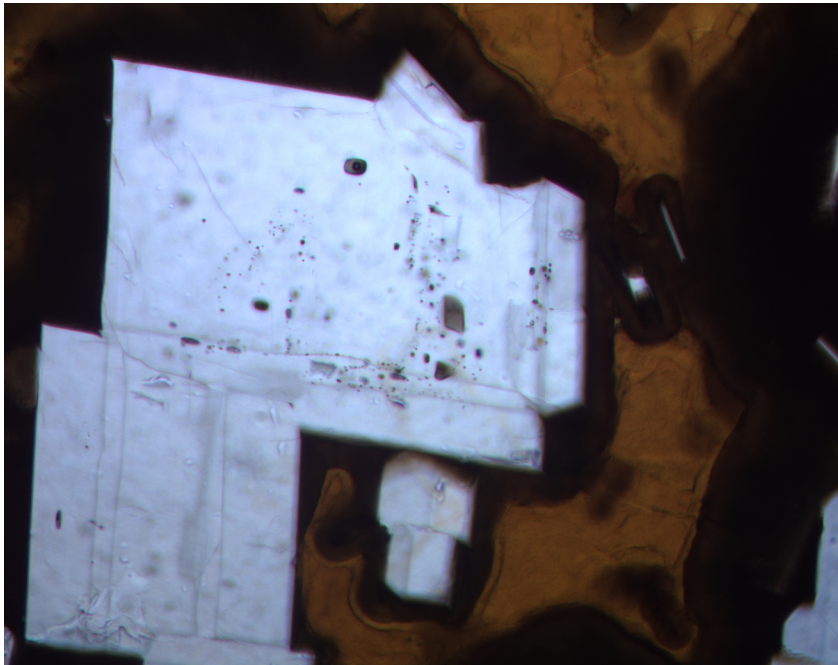
E. 197-1206A-20R-2, 85-87 cm

F. 197-1206A-23R-1, 109-111 cm

Figure F49

Figure F50

Figure F51

Figure F52

Figure F53

Figure F54

Figure F55

Figure F56
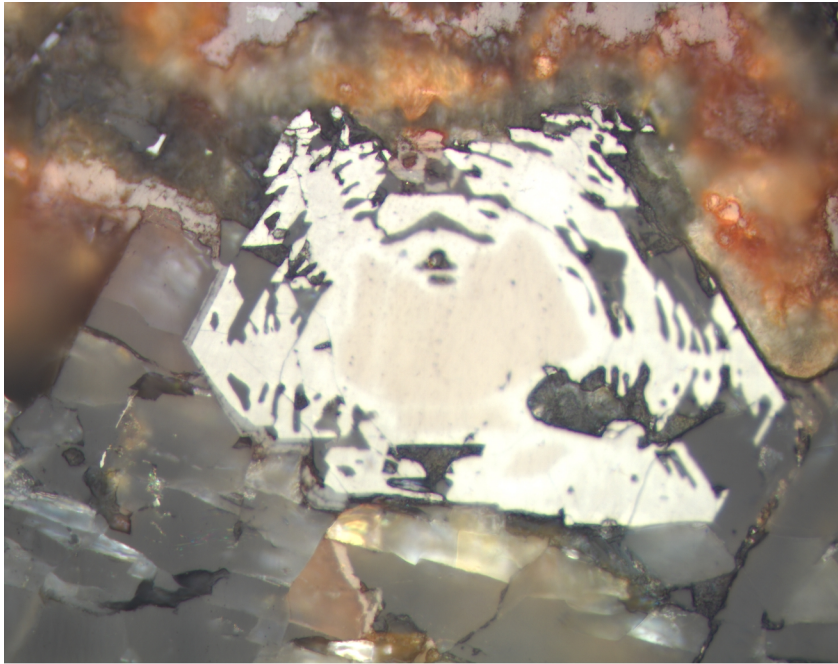
Figure F57
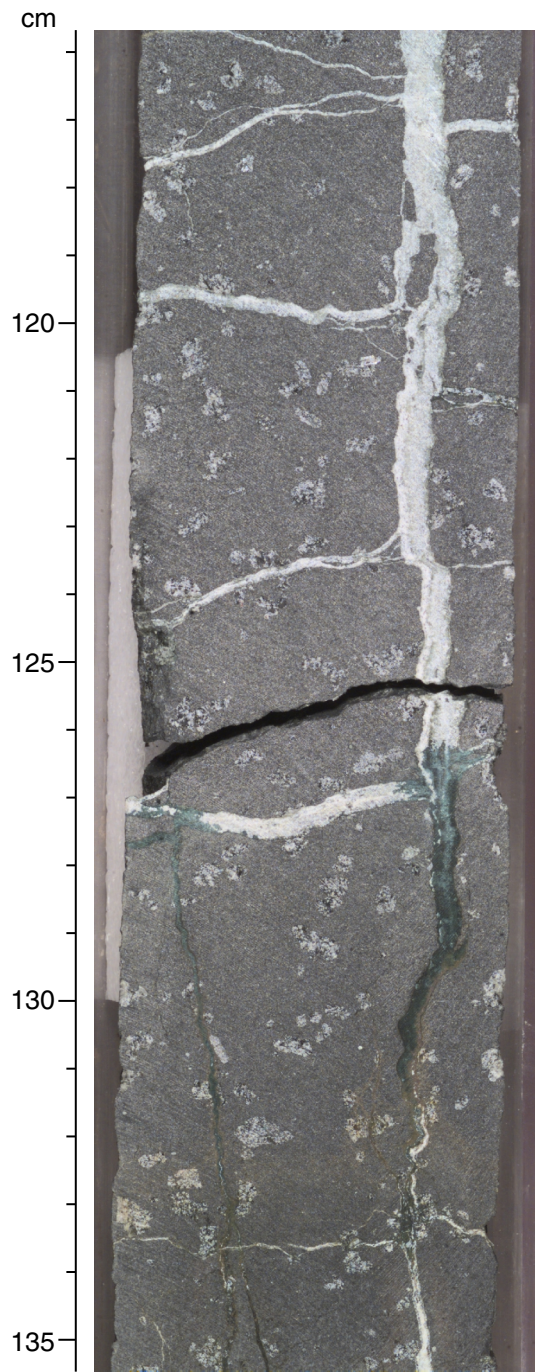
A

Figure F58

Figure F58 (continued)

Figure F59

Figure F60

Figure F61

Figure F62